Combined Turbo Coding and Turbo Equalization for Wireless Systems with Antenna Diversity

Naveen Mysore

Department of Electrical and Computer Engineering
McGill University
Montreal, Canada

January 2002

A thesis submitted to the Faculty of Graduate Studies and Research in partial fulfillment of the requirements for the degree of Master of Engineering

0-612-79086-X

Abstract

Emerging wireless communication systems strive for very high data rates, increased coverage and good quality of service. To achieve these goals under harsh conditions on many wireless channels (e.g., due to fading, multipath interference, power constraints and bandwidth limitations), both antenna diversity schemes and channel coding should be utilized.

This thesis focuses on achieving reliable transmission over a class of multi-input multi-output Rayleigh faded channels at very low Signal-to-Noise Ratios (SNRs). The transmitter and receiver designs are based on turbo coding, multiple transmit/receive antennas and turbo equalization. Simulation studies were performed for systems with different coding rates, numbers of antennas and interleaving strategies. They show the ability to achieve small bit error rates (10^{-4} – 10^{-5}) for negative values of SNR.

Sommaire

Les nouvelles technologies de communications sans fil tentent de fournir des taux de transfert de données élevés tout en offrant un maximum de couverture et une qualité de service inégalée. Afin de réaliser ces objectifs dans l'environnement hostile qu'est le canal sans fil, les techniques qui utilisent la diversité d'antennes et le codage de canal devraient être combinées.

Ce mémoire se concentre sur le problème de réaliser une communication fiable dans un système multi-entrées / multi-sorties sous un environment évanescent Rayleigh quasi-statique à rapport signal/bruit très bas. Les modèles du transmetteur et du récepteur sont basés sur les « turbo-codes », sur la diversité d'antennes en émission et en réception ainsi que sur l'égalisation turbo. Une étude comparative consistant en une série de simulations avec différents paramètres (taux de codage, nombre d'antennes, méthode d'entrelacement) a été effectuée. Les résultats montrent que les systèmes simulés sont capables d'atteindre des taux d'erreur binaire de 10^{-4}-10^{-5} pour des valeurs négatives de rapport signal/bruit.

Acknowledgements

I cannot express in words my gratefulness and appreciation to my advisor, Professor Jan Bajcsy for his patience, valuable insights and creative feedback. Working with him has been a true privilege, and I have benefited tremendously from his knowledge in science, both in depth and broadness and his enthusiasm of doing research. The guidance, encouragement and the numerous hours he gave me during the period I worked on this thesis means a great deal to me.

My special thanks go to Professor Peter Kabal, who provided initial guidance on the courses I should take and who suggested that I pursue my research interests with Professor Bajcsy. I would also like to thank Professor Kaplan who guided me in the area of space-time coding and who also taught a great course in wireless communication.

I would also like to acknowledge my friends in the Telecommunication and Signal Processing Lab: Tarun Agarwal, Charif Beainy, François Duplesis-Beaulieu, Christopher Cave, Mark Klein, Patrick Mitran, Benoît Pelletier, Wesley Periera, Aziz Shallwani, Paxton Smith, Joachim Thiemann, and Alex Wyglinski. They made my stay an enjoyable one.

Above all, I would like to express my utmost gratitude to my family: my father, Mohan, my mother, Latha, and my sister, Navya. They supported me in every aspect of my life and encouraged me every step of the way. They enriched both my life and my dreams. It is to them that I dedicate this thesis.

Na Chora-haaryam
Na Cha Raaja-haaryam
Na Bhraatru-Bhaajyam
Na Chabhaarakaari
Vyaye Krite
Vardhata Eva Nityam
Vidyaa-dhanam
Sarva Dhana Pradhaanam

- Subhashita No. 51

It cannot be stolen by thieves,
Nor can it be taken by Kings.
It cannot be divided among brothers,
And it does not cause a load on your shoulders.
If spent, it always keeps growing.
The Wealth of Knowledge is the most
Superior Wealth of all.

Contents

List Of Figures

List Of Tables

Chapter 1 Introduction

1.1 Wireless Communication Systems

Ever since Guglielmo Marconi first demonstrated the use of radio waves to carry information in 1885, wireless communication technologies have seen tremendous growth. Today's wireless communications provide people with the freedom to initiate and receive phone calls anywhere and anytime. In the future, people and devices will require reliable high data rate services. As opposed to wire line channels, wireless communications face greater challenges because of harsh conditions due to severe multipath fading interference, frequently nonexistent line of sight (LOS) between the transmitter and receiver, and bandwidth and power limitations. Hence techniques that can increase spectrum efficiency or improve link quality and capacity are of great commercial interest to meet the growth in demand for wireless services. To better understand this goal, the set-up of a cellular system will be briefly discussed followed by the motivation for systems that can support high data rates.

The radio spectrum is a finite resource and all wireless operators acquire a portion of this spectrum and must transmit only in this part. Lucky in [3] indicated that 190 billion US dollars was raised by the European nations in auctioning off spectrum for third generation wireless companies. From an industrial point of view, there is a clear incentive to use the purchased spectrum efficiently, i.e., to maximize the generated revenue, and transmit as much data as possible through the acquired spectrum. Consequently, better transmission technologies must be proposed to send more data in smaller bandwidth with less power. The last constraint is due to the finite battery power available at the mobile terminal.

A basic cellular system consists of three units: a mobile unit, a base station, and a mobile telephone switching office (MTSO), as shown in Figure 1.1. When a mobile user initiates a telephone call, the mobile unit communicates with the base station, which can utilize various multiple access schemes such as Time Division Multiple Access (TDMA), Frequency Division Multiple Access (FDMA), or Code Division Multiple Access (CDMA). The base station transmits the user's data or phone call to the MTSO, which then connects to the established telephone network or the PSTN (Public Service Telephone Network). Each cellular base station is allocated a group of radio channels to be used within a small geographic area (cell). Base stations in adjacent cells are assigned different channel groups. By limiting the coverage area to within the boundaries of a cell, the same group of channels may be reused in different cells which are separated from one another by distances large enough to keep the interference level within tolerable limits.

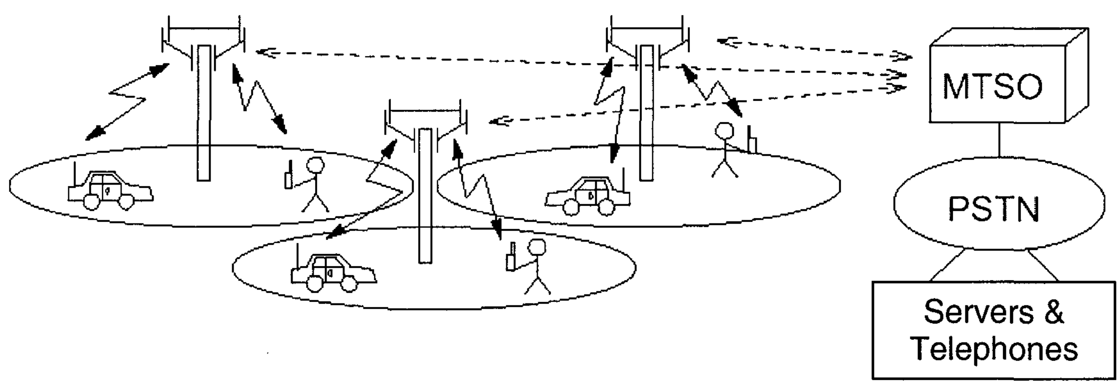

Figure 1.1: A typical cellular telephone network

As the above discussion implies, significant research and development effort has been dedicated to the problem of power and bandwidth efficient transmission over a wireless point-to-point link. This scenario occurs when a mobile unit communicates with the base station. Recent signal processing techniques strive to reach this goal by combining channel coding with antenna diversity. The following two sections provide a brief introduction to error correcting codes and systems with antenna diversity.

1.2 Error Correcting Codes for Digital Communications

Recently, error-correcting codes have been applied to a wide range of commercial applications. Examples of such systems include high-quality and high-speed voice-band modems, digital subscriber loops, personal wireless communications, mobile and direct-broadcast satellite communications [3]. These systems are required to be of low complexity, high performance and integrable into higher-level network protocols. Furthermore, they may need to provide different service rates and unequal error protection for bits from advanced source encoders.

A schematic block diagram of a point-to-point digital communication system is illustrated in Figure 1.2. The source is assumed to be discrete, memoryless with equiprobable output bits. The encoder can be thought of as a concatenation of a forward error-correcting (FEC) encoder with a modulator. The function of the modulator is to convert digital data into continuous time waveforms, which are compatible with the characteristics of the channel. Similarly, the decoder consists of a demodulator block followed by a FEC decoder. The channel generally adds noise and distortion to the transmitted signal, thus making the received waveform unreliable. As a result, the demodulator is usually unable to exactly reproduce the input to the modulator and errors are introduced into the transmitted data. One way to increase the reliability of the communication system is to introduce some structure into the transmitted sequence by adding redundancy using the FEC encoder [1]. The FEC decoder can use this redundancy to correct most channel errors (hence the term, error correcting code). The performance of the decoder is dependent on how corrupt the channel is. Shannon showed that there is a fundamental limit associated with a communication channel: the channel capacity. This quantity limits the maximum rate of reliable transmission over the channel and error-correcting codes are used to approach this limit [2].

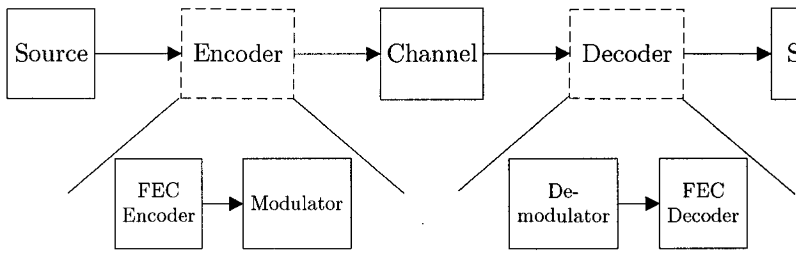

Figure 1.2: The schematic block diagram of a digital communications system

In the past 50 years, there has been significant research in designing codes that approach channel capacity. As a result, three main classes of codes have emerged, i.e., block codes, convolutional codes and concatenated codes. Block codes were originally invented by Hamming [4], and have been used extensively. These codes are based on finite field arithmetic and abstract algebra and can be used to either detect or correct errors [1]. A block code accepts k information symbols and produces n coded symbols, usually using a generator matrix. These codes are referred to as (n, k) block codes and some of the well known ones include Hamming codes, Golay codes, BCH codes and Reed Solomon codes [1]. Although the decoding techniques for these codes will not be discussed in this thesis, the decoders usually require hard quantization of the channel data. As a result, they have a tendency to perform poorly at low SNRs (due to quantization error) but can achieve very low BERs at high and medium SNRs.

Convolutional codes and their extensions are one of the most widely used channel coding techniques in practical communications systems. These codes are primarily used for real-time error correction, as they are easy to implement using the shift register structure and have a low complexity optimal decoder (the Viterbi algorithm [5]). As in the case of block codes, a convolutional encoder accepts k symbols and produces n symbols at each time instant. However, the encoded symbols do not depend only on the current k input symbols but also on past inputs. Unlike block decoders, the convolutional decoder can use the channel data directly (soft inputs) and it can also produce soft outputs (the latter is a useful feature in the next class of error correcting codes). Hence they are capable of achieving low bit error rates at low SNRs but are not as powerful as block codes at high SNRs.

A concatenated code usually consists of two separate codes, which are combined to form a larger code [1]. One example of a concatenated code is to have the block encoder in tandem with the convolutional encoder. At the receiver, the convolutional decoder forms decisions based on soft inputs and removes most of the errors in a data packet. Consequently, the data are passed onto the block decoder, which removes the isolated burst errors caused by the convolutional decoder. The concatenated system would thus achieve very low bit error rates at lower SNRs than the corresponding convolutional or block coded system. In 1993, Berrou *et al.* extended the principle of concatenation to the parallel case. This code, termed the turbo code allows construction of large block lengths using a parallel concatenation of two component convolutional codes separated by an interleaver. Berrou *et al.* also proposed an iterative decoder, which decodes the convolutional encoders separately (using soft decision decoders) and then shares the bit reliability information in an iterative manner. The above encoding and decoding scheme allows turbo codes to perform very near capacity on an Additive White Gaussian Channel (AWGN) channel [6].

1.3 Antenna Diversity Systems

Reliable wireless transmission is difficult to achieve because of the time varying multipath fading channel. This major obstacle makes wireless transmission a challenge when compared to fibre, coaxial cable and satellite transmissions. Decreasing the effective bit error rate (BER) in a multipath-fading channel is difficult, for example, in uncoded transmission, to decrease BER from 10^{-2} to 10^{-3} in an AWGN channel may require only 1 to 2 dB increase in SNR, however a fading channel requires 10 dB improvement [1]. Although BER improvement can be achieved by increasing transmitter power or bandwidth, these measures would be contrary to the efficiency requirements of next generation systems.

Diversity schemes (multiple transmissions / receptions of data packets) have been used as effective techniques to mitigate fading without increasing the transmitted power. However, frequency and time diversity schemes have the disadvantage that additional spectrum is used, which reduces the overall system efficiency. With multiple transmit and receive antennas, the received signals can be separated with spatial processing techniques, thus allowing improved overall economy and efficiency of a digital cellular system. Furthermore, Telatar [7] and Foschini [8] showed that a significant increase in the Shannon capacity of the wireless link could be achieved with multiple antennas. The first practical technique to exploit the potential of a Multi Input Multi Output (MIMO) channel has been proposed in [8]. Space-time trellis codes [9] suggested to combine trellis coding concepts and symbol mapping onto multiple transmit antennas. To further improve the performance of space-time processing, turbo codes have been recently applied to MIMO channels ([10], [11] and [12]).

1.4 Thesis Overview

The main contribution of this thesis is in proposing a practical architecture for transmission over wireless MIMO channels. The scheme combines turbo codes and turbo equalization for systems with multiple transmit and receive antennas. Simulation results of several systems are presented on MIMO channels with quasi-static Rayleigh fading where only the receiver has perfect channel state information. Significant performance gains are observed by increasing the number of transmit/receive antennas from 2 to 4 as well as by increasing the interleaver length.

Chapter 2 introduces the notation used throughout this thesis and reviews the models and capacity of MIMO faded channels, the theory of turbo codes and turbo equalization. Chapter 3 reviews previous techniques in exploiting the capacity of MIMO channels, in particular the V-BLAST architecture [8], space-time trellis codes [9] and space-time block codes [13], turbo coded modulation with antenna diversity [10] and layered space-time architecture with iterative processing [11] are considered. Chapter 4 presents the design of the proposed system and simulation results under different fading conditions and various numbers of antennas. Chapter 5 then summarises the important findings of this thesis, discusses their implications and outlines directions for future work.

Chapter 2 Preliminaries

By employing antenna diversity at both ends of the wireless link, a Multi Input Multi Output (MIMO) channel can be created. Compared to a Single Input Single Output (SISO) channel, MIMO channels offer a significant increase in the capacity of a wireless link. Coding techniques must be used to exploit this increased capacity. This chapter provides an overview of fundamental concepts that are employed throughout subsequent chapters. MIMO channel models and corresponding Shannon capacity formulas are first discussed. Following this, a development of parallel concatenated encoders and the iterative decoding scheme is presented including the concept of turbo equalization.

2.1 Multi Input Multi Output Channels

This section reviews the fading model of the single input single output channel and its extensions to the multi input multi output case.

2.1.1 Faded SISO Channels

When radiated signals are reflected or scattered by large surfaces such as buildings and (or) hills, the received signal is made up of a large number of horizontally travelling plane waves with random amplitudes, phases and angles of arrivals. Due to the finite resolution bandwidth of actual systems, the receiver cannot resolve a group of multipaths, which have almost an identical time of arrival. Hence, this group is typically treated as one signal. It has been shown that when there is no line of sight between the transmitter and receiver, then the amplitude of the received signal can be modelled as being Rayleigh distributed [14]. The probability density function of Rayleigh process is given by,

$$p(a) = \frac{2a}{\Omega} e^{-a^2/\Omega}, a \geq 0 \tag{2.1}$$

where Ω is the variance. The standard assumption that is made is that the transmitting antenna is a lossless isotropic radiator, which radiates power uniformly in all directions. Similarly, the receiver has a lossless isotropic antenna which receives power equally over its effective area [14]. For a quasi-static fading process, the channel gain can be assumed constant over a block and this type of fading will be assumed throughout the thesis.

Figure 2.1 shows the transmission model of a fading channel. It will be assumed that Binary Phase Shift Keying (BPSK) signalling and coherent detection at the receiver is used ($\Theta(t)$ is known at the receiver). Additive white Gaussian noise (AWGN), $z(t)$ has zero mean and a power spectral density, $N_0/2$ (W/Hz) (the primary source of AWGN is the front-end electronics of the receiver).

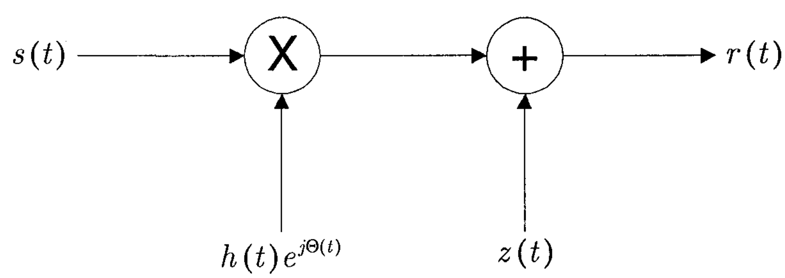

Figure 2.1: The transmission model of a fading channel with additive noise

A discrete-time baseband equivalent model can be written as,

$$\mathbf{r} = \mathbf{hs} + \mathbf{z} \tag{2.2}$$

In this representation, $\mathbf{s}$ is a BPSK vector with component values of $\pm\sqrt{E_s}$, where E_s is the transmitted energy per symbol, $\mathbf{h}$ is the Rayleigh fading vector and $\mathbf{z}$ is an AWGN vector with zero mean and variance $N_0/2$. The gain of each multipath component can be modelled as a complex Gaussian variable given by, g

$= g_x + jg_y$, where g_x and g_y are ~$N(0, ½)$ Gaussian random variables. Therefore, the variance of the complex fade is 1 and the Rayleigh fading parameter h_i at the i-th time instant is given by

$$h_i = \sqrt{g_x^2 + g_y^2}\,. \tag{2.3}$$

Figure 2.2 demonstrates the amplitude of the Rayleigh fading parameter under quasi-static or block fading conditions, where the block number refer to a block of data undergoing the same fade. Note that fades of 5 dB or more are common.

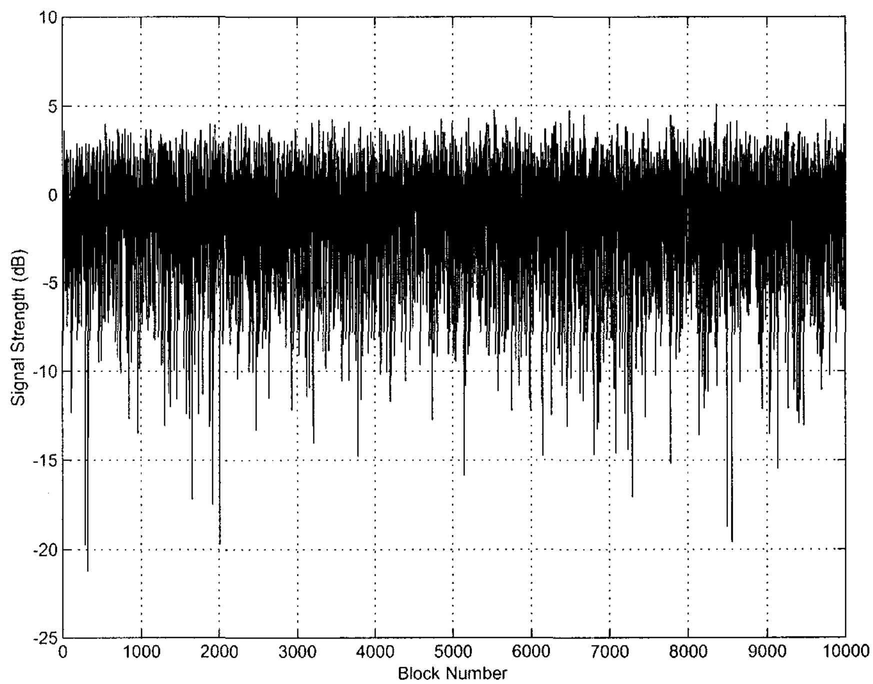

Figure 2.2: A typical received signal amplitude with quasi-static Rayleigh fading for different blocks of data

2.1.2 Faded MIMO Channels

The above model needs to be extended to systems, which incorporate antenna diversity at the transmitter and (or) receiver. For a system with n_T transmit and n_R receive antennas, the channel transfer matrix is given by,

$$\mathbf{H} = \begin{bmatrix} h^{1,1} & h^{1,2} & \cdots & h^{1,n_T} \\ h^{2,1} & h^{2,2} & \cdots & h^{2,n_T} \\ \vdots & \vdots & \ddots & \vdots \\ h^{n_R,1} & h^{n_R,2} & \cdots & h^{n_R,n_T} \end{bmatrix}. \tag{2.4}$$

$\mathbf{H}$ describes the effect of a MIMO channel and the coefficient $h^{i,j}$ is the path gain from the j-th transmit to the i-th receive antenna, $1 \leq j \leq n_T$, $1 \leq i \leq n_R$. For a wireless channel with no LOS, the fading coefficients are spatially uncorrelated, Rayleigh, quasi-static, and independent from one block to the next [15]. This assumption is an idealized version of the result that for antenna elements which are separated by half a wavelength ($\lambda/2$), the path losses are decorrelated [14]. The received vector $\mathbf{r}$ at a given time instant can be written as

$$\mathbf{r} = \mathbf{Hs} + \mathbf{z}\,, \tag{2.5}$$

where $\mathbf{s}$ is the transmitted array (of size n_T x *1*), $\mathbf{r}$ is the received vector (of size n_R x 1) and $\mathbf{z}$ is assumed to be Gaussian with zero mean and a covariance matrix $\sigma^2\mathbf{I}$ (of size n_R x n_R).

Although it may seem intuitively obvious that more antennas on either side of the communications link should improve performance, each receive antenna will receive a weighted sum of the transmitted symbols. The following example uses the signal space approach to illustrate how multiple antennas are beneficial.

Example 1

Consider the transmission of BPSK symbols over a SISO and MIMO channel. In the SISO case, if the Rayleigh fading parameter (from Equation (2.2)) is close to 0, for example, 0.1, then the receiver will find it difficult to decode the signal, as the squared Euclidean distance between the information bits 0 and 1 has reduced from 2 (between signal points -1 to 1) to 0.2 (between signal points -0.1 to 0.1). In the MIMO scenario, the transmitter demultiplexes the bit stream onto 2 antennas. The receiver is assumed to have 2 antennas and let the channel matrix be given by,

$$\mathbf{H} = \begin{bmatrix} 0.2216 & 0.6986 \\ 0.8385 & 0.9818 \end{bmatrix}. \tag{2.6}$$

Therefore, there exist four possible received signal points corresponding to inputs of the channel, which are listed in Table 1.

Table 1: Table of received points (noiseless)

s	Hs
$(-1, -1)^T$	$(-0.9202, -1.8203)^T$
$(+1, -1)^T$	$(-0.4770, -0.1433)^T$
$(-1, +1)^T$	$(0.4770, 0.1433)^T$
$(+1, +1)^T$	$(0.9202, 1.8203)^T$

In Figure 2.3, these four received signals are plotted as circles and the noisy received signals, **r** *are depicted as stars.*

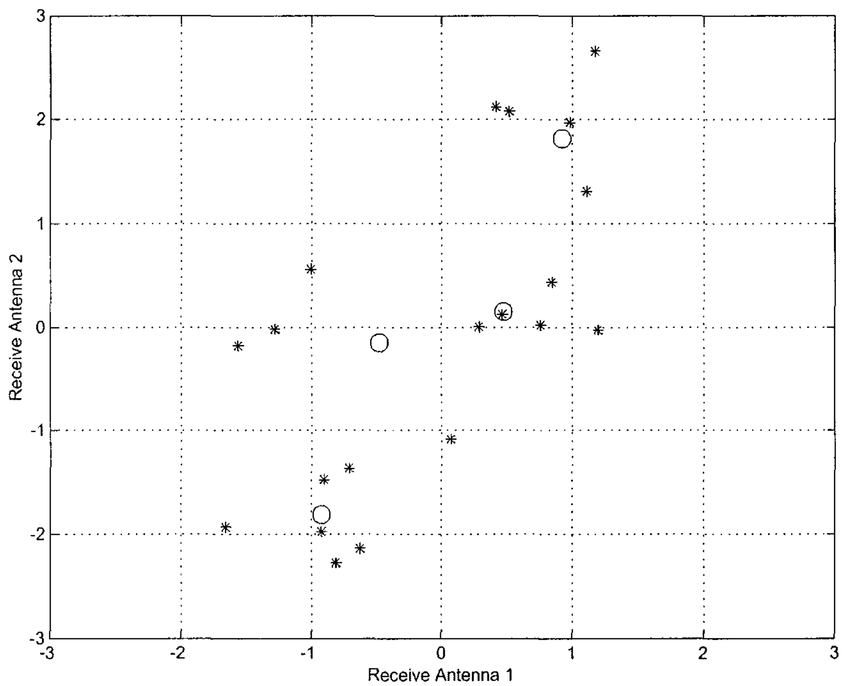

Figure 2.3: A plot illustrating diversity gain for a 2 transmit / 2 receive system

Although two of the four received points are close in the y dimension, they can be distinguished using the x dimension. Because of this extra dimension, a scenario where two points almost coincide is less likely than in the SISO case. Hence this system should have intuitively, a better performance than the SISO system.

This performance gain observed in the previous example is due to the increase in the number of antennas, and hence it is termed as the diversity gain. If more transmit and receive antennas were added, the case of two signal points being close in all dimensions becomes highly unlikely, and hence the performance of the system will further increase.

2.2 Review of the Capacity Formula

This section will focus on the motivation for capacity, the measure of SNR used in this thesis and review of the capacity formula for a multi input multi output channel with additive Gaussian noise.

2.2.1 Motivation for Channel Capacity

Shannon characterized every memoryless channel by a measure known as channel capacity [2]. In his work, he showed that if the rate of transmission is less than the capacity of a channel, arbitrarily small error rate is achievable if an appropriate encoder and decoder are used. The rate of transmission is related to the coding rate by,

$$R = n_T R_m R_c \,, \tag{2.7}$$

where n_T is the number of transmit antennas, R_m is the factor introduced by modulation scheme. The coding rate, R_c is given by,

$$R_c = \frac{k}{n}, \tag{2.8}$$

where k bit message sequence is represented as a n bit coded sequence. Given a particular modulation (R_m is constant), the rate of transmission is directly proportional to the coding rate; in the case of BPSK modulation, $R = n_T R_c$. Hence, capacity is often used as the fundamental benchmark for the goodness of a code. From an alternative point of view, the channel capacity allows the calculation of the lowest SNR a system can operate using a rate of transmission, R (in this situation, the capacity is set to R and the SNR limit is solved for). In this thesis the normalized SNR, which is the bit energy over the power spectral density of the noise, E_b/N_0, will be used. If a system that has a rate of transmission R, a power constraint of P and a noise variance of $\sigma^2 = N_0/2$, then the normalized SNR can be expressed as,

$$\frac{E_b}{N_0} = \frac{P}{2n_T R_m R_c \sigma^2} = \frac{P}{2R\sigma^2}. \tag{2.9}$$

Normalizing all plots to E_b/N_0 allows comparisons between systems that have different spectral efficiencies (different Rs).

2.2.2 The Shannon Capacity Formulas

In this section, the capacity formula for an AWGN channel, SISO and MIMO channels under different conditions will be discussed. A discrete time Gaussian channel with input power constraint, P at time $i = 1, 2, \ldots$ can be expressed as,

$$Y_i = X_i + Z_i, \tag{2.10}$$

where Z_i is a zero mean Gaussian random variable with variance σ^2. In this case, the capacity of a real AWGN single input single output channel is [2],

$$C_{AWGN} = \frac{1}{2}\log_2\left(1 + \frac{P}{\sigma^2}\right) \tag{2.11}$$

and the units are bits per channel use. Hence, if the transmission rate is lower than C_{AWGN}, with the proper coding scheme, any desired bit error rate can be achieved.

The corresponding MIMO channel with n_T transmit and n_R receive antennas can be expressed as,

$$\mathbf{Y}_i = \mathbf{H}\mathbf{X}_i + \mathbf{Z}_i, \tag{2.12}$$

where the real channel matrix $\mathbf{H}$ is unknown at the transmitter, but is perfectly known at the receiver. The MIMO capacity formula is given by [16],

$$C_{fixed} = \frac{1}{2}\log_2 \det\left(\mathbf{I} + \frac{P}{n_T\sigma^2}\mathbf{H}\mathbf{H}^\dagger\right), \tag{2.13}$$

where the input power P is split evenly amongst the n_T antennas and the Hermitian operation is denoted by †. Assuming parallel orthogonal channels, then $\mathbf{H} = \mathbf{I}$, and Equation (2.13) reduces to,

$$C_{parallel} = \frac{n_T}{2}\log_2\left(1+\frac{P}{n_T\sigma^2}\right), \qquad (2.14)$$

which is a multi-dimensional generalization of the 1-D solution.

If the channel matrix changes in time, the value of capacity is given by [7],

$$C_{MIMO} = E\left[\frac{1}{2}\log_2\left(\det\left(\mathbf{I}+\frac{P}{n_T\sigma^2}\mathbf{H}\mathbf{H}^\dagger\right)\right)\right]. \qquad (2.15)$$

Although Telatar in [7] has found an analytical expression for this expectation; it is very difficult to evaluate. Instead a numerical technique will be used to calculate C_{MIMO}. Since the matrices **H** that are observed in time are stationary and ergodic, the statistical average of the capacity in Equation (2.15) is equal to its time average. This implies that C_{MIMO} can be approximately calculated by averaging C_{fixed} from Equation (2.13) over a large number of realizations of **H** as shown in Equation (2.16),

$$C_T = \frac{1}{2T}\sum_{i=1}^{T}\log_2\left(\det\left(\mathbf{I}+\frac{P}{n_T\sigma^2}\mathbf{H}_i\mathbf{H}_i^\dagger\right)\right)\underset{T\to\infty}{\longrightarrow} C_{MIMO}\,. \qquad (2.16)$$

For large T, C_T is a very good approximation of C_{MIMO}. Equation (2.13) and Equation (2.16) can also be applied to a faded SISO channel, where **H** is replaced by h and **I** with 1. If the channel matrix is complex then the ½ is dropped in Equations (2.11) and (2.13) to (2.16). Figure 2.4 and Figure 2.5 illustrate the relationship between C_T, the number of antennas ($n_T = n_R$) and E_b/N_0. The capacity grows linearly with E_b/N_0 and logarithmically with the number of antennas [8]. At an E_b/N_0 of 1 dB, 70.4 bits per channel use can be transmitted with a 16 antenna system, compared to 3.5 bits in the corresponding SISO case.

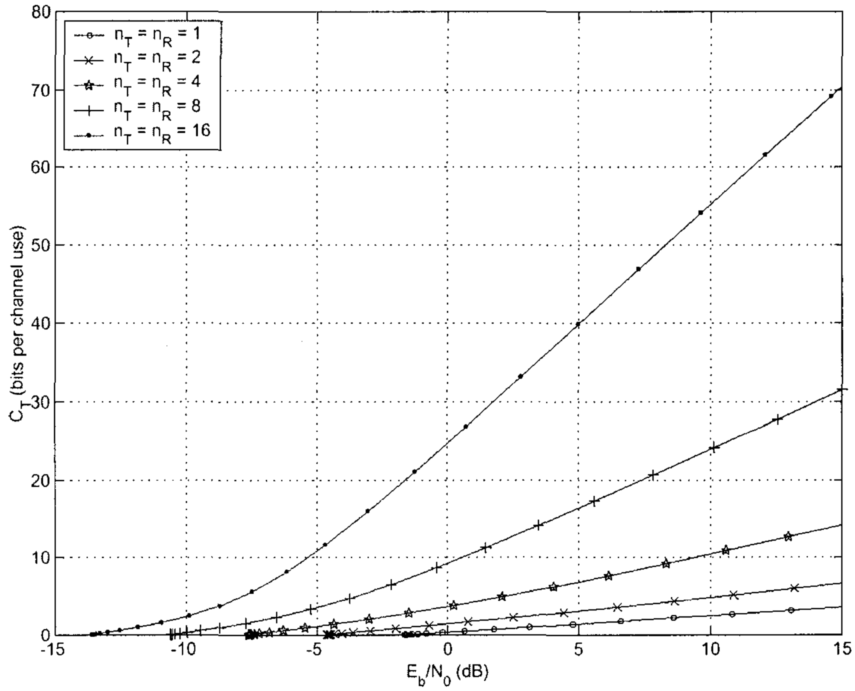

Figure 2.4: A linear plot of C_T vs. E_b/N_0 for different number of antennas

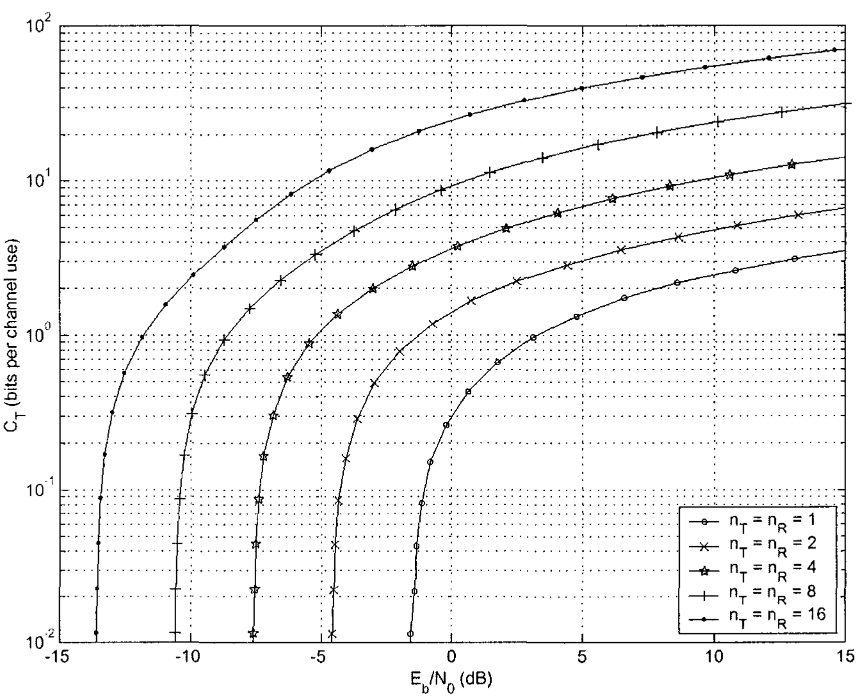

Figure 2.5: A semi-log plot of C_T vs. E_b/N_0 for different number of antennas

2.3 Encoders

In this section, the encoder structure of a general communications system will be discussed. To begin with, the concepts from graph theory will be considered as convolutional encoders and more generally, finite state machine encoders require graph based techniques. Then the discussion will focus on the trellis description of FSM encoders. This section will then conclude with a brief discussion on representing MIMO channels as block encoders.

2.3.1 Concepts from Graph Theory

In this section, the concepts from graph theory will be considered, where the notation follows from class notes given in [17]. A directed graph $\mathcal{G}$ consists of a set of vertices or nodes $V(\mathcal{G})$, an edge set $E(\mathcal{G})$ and an incidence relationship, $I(u, v, e)$. Edge e connects vertex u to vertex v if the following incidence relation is satisfied [17],

$$I(u,v,e) = \begin{cases} 1, \text{ if } u \text{ and } v \text{ are connected} \\ 0, \text{ otherwise} \end{cases} . \tag{2.17}$$

If $I(u, v, e)$ is 1, the head and tail of the edge is given by u and v, respectively. A directed graph is shown in Figure 2.6.

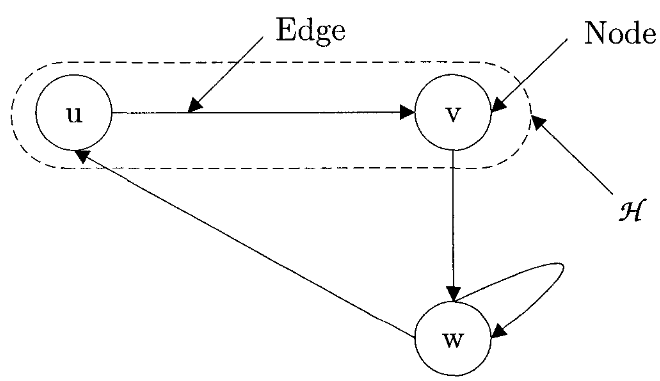

Figure 2.6: A general directed graph

A subgraph $\mathcal{H}$ of a directed graph $\mathcal{G}$ is a directed graph with $V(\mathcal{H}) \subseteq V(\mathcal{G})$ and $E(\mathcal{H}) \subseteq E(\mathcal{G})$, such that every edge of $\mathcal{H}$ has the same head and tail in $\mathcal{H}$ as in $\mathcal{G}$.

For example, $\mathcal{H}$ is the subgraph that contains u and v in Figure 2.6. A path in $\mathcal{G}$ is a subgraph of $\mathcal{G}$ such that the node set and edge set can be numbered as $\{v_1 \ldots v_{N+1}\}$ and $\{e_1 \ldots e_N\}$, respectively, so that e_w is the edge which connects v_w to v_{w+1}, $w = 1 \ldots N$. A trellis is a layered directed graph where the nodes in $V(\mathcal{G})$ can be partitioned into sets $V_1 \ldots V_{N+1}$, so that the edges can only go from V_w to V_{w+1} in the w-th time instant. Figure 2.7 illustrates a trellis.

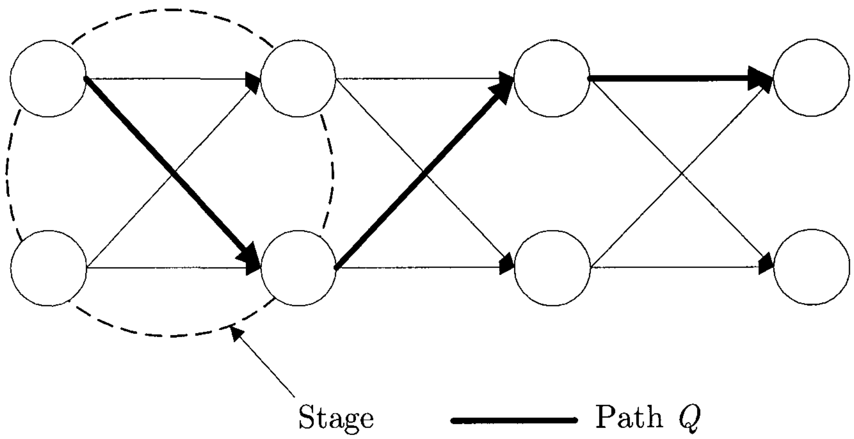

Figure 2.7: The depiction of a layered directed graph (trellis)

A trellis encoder can be thought of as a mapping between a set of messages $\mathcal{M}$ to a codebook C,

$$f : \mathcal{M} \rightarrow C \subseteq \mathcal{S}, \tag{2.18}$$

where the codebook C is a subset of allowed channel input sequences $\mathcal{S}$. Therefore, a trellis encoder is a Finite State Machine (FSM) that has a trellis $\mathcal{G}$, input label $l_I(e)$ and output label $l_O(e)$ along every edge $e \in E(\mathcal{G})$. The input and the present state determine the output and the next state. In a trellis, all FSM states are depicted as a column of dots and are repeated at each time instant. A trellis stage corresponds to proceeding from one column to the next and a trellis path is a sequence of states that an encoder has visited based on the input bits. In Figure 2.7, a trellis stage and a typical path, Q is shown.

2.3.2 FSM Encoders

As indicated in section 1.2, convolutional codes differ from block codes as they introduce memory into the encoded data by using a shift register structure. Since convolutional encoders have finite memory, they form a particular subclass of finite state machine (FSM) encoders, as illustrated in Figure 2.8. Although general FSM encoders are completely described by a trellis, they may not have a shift register structure.

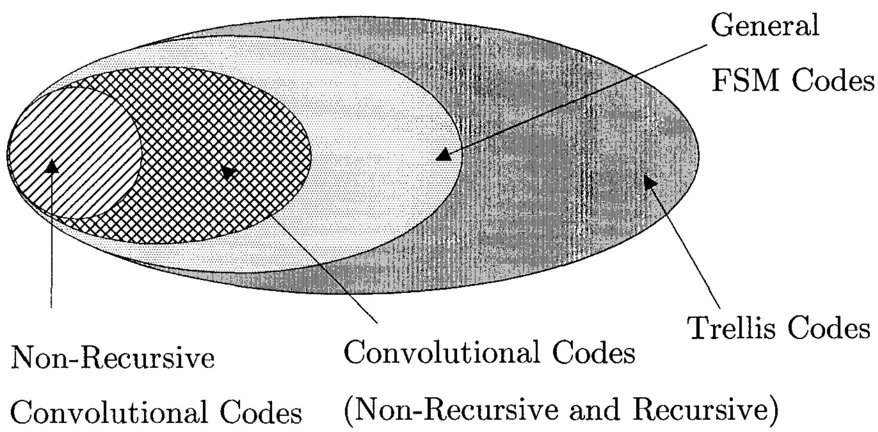

Figure 2.8: Illustration of the different classes in general FSM codes

In the following discussion, several recursive systematic convolutional (RSC) encoders and a sample FSM (non-convolutional) encoder will be presented.

Berrou *et al.* in [6] used RSC encoders to construct the original turbo codes based on parallel concatenation, which will be discussed in section 2.5.1. The recursive systematic convolutional encoders get their name as one of the outputs is the message stream and the next input into the shift register is obtained by feeding back a weighted sum of shift register contents. A sample block diagram for a rate 1/2 RSC encoder is shown in Figure 2.9.

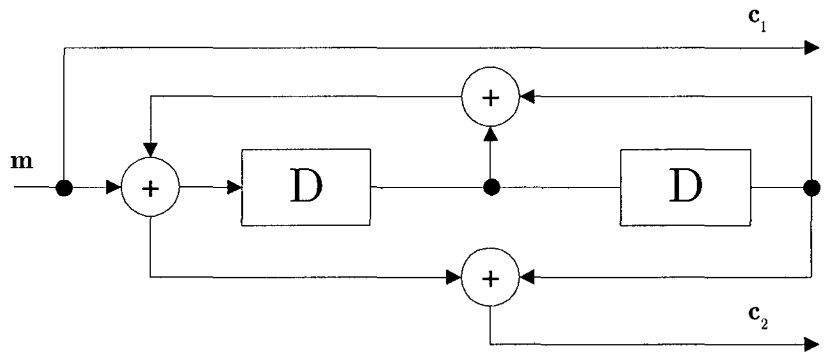

Figure 2.9: A sample block diagram of a rate 1/2 recursive systematic convolutional encoder

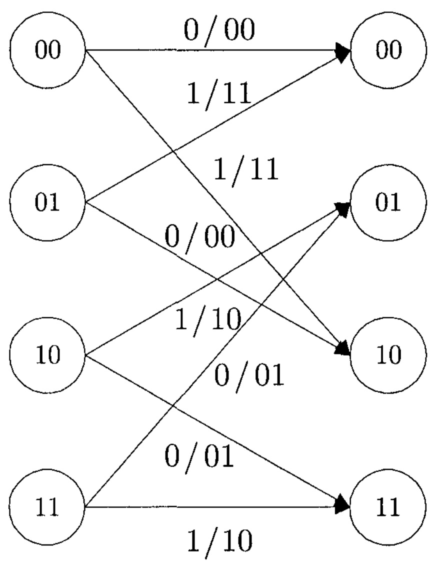

Figure 2.10: One stage of the trellis of the RSC encoder shown in Figure 2.9

An RSC encoder can be described by the generator polynomial, $\mathbf{G} = [1, \mathbf{g}_2/\mathbf{g}_1]$, where 1 denotes the systematic output, $\mathbf{g}_1$ and $\mathbf{g}_2$ are the feedback and feedforward polynomials, respectively. In Figure 2.9, $\mathbf{g}_1$ is 7_{oct} and $\mathbf{g}_2$ is 5_{oct} while one stage of the trellis for this encoder is shown in Figure 2.10.

The nature of recursive versus nonrecursive convolutional encoders can best be illustrated through an example. Figure 2.11 shows a nonrecursive convolutional encoder with generator polynomial, $\mathbf{G} = [\mathbf{g}_1, \mathbf{g}_2]$, where $\mathbf{g}_1 = 3_{oct}$ and $\mathbf{g}_2 = 2_{oct}$.

Figure 2.12 shows a similar recursive convolutional encoder, with generator ploynomial, $\mathbf{G} = [1, \mathbf{g}_2/\mathbf{g}_1]$, where the generator sequences are the same as above.

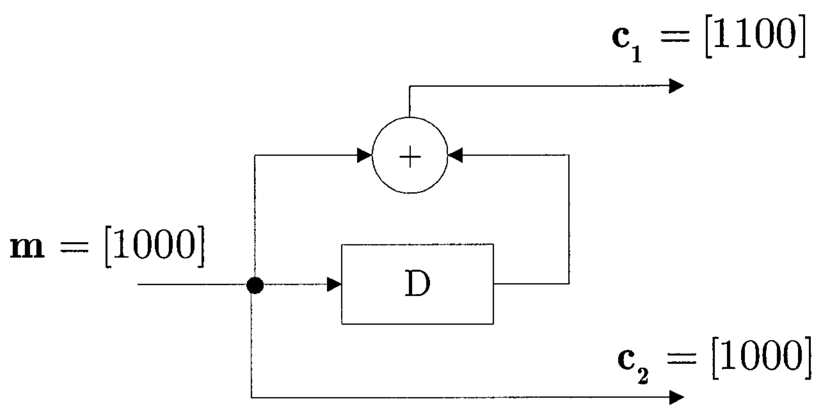

Figure 2.11: The schematic block diagram of a rate 1/2 nonrecursive convolutional encoder

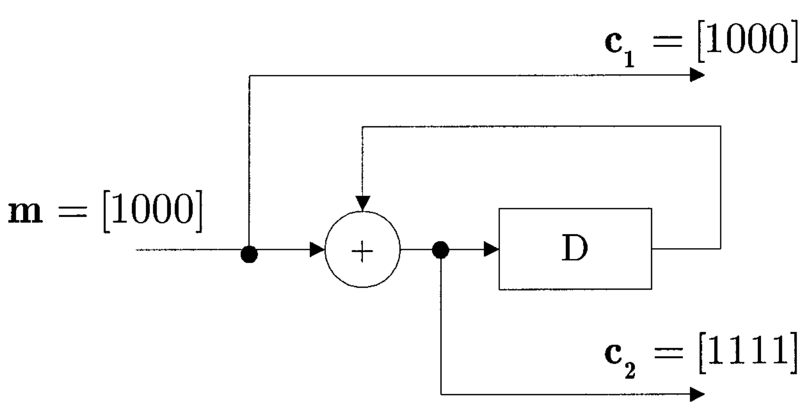

Figure 2.12: The schematic block diagram of a rate 1/2 recursive convolutional encoder

Given the same input sequence, the nonrecursive encoder produces an output codeword of weight 3 and the recursive encoder produces an output codeword of weight 5. This demonstrates the potential of recursive convolutional encoders to produce codewords with increased weights relative to nonrecursive encoders. This results in a larger distance between codewords with lower weights, which in turn leads to better performance.

As can be seen in Figure 2.8, general FSM codes can include a wide variety of codes that can be represented by a trellis, including non-linear codes. Hence they provide a lot of flexibility to the designer, as codes can be constructed based on a system's constraints. An intuitive reason as to why a designed code may perform better is that code optimization (search for the best code) is performed over a larger set (shown in Figure 2.8) rather than a subclass. An example of a general FSM code is shown in Figure 2.13 and it should be noted that this code does not have a shift register structure. Although this trellis is similar to the one shown in Figure 2.10 with respect to input labels and state transitions, the output labels differ on some of the edges.

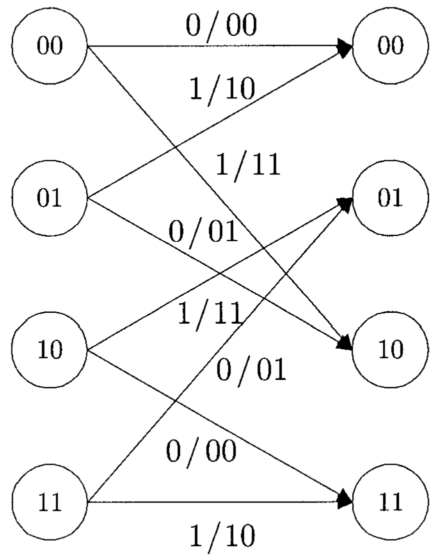

Figure 2.13: One stage of the trellis of a general FSM encoder

2.3.3 Trellis Closing

Graph based decoders as described in section 2.4 require knowledge of the final state of the trellis. As a convention, state '0' is always assumed to be the starting and finishing state. The process of adding tail bits to force the state machine to end in a predefined state is known as trellis closing. For nonrecursive convolutional codes, trellis closing is accomplished by shifting K-1 input zeros, where K is the constraint length. However, this will not work for RCS and general FSM encoders as the tail bits are dependent on the final state of the encoder. The smallest number of these bits corresponds to the shortest path from the final state of the encoder to state '0'. The shortest path can be found using the Viterbi algorithm, and the tail bits from this path can then be appended to the encoded output.

2.3.4 MIMO Channels as Block Encoders

Block encoders are a class of encoders, which accepts an input block and output a block of data. In a block code the information sequence is divided into blocks of length k, and each block is mapped into outputs of length n. This mapping is independent from the previous blocks, i.e., there exists no memory from one block to the next. The MIMO channel described in section 2.1.2 is an example of a block encoder. In this case, Table 1 represents the look up table, where the input block (which is 2 bits) must match the entry in the left column. Then the corresponding output in the right column can be read out.

2.4 Decoders

This section will introduce different types of soft decision decoders. Initially a discussion of what a soft decision decoder is trying to calculate will be provided. Then different techniques such as the BCJR [19] and SOVA ([20] and [21]) algorithms and soft decision block decoding will be considered. Without loss of generality, it shall be assumed that the encoder is of rate $1/n$, i.e., $k = 1$.

2.4.1 Decoders as Mappings and Probabilistic Decoding

Parallel concatenation of constituent encoders offer the ability to build powerful codes, which utilize a relatively simple soft decision-decoding algorithm. This is possible because the turbo decoder is constructed from simple constituent decoders which share bit reliability measures. Similar to the encoder, the channel can be thought of as a mapping from the set of allowed channel inputs $\mathcal{S}$ to the set of received messages $\mathcal{R}$,

$$g : \mathcal{S} \rightarrow \mathcal{R} \,. \tag{2.19}$$

The decoder can also be thought of as a mapping between the received set and the decision set,

$$\varphi : \mathcal{R} \rightarrow \mathcal{D}. \tag{2.20}$$

Hence, the whole communications system can be thought of as going from $\mathcal{M}$ (the message set) $\rightarrow \mathcal{D}$. To minimize the message error probability going from $\mathcal{M}$ to $\mathcal{D}$ is to maximize the aposteriori probability,

$$\hat{\mathbf{m}} = \arg\max_{\mathbf{m}\in\mathcal{M}} P(\mathbf{m}|\,\mathbf{y}), \tag{2.21}$$

where $\mathbf{y}$ is the received sequence and $\hat{\mathbf{m}}$ is the decoded sequence. Alternatively, if one wants to obtain a soft decision of the message bits, the array of probabilities can be evaluated,

$$\begin{bmatrix} P\left(m_1 = 0\middle|\mathbf{y}\right) \\ P\left(m_1 = 1\middle|\mathbf{y}\right) \end{bmatrix} \cdots \begin{bmatrix} P\left(m_N = 0\middle|\mathbf{y}\right) \\ P\left(m_N = 1\middle|\mathbf{y}\right) \end{bmatrix}. \tag{2.22}$$

Although neither $P(\mathbf{m}|\mathbf{y})$ nor $P(m_w = 0|\mathbf{y})$ can be evaluated directly, they can be rewritten in terms of known quantities. Using Bayes' Rule, the aposteriori probability is given by,

$$\begin{aligned} P(\mathbf{m}|\,\mathbf{y}) &= P(\mathbf{c}|\,\mathbf{y}) \\ &= \frac{P\left(\mathbf{y}\middle|\mathbf{c}\right)P(\mathbf{c})}{P(\mathbf{y})} \\ &= \frac{P\left(\mathbf{y}\middle|\mathbf{c}\right)P(\mathbf{m})}{P(\mathbf{y})} \\ &= \frac{\left(\prod_{j=1}^{n} P\left(y_j\middle|c_j\right)\right)P(\mathbf{m})}{P(\mathbf{y})} \end{aligned}, \tag{2.23}$$

where it is assumed that the source is binary, memoryless and has equiprobable outputs, the encoder is a one to one mapping from the message bits to the codeword bits and the channel is memoryless.

Assuming an AWGN channel, the probabilities can be replaced with probability density functions evaluated for a given y_j and c_j. Hence the probability $P(\mathbf{m}|\mathbf{y})$ can be written as,

$$P(\mathbf{m}|\mathbf{y}) = \frac{\left(\prod_{j=1}^{n} e^{-\|y_j - c_j\|^2 / 2\sigma^2}\right) P(\mathbf{m})}{\left(\sqrt{2\pi}\sigma\right)^n P(\mathbf{y})}. \tag{2.24}$$

$P(\mathbf{y})$ is usually not evaluated as it is common to all terms and is a constant.

2.4.2 Maximum Likelihood Decoding

Maximum Likelihood (ML) decoding for convolutionally encoded messages was first proposed by Viterbi [22], while Forney [5] introduced the trellis diagram and explained the Viterbi algorithm as the shortest path problem. Assuming that the prior probabilities on all the message bits are equal and $P(m_w = 0) = P(m_w = 1) = ½$, the ML decoder computes the nearest message given the received channel vector. Using the probabilistic decoding lemma in [23], the probability in Equation (2.23) can be expressed as

$$P(\mathbf{m}|\mathbf{y}) = \frac{1}{P(\mathbf{y})} \prod_{c_w \in E(Q_{\mathbf{m}})} \gamma(e_w), \tag{2.25}$$

where $\gamma(e_w)$ is the trellis edge weights and $Q_{\mathbf{m}}$ is the path corresponding to message $\mathbf{m}$ and codeword $\mathbf{c}$. Going from equation (2.23) to (2.25), the products have been reindexed from coordinate indices to edges along the trellis path corresponding to $\mathbf{m}$, where edge $e_w \in \mathrm{E}(Q_{\mathbf{m}})$ corresponds to the $k = 1$ message bit and n coded bits in the w-th time instant. The trellis edge weight, $\gamma(e_w)$, is given by,

$$\gamma(e_w) = \frac{1}{2} \prod_{j=1}^{n} P\left(y_{jw} \middle| c_{jw} = l_O(e_w)\right). \tag{2.26}$$

Based on the probabilistic decoding lemma, the maximum aposteriori problem becomes equivalent to finding a path $\hat{Q}_{\mathbf{m}}$ (ML decoding) in the trellis such that

$$\begin{aligned} \hat{Q}_{\mathbf{m}} &= \arg\max_{Q_{\mathbf{m}}} \frac{1}{P(y)} \prod_{c_w \in E(Q_{\mathbf{m}})} \gamma(e_w) \\ &= \arg\max_{Q_{\mathbf{m}}} \exp\left(\sum_{c_w \in E(Q_{\mathbf{m}})} \log\left(\gamma(e_w)\right) \right), \\ &= \arg\min_{Q_{\mathbf{m}}} \sum_{c_w \in E(Q_{\mathbf{m}})} d(e_w) \end{aligned} \tag{2.27}$$

where the exponent has been dropped from the last expression as it is a monotonically increasing function. The trellis distances are defined as,

$$d(e_w) = -\log(\gamma(e_w)). \tag{2.28}$$

The term, $d(e_w)$ can be thought of as a distance measure between the received vector $\mathbf{y}$ and a particular codeword $\mathbf{x}$. Thus, the shortest path through the trellis $\mathcal{G}$, with these edge weights, correspond to the optimum solution and the input and output label specify $\hat{\mathbf{m}}$ and $\hat{\mathbf{c}}$, respectively.

The recursive algorithm for finding the shortest path from u to v can be expressed as [34],

1. Initialize $w = 1$, $P_1 = \{0\}$ and $d(P_1) = 0$ ($d(\cdot)$ is the distance of the edge or path).
2. For every $v \in V_{w+1}$ (the set of all possible states in the $w+1$-th stage), find the shortest path from 0 (start) to v. Let the shortest path from 0 to u (the state at time w) be denoted by P_u, then the shortest path from 0 to v corresponds to the edge $e_w = uv$ that minimizes $d(P_u) + d(e_w)$. Update the shortest paths and their lengths as follows,

$$\begin{aligned} P_v &= \{P_u, e_w\} \\ d(P_v) &= d(P_u) + d(e_w) \end{aligned} . \tag{2.29}$$

3. If $w = N$ (The end of the trellis), then output the overall shortest path from $0 \in V_1$ to $t \in V_N$, else increase w by 1 and go to step 2.

The distance metric used in the algorithm is the Euclidean distance for an AWGN channel. To decode the message, it is assumed that the trellis starts and finishes in the 0-th state. Example 1 illustrates the Viterbi algorithm on a simple trellis.

Example 1

Consider the following trellis, where the first label on the edge is the input and output and the second label is the Euclidean distance of that edge assuming that the received sequence was [0.8408 -0.3381 -0.0254].

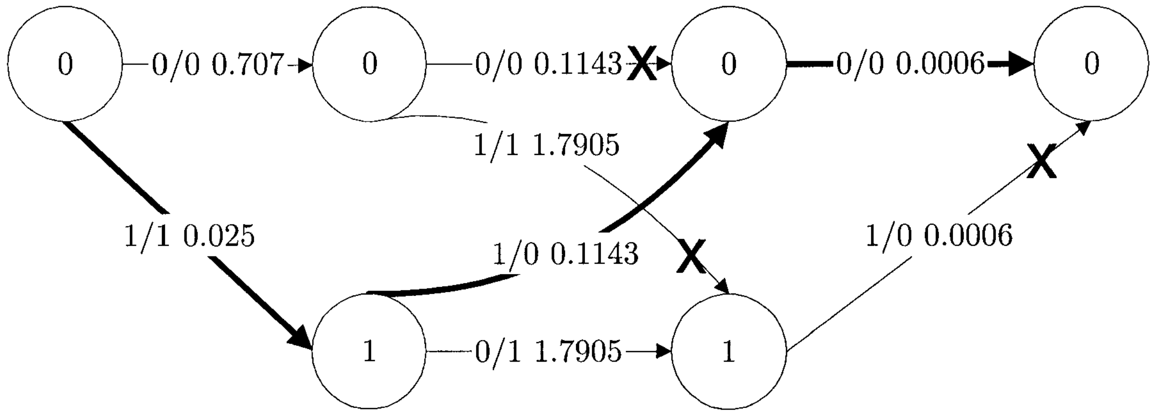

Figure 2.14: The trellis diagram illustrating the Viterbi algorithm

To apply the Viterbi algorithm in an efficient manner, two support quantities need to be defined:

Path Metric at a state u: The distance of a path from the 0-th state to state u.

Node Metric at the w-th stage: is a L x 1 vector of minimum path metrics for all L states in the w-th stage.

To illustrate these two quantities, the node metric (NM_w) for each of the w = 1...3 stages in the above trellis can be calculated. The node metric is initialized to $[0, \infty]^T$. *In the first stage,*

$$\begin{aligned} NM_1(0) &= \min\left\{\begin{bmatrix}0\\\infty\end{bmatrix}+\begin{bmatrix}0.707\\\infty\end{bmatrix}\right\} = 0.707, \text{0-th } \textit{state} \\ NM_1(1) &= \min\left\{\begin{bmatrix}0\\\infty\end{bmatrix}+\begin{bmatrix}0.025\\\infty\end{bmatrix}\right\} = 0.025, \text{0-th } \textit{state} \end{aligned} \quad . \tag{2.30}$$

Similarly, the node metrics for the second and third stages are,

$$\begin{aligned} NM_2 &= \begin{bmatrix}0.1397\\1.8158\end{bmatrix}, \begin{bmatrix}\text{1st state}\\\text{1st state}\end{bmatrix} \\ NM_3 &= \begin{bmatrix}0.1403\\\infty\end{bmatrix}, \begin{bmatrix}\text{0-th state}\\\text{Don't Care}\end{bmatrix} \end{aligned} . \tag{2.31}$$

Equation (2.30) & (2.31) also indicates which starting state gave the smallest distance. Once the end of the trellis is reached, a back track operation through these states will give the corresponding inputs. In this case,

0-th → 1-st → 0-th.

The corresponding message is '110'. The highlighted path is shown in Figure 2.14.

2.4.3 The BCJR Decoder

The BCJR (named after its authors: Bahl, Cocke, Jelinek and Raviv) algorithm is an efficient way of performing soft decision decoding [19]. Consider a message **m**, encoded by a trellis encoder and transmitted over a memoryless channel. The posterior bit/symbol probability, e.g., $P(m_w = 0 \mid \mathbf{y})$ can be written as,

$$P\left(m_w = 0 \middle| \mathbf{y}\right) = \sum_{\substack{m \in \mathcal{M} \\ \text{such that } m_w = 0}} P(\mathbf{m} | \mathbf{y})$$

$$= \frac{\sum_{\substack{m \in \mathcal{M} \\ \text{such that } m_w = 0}} P(m_w) \prod_{j=1}^{n} P\left(y_{jw} \middle| x_j\right)}{\sum_{m \in \mathcal{M}} P(m_w) \prod_{j=1}^{n} P\left(y_{jw} \middle| x_j\right)} \tag{2.32}$$

$$P\left(m_w = 0 \middle| \mathbf{y}\right) = \frac{\sum_{\substack{Q_m : \\ E(Q_m) \cap S \neq 0}} \prod_{c_w \in E(Q_m)} \gamma(e_w)}{\sum_{Q_m} \prod_{c_w \in E(Q_m)} \gamma(e_w)}, \tag{2.33}$$

where the trellis edge weights $\gamma(e_w)$ are given by,

$$\gamma(e_w) = P\left(m_w = l_I(e_w)\right) \prod_{j=1}^{n} P\left(y_{jw} \middle| x_{jw} = c_{jw} = l_O(e_w)\right). \tag{2.34}$$

Intuitively, $\gamma(e_w)$ is the number of distinct paths through the edge, e_w. The BCJR decoder will evaluate the above probability for all bits in the packet. To do this efficiently, the BCJR decoder will first set up the edge weight matrix, $\boldsymbol{\Gamma}$, where the entries of the matrix are δ_{wfg}, which is the edge weight (calculated using Equation (2.34)) going from state f to g in the w-th stage (N is the size of the data packet and L is the total number of states in a stage),

$$\boldsymbol{\Gamma} = \left[\boldsymbol{\Gamma}_1 \middle| \cdots \middle| \boldsymbol{\Gamma}_N\right] = \left[\begin{array}{ccc|c|ccc} \gamma_{111} & \cdots & \gamma_{11L} & & \gamma_{N11} & \cdots & \gamma_{N1L} \\ \vdots & \ddots & \vdots & \cdots & \vdots & \ddots & \vdots \\ \gamma_{1L1} & \cdots & \gamma_{1LL} & & \gamma_{NL1} & \cdots & \gamma_{NLL} \end{array}\right]. \tag{2.35}$$

Also, the decoder calculates two support quantities: the forward and backward metrics ($\boldsymbol{\alpha}$, $\boldsymbol{\beta}$, respectively) for each stage. The forward metric is the sum of all weighted paths from 0-th state to each of the states in a stage. The forward metric, $\boldsymbol{\alpha}_w$, for the w-th stage can be calculated in a recursive fashion:

$$\boldsymbol{\alpha}_w = \boldsymbol{\alpha}_{w\text{-}1}\boldsymbol{\Gamma}_w , \tag{2.36}$$

where $\boldsymbol{\alpha}_w$ is a 1 x L matrix. Similarly, the backward metric is defined as,

$$\boldsymbol{\beta}_{w-1} = \boldsymbol{\Gamma}_w\boldsymbol{\beta}_w , \tag{2.37}$$

where $\boldsymbol{\beta}_w$ is a L x 1 matrix and the initial conditions are $\alpha_0 = \beta_N = 1$. Conceptually, the backward metric is the same as the forward metric, except that it is evaluated starting from the end of the trellis. Therefore the sum of the weighted paths from the 0-th state to the w-th stage in a trellis is given by,

$$Total = \boldsymbol{\alpha}_w\boldsymbol{\beta}_w = \sum_{all\ states\ L} \alpha_w(l)\beta_w(l) \ . \tag{2.38}$$

According to probabilistic decoding lemma [19], the probability, $P(m_w = 0|\mathbf{y})$ (Equation (2.33)) is equivalent to finding the number of paths passing through the edge having $m_w = 0$ over the total sum,

$$P\left(m_w = 0\middle|\mathbf{y}\right) = \frac{\boldsymbol{\alpha}_{w\text{-}1}\boldsymbol{\Gamma}^*_w\boldsymbol{\beta}_w}{\boldsymbol{\alpha}_w\boldsymbol{\beta}_w} , \tag{2.39}$$

where * indicates a modified $\boldsymbol{\Gamma}_w$. Example 2 illustrates the computation of (2.39).

Example 2

Consider the trellis shown in Figure 2.15. The trellis edge weights (the second label) were found using Equation (2.34). Based on the above trellis, the $\boldsymbol{\Gamma}$ matrix is given by,

$$\boldsymbol{\Gamma} = \left[\begin{array}{cc|cc|cc} 0.1 & 0.9 & 0.5 & 0.3 & 0.2 & 0 \\ 0 & 0 & 0.3 & 0.5 & 0.4 & 0 \end{array}\right]. \tag{2.40}$$

The support quantities are,

$$\alpha_1 = \begin{bmatrix} 0.1 & 0.9 \end{bmatrix}, \alpha_2 = \begin{bmatrix} 0.32 & 0.48 \end{bmatrix}, \alpha_3 = [0.256], \tag{2.41}$$

$$\beta_3 = [1], \beta_2 = \begin{bmatrix} 0.2 & 0.4 \end{bmatrix}^{\mathrm{T}}, \beta_1 = \begin{bmatrix} 0.22 & 0.26 \end{bmatrix}^{\mathrm{T}}. \tag{2.42}$$

To find the probability of the 2^{nd} bit being zero, then Equation (2.39) is evaluated, where $\boldsymbol{\Gamma}^*_2$ is,

$$\boldsymbol{\Gamma}^*_2 = \begin{bmatrix} 0.5 & 0 \\ 0 & 0.5 \end{bmatrix}. \tag{2.43}$$

The allowed paths are highlighted in Figure 2.15. Substituting in Equation (2.39),

$$P\left(m_2 = 0 \middle| \mathbf{y}\right) = \frac{0.19}{0.256} = 0.742\,. \tag{2.44}$$

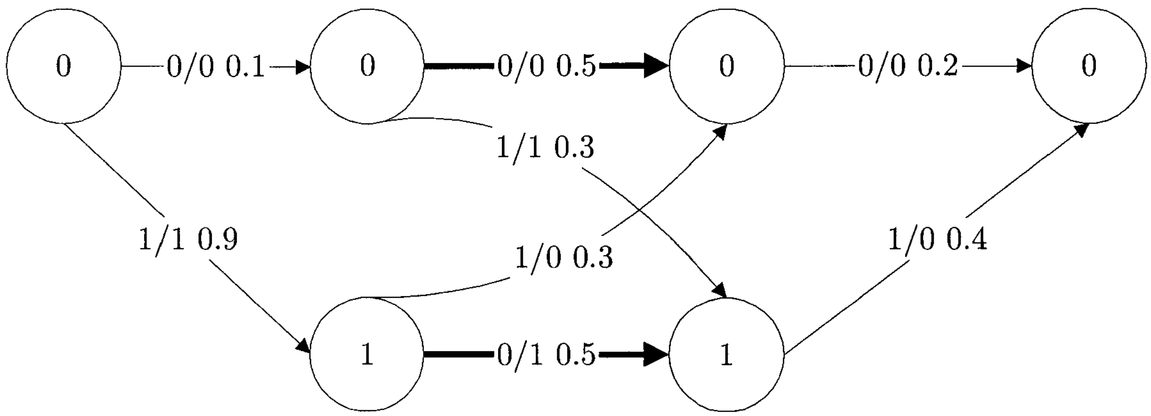

Figure 2.15: The trellis diagram illustrating the BCJR algorithm

2.4.4 Implementation of the SOVA Decoder

Soft Output Viterbi Algorithm (SOVA) decoder is a variation of the Viterbi or the minimum distance decoder, but it also outputs reliability values as well as the hard decision outputs. SOVA was initially proposed in 1989 [20], however, the algorithm only considered the most likely path for the computation of the reliability values. Hence, the performance of this version of SOVA in a turbo decoder was about 0.7 dB worse than using a BCJR decoder. In 1997, a computationally efficient implementation of SOVA involved applying the Viterbi Algorithm bi-directionally [21]. In this implementation, it was possible to consider all paths in the computation of the reliability values, hence allowing the performance to be within 0.3 dB of the BCJR decoder. This section will focus on this implementation of SOVA. Similar data structures as those defined in the BCJR decoder are used here, i.e., $\boldsymbol{\Gamma}$, $\boldsymbol{\alpha}$, $\boldsymbol{\beta}$. However, the distance matrix, $\mathbf{D}$, will replace the trellis edge weight matrix, $\boldsymbol{\Gamma}$,

$$\mathbf{D} = -\ln(\boldsymbol{\Gamma})\,. \tag{2.45}$$

The forward metrics can be calculated using Equation (2.46),

$$\boldsymbol{\alpha}_w = \min_{\substack{\text{along}\\\text{each}\\\text{column}}} \left(\left[\boldsymbol{\alpha}_{w-1} \overset{L \text{ times}}{\cdots} \boldsymbol{\alpha}_{w-1} \right] + \mathbf{D}_{w-1} \right), w = 1 \ldots N, \tag{2.46}$$

where $\boldsymbol{\alpha}_0$ is initialized to $[0, \infty \ldots \infty]^{\mathrm{T}}$ ($(L - 1)$ infinities). To find the backward metrics, each stage matrix is transposed, $\boldsymbol{\Gamma}_w$, $w = 1 \ldots N$ and their orders are reversed,

$$\boldsymbol{\Gamma}_{\text{back}} = \left[\boldsymbol{\Gamma}_N^{\mathrm{T}} \middle| \boldsymbol{\Gamma}_{N\text{-}1}^{\mathrm{T}} \middle| \cdots \middle| \boldsymbol{\Gamma}_1^{\mathrm{T}} \right]. \tag{2.47}$$

Similarly the backward metrics are given by,

$$\boldsymbol{\beta}_{w-1} = \min_{\substack{\text{along}\\\text{each}\\\text{column}}} \left(\left[\boldsymbol{\beta}_w \overset{L \text{ times}}{\cdots} \boldsymbol{\beta}_w \right] + \mathbf{D}_{\text{back } w} \right), w = N \ldots 1, \tag{2.48}$$

where $\mathbf{D}_{\text{back}} = -\ln(\boldsymbol{\Gamma}_{\text{back}})$ and $\boldsymbol{\beta}_N$ is $[0, \infty \ldots \infty]^{\mathrm{T}}$ ($(L - 1)$ infinities).

To find the reliability values on each bit, Δ_w, the distance matrix, $\mathbf{D}_w$, needs to be modified. Specifically, the distance matrix is altered so that the smallest path metric in the stage that has a different message bit (in the w-th position) can be found. Intuitively, this means that the confidence in the w-th decoded bit is proportional to how close the closest neighbouring message point is (who is different in the w-th position). Equation (2.49) expresses this concept mathematically,

$$\Delta_w = \min\left(\boldsymbol{\alpha}_w + \mathbf{D}_w^* + \boldsymbol{\beta}_w \right) - \textit{shortest}, \tag{2.49}$$

where *shortest* is the path metric of the decoded message. The function, min in Equation (2.49) will find the smallest element in the matrix. The difference between $\mathbf{D}_w^*$ and $\mathbf{D}_w$ is that the edges, which correspond to the same message bit as the decoded message, are set to infinity, and all other distances are kept finite. As in the BCJR decoder, the soft decisions are the probabilities on the decoded bits. These probabilities are given by [20],

$$P\left(m_w = \hat{m}_w \middle| \mathbf{y} \right) = \frac{e^{\Delta_w}}{1 + e^{\Delta_w}}. \tag{2.50}$$

Example 3 illustrates the SOVA algorithm using the same trellis as in Example 2.

Example 3

Once again, consider the same trellis,

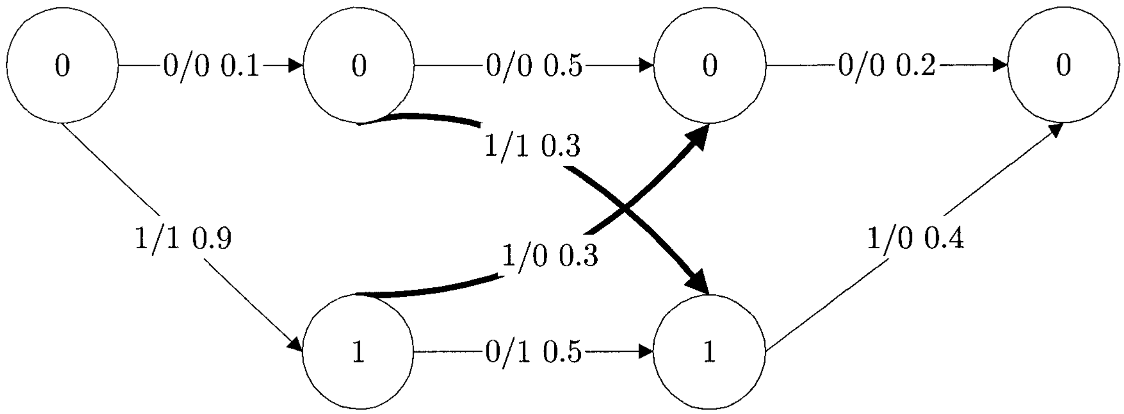

Figure 2.16: The trellis diagram illustrating the SOVA algorithm

The distance matrices are

$$\mathbf{D} = \left[\begin{array}{cc|cc|cc} 2.302 & 0.105 & 0.693 & 1.204 & 1.609 & \infty \\ \infty & \infty & 1.204 & 0.693 & 0.916 & \infty \end{array}\right]$$

$$\mathbf{D}_{\text{back}} = \left[\begin{array}{cc|cc|cc} 1.609 & 0.916 & 0.693 & 1.204 & 2.302 & \infty \\ \infty & \infty & 1.204 & 0.693 & 0.105 & \infty \end{array}\right] \quad . \tag{2.51}$$

The support quantities can be found by applying the Viterbi algorithm to the above trellis,

$$\boldsymbol{\alpha} = \left[\begin{array}{c|c|c} 2.302 & 1.309 & 1.714 \\ 0.105 & 0.798 & \infty \end{array}\right]$$

$$\boldsymbol{\beta} = \left[\begin{array}{c|c|c} 1.609 & 2.120 & 1.714 \\ 0.916 & 0.916 & \infty \end{array}\right] \quad . \tag{2.52}$$

The decoded message is '101' and the path metric for this decoded message is (shortest =) 1.714. To find Δ_2, $\boldsymbol{D}_2$ *must be modified,*

$$\mathbf{D}^*_2 = \begin{bmatrix} \infty & 1.204 \\ 1.204 & \infty \end{bmatrix}. \tag{2.53}$$

The finite path edges are highlighted in Figure 2.16. Substituting this into (2.49),

$$\begin{aligned} \Delta_2 &= \min\left(\begin{bmatrix} 1.309 & 1.309 \\ 0.798 & 0.798 \end{bmatrix} + \begin{bmatrix} \infty & 1.204 \\ 1.204 & \infty \end{bmatrix} + \begin{bmatrix} 2.120 & 2.120 \\ 0.916 & 0.916 \end{bmatrix} \right) - 1.714 \\ &= \min\left(\begin{bmatrix} \infty & 4.633 \\ 2.918 & \infty \end{bmatrix} \right) - 1.714 \\ &= 1.204 \end{aligned} \tag{2.54}$$

The corresponding probability is,

$$P\left(m_2 = 0 \middle| \mathbf{y}\right) = \frac{e^{1.204}}{1 + e^{1.204}} = 0.769\,, \tag{2.55}$$

which is close to the BCJR decoder output of 0.742.

2.4.5 Soft Decision Block Equalization

This section will consider channel equalization as an example of decoding of block encoders. Conventionally an equalizer is a filter that accepts a soft input and produces a hard output. Alternatively, a soft decision equalizer accepts soft inputs and produces soft outputs, i.e., the probabilities on the input symbols. As stated in section 2.3.4, the outputs of a MIMO channel do not have any memory and are only dependent on the present input. Hence the equalizer will not require graph based techniques to evaluate $P(\mathbf{m}|\mathbf{y})$. Instead, the probability of the input symbol is found by appropriately summing the probabilities on the output symbols. In this case, the message $\mathbf{m}$ is the transmitted symbol, the coded symbol is $\mathbf{Hs}$ and $\mathbf{r}$ is the received sequence, where it is assumed that the receiver has perfect channel state information. Let a general realization of the channel matrix for a 2 transmit / 2 receive antenna be given by,

$$\mathbf{H} = \begin{bmatrix} a_{11} & a_{12} \\ a_{21} & a_{22} \end{bmatrix}. \tag{2.56}$$

Then the four possible outputs, given the inputs are shown in Table 2.

Table 2: The outputs of the fading channel (noiseless)

s	Hs
$(-1, -1)^T$	$(-a_{11}-a_{12}, -a_{21}-a_{22})^T$
$(1, -1)^T$	$(a_{11}-a_{12}, a_{21}-a_{22})^T$
$(-1, 1)^T$	$(-a_{11}+a_{12}, -a_{21}+a_{22})^T$
$(1, 1)^T$	$(a_{11}+a_{12}, a_{21}+a_{22})^T$

The soft decision equalizer is at the front end of the receiver, where it receives a noisy version of the signals in Table 2. It calculates the probabilities of these symbols, which is a multivariable Gaussian as shown in Equation (2.57),

$$P\left[\mathbf{r}\,|\mathbf{Hs}\right] = \frac{1}{\left(\sqrt{2\pi}\sigma\right)^{n_R}} e^{-\frac{\|r-\mathbf{Hs}\|^2}{2\sigma^2}}. \tag{2.57}$$

The probability that the first transmitted BPSK symbol is a –1 given the output of the quasi-static Rayleigh faded channel is

$$P\left[\mathrm{s}_1 = -1\middle|\mathbf{r}\right] = \frac{1}{P[\mathbf{r}]}\begin{pmatrix} P\left[\mathbf{r}\middle|\mathbf{Hs} = \left(-a_{11} - a_{12}, -a_{21} - a_{22}\right)^T\right] P[\mathbf{Hs}] \\ +P\left[\mathbf{r}\middle|\mathbf{Hs} = \left(-a_{11} + a_{12}, -a_{21} + a_{22}\right)^T\right] P[\mathbf{Hs}] \end{pmatrix}, \tag{2.58}$$

where the channel was assumed to be a one to one mapping. The terms, $P[\mathbf{r}]$ and $P[\mathbf{Hs}]$ can be ignored in the calculation of the probabilities as they are constants. The probabilities from Equation (2.58) are assumed to be the channel observations and can be fed to a subsequent soft input channel decoder.

2.5 Concatenated Encoders and Turbo Decoding

This section will introduce the concept of turbo encoding and decoding, while turbo equalization will also be discussed. In the latter, a soft decision equalizer is moved into an iterative loop with the turbo decoder to improve the overall system performance.

2.5.1 The Parallel Concatenated Encoder

Figure 2.17 and Figure 2.18 illustrate a rate 1/3 and 1/5 parallel concatenated encoder, respectively. A parallel concatenated encoder is composed of two primary components: constituent encoders and interleavers. The constituent encoders are usually identical and the interleavers (denoted π_1, π_2, etc.) permute the data sequence in some predetermined manner.

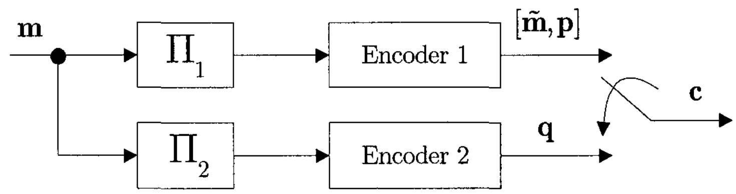

Figure 2.17: The block diagram of a rate 1/3 parallel concatenated encoder

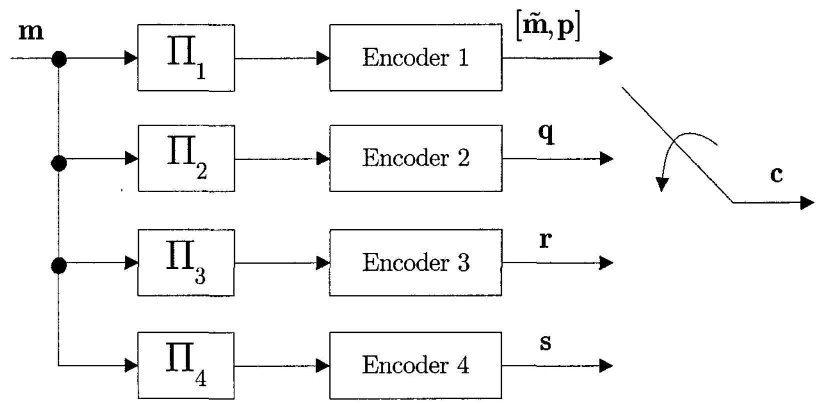

Figure 2.18: The block diagram of a rate 1/5 parallel concatenated encoder

In reference to Figure 2.17, $\tilde{\mathbf{m}}$ is the interleaved version of the message and the parity output vectors are given by $\mathbf{p}$ and $\mathbf{q}$. A concatenated code, which uses multiple encoders joined via interleaving, can increase the free distance over a non-interleaved counterpart [24]. Also the choice of the constituent encoders has a large impact on this free distance. The recursive and non-recursive codes that were considered in section 2.3.2 have the same minimum free distance and hence have the same first error event probability [1]. However these two codes when used in the context of a concatenated encoding scheme have significantly different performances. Regardless of the type of interleaver used, the non-recursive encoders produce low weight codewords for low weight messages. Therefore, the free distance of the concatenated code is limited in this case. However, when a single '1' is fed into a RSC, the encoder will enter a state other than the all zero state and not return to the zero state for as long as the encoder will run. Therefore, a packet with a single '1' will have a high weight codeword and is no longer a limiting case on the free distance of the parallel concatenated encoder. Hence using a RSC constituent encoder will result in an increased minimum distance, and better performance. As a final note, a systematic constituent encoder is preferred to a non-systematic one, as the message bits in the codewords (the systematic part) provide a good starting point for the turbo decoder.

Although a RSC encoder may be used, there is still a chance of a low weight codeword occurring in both branches of the parallel concatenated encoder. Therefore to ensure high weight outputs of the concatenated code, the interleaver should ensure that low weight encodings of one permutation coincide with the high weight encodings of the other branch. Clearly, a system having a larger interleaver will have a larger d_{min} (and better performance) than a smaller interleaver. Apart from the interleaving shown in Figure 2.18, a second block of interleaving may be added to prevent burst errors due to the channel as shown in Figure 2.19. After multiplexing the output of the encoder, it can be modulated and transmitted on the channel (not shown).

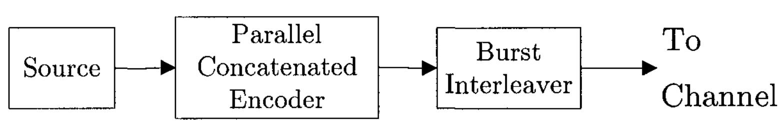

Figure 2.19: The schematic block diagram of a SISO transmitter showing the burst interleaver

2.5.2 The Iterative Turbo Decoder

The block diagram of the turbo decoder for a parallel-concatenated code is shown in Figure 2.20 where $\mathbf{r}$ is the received vector from the channel and $\mathbf{y}_1$ and $\mathbf{y}_2$ are the noisy version of $[\tilde{\mathbf{m}}\,\mathbf{p}]$ and $\mathbf{q}$, respectively. It is assumed that the appropriate deinterleaving / interleaving are the front and back ends of each decoder.

The equations for the turbo decoder can be written as

$$\begin{aligned} \mathbf{x}_2^{\mathrm{i}} &= \varphi_2\left(\mathbf{y}_2, \mathbf{x}_1^{\mathrm{i-1}}\right) - \mathbf{x}_1^{\mathrm{i-1}} \\ \mathbf{x}_1^{\mathrm{i}} &= \varphi_1\left(\mathbf{y}_1, \mathbf{x}_2^{\mathrm{i}}\right) - \mathbf{x}_2^{\mathrm{i}} \end{aligned}, \tag{2.59}$$

where φ is the soft decision decoder (i.e., BCJR or SOVA) and $\mathbf{x}_{\mathrm{j}}^{\mathrm{i}}$ is the extrinsic information at decoder j in iteration i. As can be seen in Equation (2.59), the turbo decoder consists of constituent decoders functionally iterating over the received sequence. The initial condition is chosen to be $\mathbf{x}_1^0 = \mathbf{0}$. The vectors of extrinsic information, are treated as if they contain independent probabilities on the message bits, $\mathbf{m}$ ($\mathbf{x}_{\mathrm{j}}^{\mathrm{i}}$ is treated as an independent Gaussian random variable with a mean (½…½) (N elements as $k = 1$) and an identity covariance matrix).

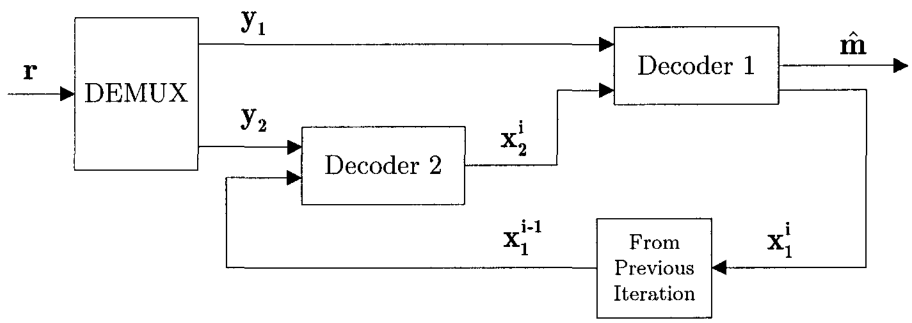

Figure 2.20: The block diagram illustrating the turbo-decoding algorithm

In section 2.4.3 and section 2.4.4, the aposteriori probability was conditioned only on the received sequence $\mathbf{y}$. In the turbo decoder, the aposteriori probability must be conditioned on both the received sequence and the extrinsic information

$$P\left(\mathbf{m}|\,\mathbf{y}_2,\mathbf{x}_1^{\mathrm{i-1}}\right)=\frac{P(\mathbf{y}_2|\mathbf{c})P\left(\mathbf{x}_1^{\mathrm{i-1}}|\mathbf{m}\right)}{P\left(\mathbf{y}_2,\mathbf{x}_1^{\mathrm{i-1}}\right)}$$
$$=\frac{\left(\prod_{j=1}^{n}P\left(y_{2j}|c_j\right)\right)\left(P\left(\mathbf{x}_1^{\mathrm{i-1}}|\mathbf{m}\right)\right)}{P\left(\mathbf{y}_2,\mathbf{x}_1^{\mathrm{i-1}}\right)}. \tag{2.60}$$

Therefore, the trellis edge weights that are used in the BCJR and SOVA decoders are redefined as,

$$\gamma\left(e_w\right)=P\left(x_{1w}^{i-1}\middle|m_w=l_I\left(e_w\right)\right)\prod_{j=1}^{n}P\left(y_{2jw}\middle|c_{jw}=l_O\left(e_w\right)\right) \tag{2.61}$$

and $P\left(\mathbf{m}|\,\mathbf{y}_2,\mathbf{x}_1^{\mathrm{i-1}}\right)$ replaces $P(\mathbf{m}|\mathbf{y})$ in equation (2.32). With these new definitions the probabilities can be calculated using BCJR or SOVA algorithms. After computing the aposteriori probabilities, the following array of probabilities must be evaluated,

$$\begin{bmatrix}P\left(m_1=0|\mathbf{y}\right)\\P\left(m_1=1|\mathbf{y}\right)\end{bmatrix}\cdots\begin{bmatrix}P\left(m_N=0|\mathbf{y}\right)\\P\left(m_N=1|\mathbf{y}\right)\end{bmatrix}. \tag{2.62}$$

This array is the output of φ_k and to find the extrinsic information, the array of the current decoder must be divided by the array calculated by the previous decoder, as depicted by the log domain equation in Equation (2.59). The hard decision outputs are given by the maximum in each column of Equation (2.62).

The corresponding equations describing a system with four constituent decoders are given by,

$$\begin{aligned}
\mathbf{x}_4^{\mathrm{i}}&=\varphi_4\left(\mathbf{y}_4,\mathbf{x}_3^{\mathrm{i-1}},\mathbf{x}_2^{\mathrm{i-1}},\mathbf{x}_1^{\mathrm{i-1}}\right)-\mathbf{x}_3^{\mathrm{i-1}}-\mathbf{x}_2^{\mathrm{i-1}}-\mathbf{x}_1^{\mathrm{i-1}}\\
\mathbf{x}_3^{\mathrm{i}}&=\varphi_3\left(\mathbf{y}_3,\mathbf{x}_4^{\mathrm{i}},\mathbf{x}_2^{\mathrm{i-1}},\mathbf{x}_1^{\mathrm{i-1}}\right)-\mathbf{x}_4^{\mathrm{i}}-\mathbf{x}_2^{\mathrm{i-1}}-\mathbf{x}_1^{\mathrm{i-1}}\\
\mathbf{x}_2^{\mathrm{i}}&=\varphi_2\left(\mathbf{y}_2,\mathbf{x}_4^{\mathrm{i}},\mathbf{x}_3^{\mathrm{i}},\mathbf{x}_1^{\mathrm{i-1}}\right)-\mathbf{x}_4^{\mathrm{i}}-\mathbf{x}_3^{\mathrm{i}}-\mathbf{x}_1^{\mathrm{i-1}}\\
\mathbf{x}_1^{\mathrm{i}}&=\varphi_1\left(\mathbf{y}_1,\mathbf{x}_4^{\mathrm{i}},\mathbf{x}_3^{\mathrm{i}},\mathbf{x}_2^{\mathrm{i}}\right)-\mathbf{x}_4^{\mathrm{i}}-\mathbf{x}_3^{\mathrm{i}}-\mathbf{x}_2^{\mathrm{i}}
\end{aligned}, \tag{2.63}$$

where the decoded message is found by hard thresholding $\mathbf{x}_1^{\mathrm{i}}$. As can be seen in Equation (2.63), in every iteration, each constituent decoder uses all the available extrinsic information. The block diagram of the parallel concatenated decoder using four constituent decoders is shown in Figure 2.21.

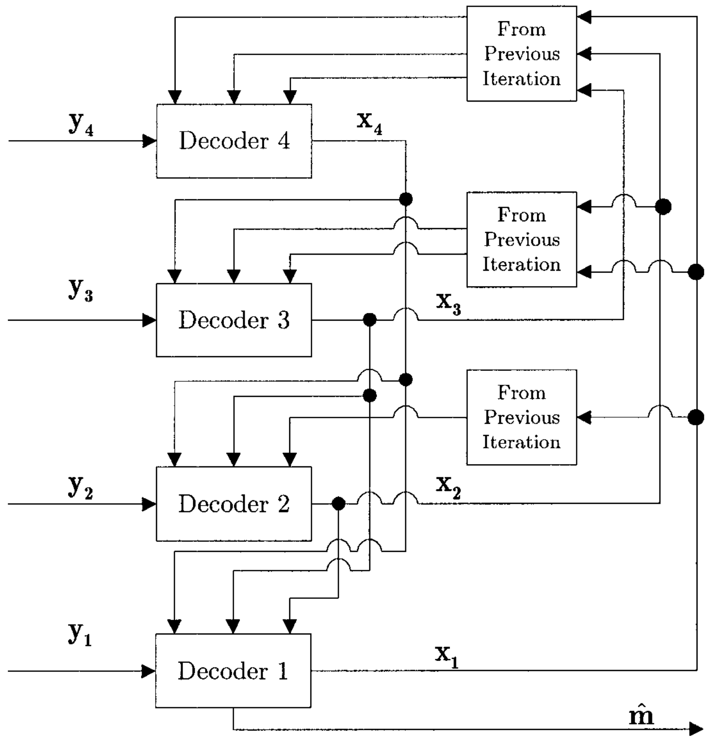

Figure 2.21: The block diagram of the turbo decoder using four constituent decoders

The interleaver that is between the encoded streams in Figure 2.17 prevents the construction of a joint trellis at the receiver. Hence the iterative turbo decoder is sub-optimal, as it does not necessarily choose the most likely sequence or bit values for a received codeword.

2.5.3 Turbo Equalization

Since the quasi-static fading channel can be treated as a block encoder, the receiver can consider it as a serially concatenated with the parallel concatenated encoder. Raphaeli first proposed turbo equalization in 1998 [25], where the equalizer was moved into the iterative decoding loop, which resulted in a significant performance improvement [26]. Unlike the constituent decoders in the iterative loop, which exchange extrinsic information on the message bits, information on the codewords needs to be exchanged. The equations which describe this operation for the $n_R = 2$ antenna system is given by,

$$\begin{aligned}
&\mathbf{w}^{i} = \phi\left(\mathbf{r}, \mathbf{w}^{i\text{-}1}\right) - \mathbf{w}^{i\text{-}1} \\
&\text{Demux } \mathbf{w}^{i} \text{ to form } \mathbf{y}_1 \text{ and } \mathbf{y}_2 \\
&\mathbf{x}_2^{i} = \varphi_2\left(\mathbf{y}_2, \mathbf{x}_1^{i\text{-}1}\right) - \mathbf{x}_1^{i\text{-}1} \\
&\mathbf{z}_2^{i} = \varphi_2\left(\mathbf{y}_2, \mathbf{z}_1^{i\text{-}1}\right) - \mathbf{z}_1^{i\text{-}1} \\
&\mathbf{x}_1^{i} = \varphi_1\left(\mathbf{y}_1, \mathbf{x}_2^{i}\right) - \mathbf{x}_2^{i} \\
&\mathbf{z}_1^{i} = \varphi_1\left(\mathbf{y}_1, \mathbf{z}_2^{i}\right) - \mathbf{z}_2^{i} \\
&\text{Mux } \mathbf{z}_1^{i} \text{ and } \mathbf{z}_2^{i} \text{ to form } \mathbf{w}^{i\text{-}1}
\end{aligned} \quad . \tag{2.64}$$

In Equation (2.64), the operation of the soft decision equalizer is depicted by ϕ. The symbols $\mathbf{z}_1^i$ and $\mathbf{z}_2^i$ are the log-likelihoods on the codeword bits corresponding to the message bits ($\mathbf{x}_1^i$ and $\mathbf{x}_2^i$). Although each of the constituent decoders is repeated twice, the log-likelihoods on codeword and message bits are calculated in one pass. The block diagram of the combined receiver is shown in Figure 2.22.

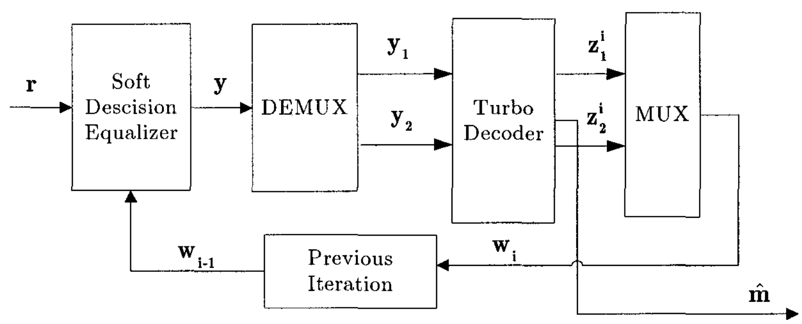

Figure 2.22: The schematic block diagram of the turbo equalizer for a SISO system

2.6 Chapter Summary

This chapter focused on reviewing concepts that are fundamental in the area of communications and the particular topic of turbo codes.

The multipath-fading model, which is based on field observations, was shown to be mathematically tractable using a Rayleigh distributed fading parameter. This mathematical model was then extended to a MIMO channel. The capacities of various channels were then discussed. In particular the capacity equations for a fixed and variable MIMO channel were studied.

Using the channel and FSM encoders as examples, the encoding and decoding processes for the block and graph (trellis) based techniques were discussed. Block decoding was illustrated by equalizing (i.e., 'decoding') the channel. An introduction to graph theory was provided to describe the algorithmic implementation of the maximum likelihood decoder and two soft decision trellis decoders.

Finally these encoders and decoders were combined into the structure of a parallel concatenated encoder and turbo decoder. Furthermore, it was shown that by moving the soft decision equalizer into the iterative loop, turbo equalization can be performed.

Chapter 3 A Review of Coded Space-Time Processing

In a typical urban environment where a fixed base station communicates with a mobile terminal, a line of sight (LOS) path rarely exists. Hence, the received signal will consist of a weighted sum of delayed versions of the transmitted signal. The resulting amplitude variation in the received signal is known as fading. Diversity schemes have been shown as an effective means to combat fading. These methods require a number of signal branches, all carrying the same message but having independent fading statistics. The success of diversity techniques depends on the degree to which the signals on the different branches are uncorrelated. Space-time coding schemes combine spatial diversity with channel coding and (or) equalization. In this chapter, previous work in the field of space-time coding will be discussed, starting with the Bell Labs layered space-time architecture prototype. Following this, space-time trellis codes and space-time block codes will be considered. Finally this chapter will conclude with a discussion of antenna diversity, which make use of turbo codes and iterative processing techniques.

3.1 Layered Space-Time Architecture

Foschini *et al.* [27] investigated the capacity of MIMO channels and have shown that the capacity of the channel grows linearly with the number of transmit and receive antennas where the total transmit power is the same as the corresponding SISO case. This framework has led to the vertical BLAST (Bell Laboratories Layered Space Time) or V-BLAST system, which has a high rate of transmission in indoor environments [28]. The block diagram of a V-BLAST system is shown in Figure 3.1.

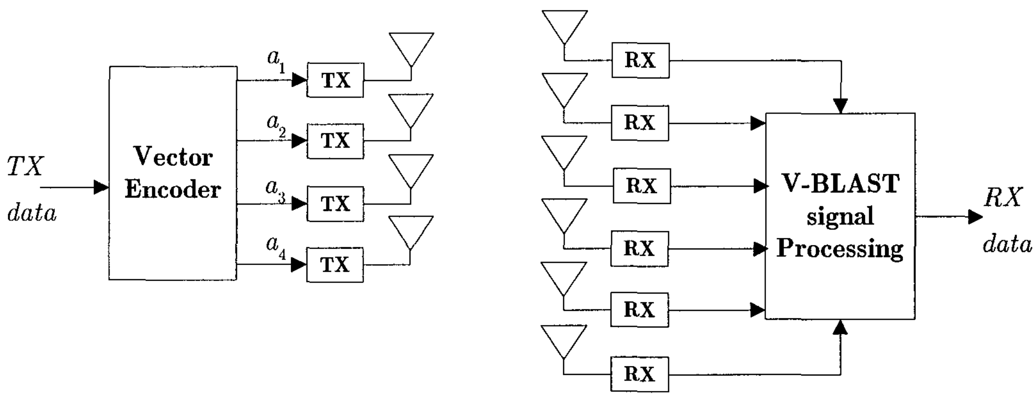

Figure 3.1: The schematic block diagram of the V-BLAST system (courtesy of [13])

Each stream is encoded using a 1 D encoder, where the input data can be read out in a vertical or diagonal direction. The diagonal BLAST (D-BLAST) system performs better than the V-BLAST system, however, coding constraints, and a higher decoder complexity prevent it from being used [28]. The V-BLAST system achieves lower capacity than the diagonal system, however the lower encoder and decoder complexity make it very attractive from an implementation perspective [28]. The V-BLAST transmission architecture is shown in Figure 3.2.

Each encoded stream is QAM modulated and transmitted from n_T transmitters. The power of the transmitted symbol is proportional to $1/n_T$ so that the total radiated power is constant and independent of n_T [28]. The receiver consists of n_R receivers ($n_R \geq n_T$), whose outputs are fed to a V-BLAST decoder. The vector decoding process is simply a demultiplexing operation followed by a bit to symbol mapping.

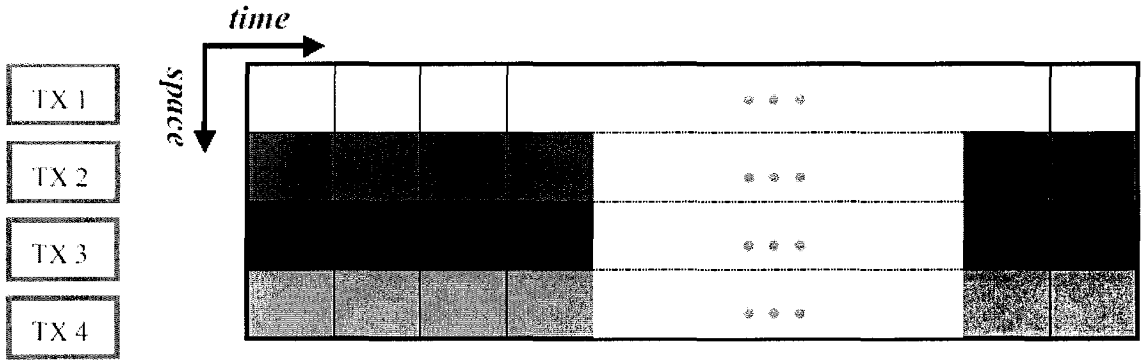

Figure 3.2: The V-BLAST transmission architecture (courtesy of [51])

There are 3 main differences of the V-BLAST system over traditional multi-access techniques. Unlike CDMA, the V-BLAST system does not require a large channel bandwidth; it only requires a small fraction in excess of the symbol rate – similar to conventional QAM systems. Unlike FDMA, the transmitted symbol occupies the entire system bandwidth and unlike TDMA, the entire system bandwidth is used simultaneously. Taken together, these differences account for the high spectral efficiencies that V-BLAST is able to achieve [28].

The detection process of the vector of transmitted symbols will now be considered. It shall be assumed that the receiver has symbol synchronous sampling and ideal timing. Let $\mathbf{a}^1 = \left[a_1^1, a_2^1, \ldots, a_{n_T}^1\right]^{\mathrm{T}}$ denote the vector of transmitted symbols, then the corresponding received n_R vector at the first time instant is given by,

$$\mathbf{r}_{(1)}^1 = \mathbf{H}\mathbf{a}^1 + \mathbf{z}\,, \tag{3.1}$$

where $\mathbf{z}$ is the additive white Gaussian noise. The detection algorithm produces the decision statistics: $y_1^1 \ldots y_{n_T}^1$ from $\mathbf{r}_{(1)}^1$. Quantizing y_k^1, $k = 1\ldots\ n_T$ will produce the data symbols. The detection process uses linear combinatorial nulling and symbol cancellation to successively compute y_k^1 [29]. It was shown in [28] that the optimal order to find these decision statistics is in the order of highest SNR to the lowest SNR. Without loss of generality, y_1^1 will correspond to the most confident decision statistic and $y_{n_T}^1$ corresponds to the least confident (based on SNR). The procedure to calculate the decoded symbols $\hat{a}_k^1$ is shown in [29] and is summarised here:

Step 1: Using the nulling vector, $\mathbf{w}_1^1$, form a linear combination of the components of $\mathbf{r}_{(1)}^1$, to yield y_1^1

$$y_1^1 = \left(\mathbf{w}_1^1\right)^{\mathrm{T}} \mathbf{r}_{(1)}^1. \tag{3.2}$$

Step 2: y_1^1 is then quantized to obtain $\hat{a}_1^1$:

$$\hat{a}_1^1 = Q\left(y_1^1\right), \tag{3.3}$$

where Q(·) denotes a thresholding operation appropriate to the constellation that is used.

Step 3: Assuming that $\hat{a}_1^1 = a_1^1$, $\hat{a}_1^1$ is subtracted from the received vector $\mathbf{r}_{(1)}^1$, resulting in the modified received vector $\mathbf{r}_{(2)}^1$,

$$\mathbf{r}_{(2)}^1 = \mathbf{r}_{(1)}^1 - \hat{a}_1^1 (\mathbf{H})_1, \tag{3.4}$$

where $(\mathbf{H})_1$ denotes the 1st column of **H**. Steps 1-3 are repeated for antennas 2 to n_T by operating on the modified received vectors $\mathbf{r}_{(2)}^1$ to $\mathbf{r}_{(\mathbf{n}_T)}^1$. The nulling vector that is used in the above procedure is found using the MMSE or the zero forcing criterions. The above procedure is very similar to the operation of the decision feedback equalizer [28]. As in the DFE, if the detector makes an error on $\hat{a}_k^w$, the remaining $\hat{a}_{k+1}^w$ to $\hat{a}_{n_T}^w$ could be in error (error propagation). Hence, the reason for the ordering is that the detector would be most confident (correct) in detecting the bit with the highest SNR, which results in a smaller probability of error propagation. Figure 3.3 shows the results obtained using a V-BLAST setup where $n_T = 8$ transmitters, $n_R = 12$ receivers and the above ordering scheme. Since each block consists of 8×100 symbols (4 bits /symbol), the system reaches 10^{-5} at a channel SNR (P/σ^2) of 23.8 dB or an E_b/N_0 value of 6.8 dB. The system was operated at a carrier frequency of 1.9 GHz and a bandwidth of 30 kHz. Uncoded 16 QAM at each transmitter yields a raw spectral efficiency of 25.9 bits/s/Hz [29].

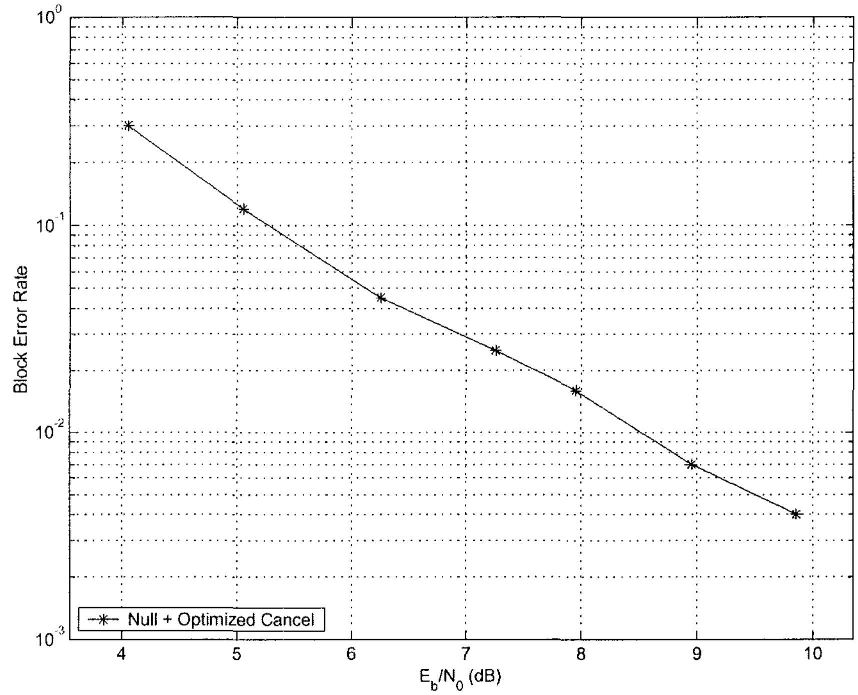

Figure 3.3: Performance of the V-BLAST system with 16 QAM, $n_T = 8$, $n_R = 12$ and 25.9 bps/Hz (courtesy of [29])

3.2 Space-time Trellis Codes

Tarokh *et al.* originally proposed Space-Time Trellis Codes (STTC) [9], which combines channel coding and symbol mapping onto multiple transmit antennas. The STTC scheme achieves the same diversity advantage as the Maximal Ratio Receive Combining (MRRC) technique. The system diagram is shown in Figure 3.4.

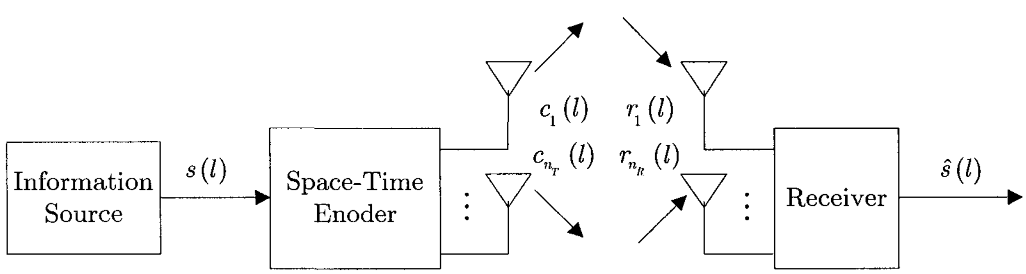

Figure 3.4: The schematic block diagram of the space-time trellis code system (courtesy of [42])

There are two criterions, which drive the construction of the code: the rank and determinant criterions. In [9], Tarokh *et al.* considered the probability that the receiver decides erroneously in favour of

$$\mathbf{e} = e_1^1 e_1^2 \cdots e_1^{n_T} e_2^1 e_2^2 \cdots e_2^{T} \cdots e_N^1 e_N^2 \cdots e_N^{n_T} \tag{3.5}$$

assuming that

$$\mathbf{c} = c_1^1 c_1^2 \cdots c_1^{n_T} c_2^1 c_2^2 \cdots c_2^{n_T} \cdots c_N^1 c_N^2 \cdots c_N^{n_T} \tag{3.6}$$

was transmitted, where c_t^i is the symbol transmitted from the i-th antenna at the t-th transmission time. The rank criterion states that in order to achieve maximum diversity ($n_T n_R$, where n_T and n_R is the number of transmit and receive antennas), $\mathbf{B}(\mathbf{c}, \mathbf{e})$ must be full rank for any codewords $\mathbf{c}$ and $\mathbf{e}$, where $\mathbf{B}(\mathbf{c}, \mathbf{e})$ is,

$$\mathbf{B}(\mathbf{c},\mathbf{e}) = \begin{pmatrix} e_1^1 - c_1^1 & e_2^1 - c_2^1 & \cdots & \cdots & e_N^1 - c_N^1 \\ e_1^2 - c_1^2 & e_2^2 - c_2^2 & \cdots & \cdots & e_N^2 - c_N^2 \\ e_1^3 - c_1^3 & e_2^3 - c_2^3 & \cdots & \cdots & e_N^3 - c_N^3 \\ \vdots & \vdots & \ddots & \ddots & \vdots \\ e_1^{n_T} - c_1^{n_T} & e_2^{n_T} - c_2^{n_T} & \cdots & \cdots & e_N^{n_T} - c_N^{n_T} \end{pmatrix}. \tag{3.7}$$

If $\mathbf{B}(\mathbf{c}, \mathbf{e})$ has a rank of r, then the diversity of the system is rn_R. To achieve the largest coding gain, the minimum of the n_T-th roots of the sum of the determinants of all n_T x n_T cofactors of $\mathbf{B}(\mathbf{c}, \mathrm{e})\mathbf{B}^{\dagger}(\mathbf{c}, \mathbf{e})$ must be maximized (where † is the transpose conjugate operator). These criterions translate to the following design rules for designing the space-time encoder:

- Transitions departing from the same state differ in the second symbol
- Transitions arriving at the same state differ in the first symbol

Figure 3.5 shows the 4 PSK, 4 states, 2 antenna space-time code. The edge label x_1x_2 indicates that the signal x_1 is transmitted over antenna 1 and x_2 is transmitted over antenna 2. Therefore the block diagram of the space-time encoder is as shown in Figure 3.6, where encoder 1 and 2 are finite state machines, which produce different outputs for the same input and present state.

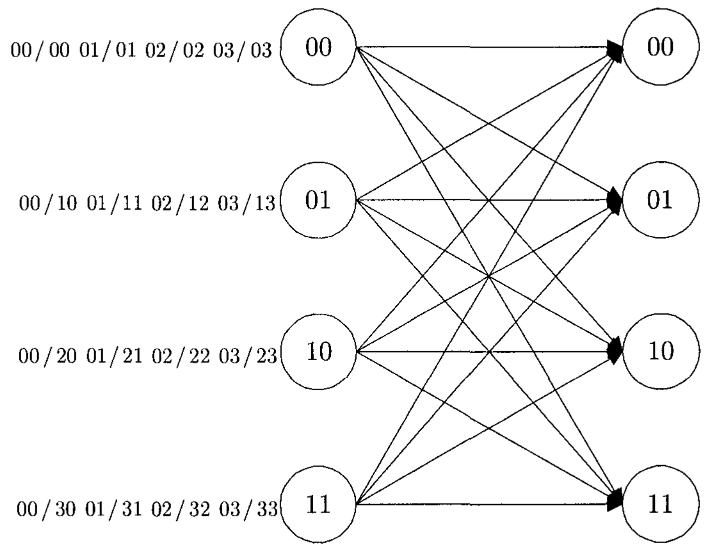

Figure 3.5: The trellis of the space-time trellis code for 4-PSK, 4 States and 2 bits/s/Hz (courtesy of [9])

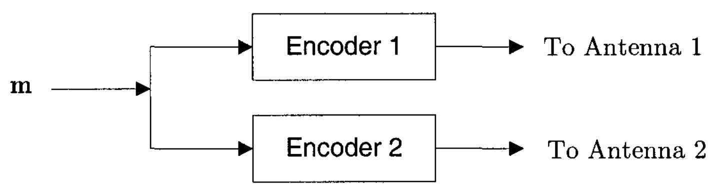

Figure 3.6: The block diagram of the space-time trellis encoder

Suppose that the code vector **c** was transmitted, and the receive vector, **r** was received,

$$\mathbf{r} = r_1^1 r_1^2 \cdots r_1^{n_R} r_2^1 r_2^2 \cdots r_2^{n_R} \cdots r_N^1 r_N^2 \cdots r_N^{n_R} . \tag{3.8}$$

Optimum decoding at the receiver implies that an **e** is chosen such that the aposteriori probability

$$P(\mathbf{e} | \mathbf{r}, \mathbf{H}(t), t = 1, \cdots, N) \tag{3.9}$$

is maximized, where $\mathbf{H}$(t) is of size n_R x n_T. Assuming that all codewords are equiprobable and that the channel is AWGN, then the optimum decoder is [9],

$$\mathbf{e} = \arg \min_{\mathbf{e}=\mathbf{e}(1),\ldots\mathbf{e}(N)} \sum_{t=1}^{N} \left\| \mathbf{r}(t) - \sqrt{E_s}\mathbf{H}(t)\mathbf{c}(t) \right\|^2 . \tag{3.10}$$

Hence, the decoder constructs a joint trellis (from the data of each antenna) and using a vector form of the Viterbi decoder, the corresponding message can be decoded. However, if the number of antennas is fixed, the decoding complexity of the space-time trellis code increases exponentially as a function of the diversity level and transmission rate [9]. The performance of an 8 PSK, 64 state space-time code over a block faded channel is shown in Figure 3.7. The path gains are assumed to be constant for 130 channel uses. There are two transmit and two receive antennas and the rate of this system is 3 bits/s/Hz. Based on the curve shown in Figure 3.7, a BER of 1.3 x 10^{-5} is reached at a channel SNR (P/σ^2) of 16.8 dB or an E_b/N_0 value of 9 dB with a frame size of 2×130 symbols (3 bits per symbol).

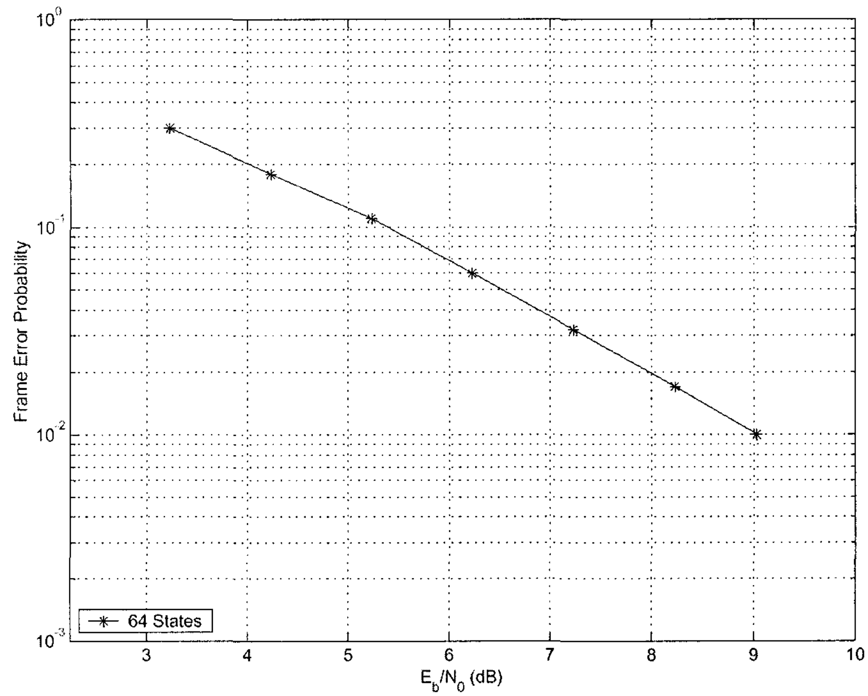

Figure 3.7: Performance of the 64 state space-time trellis coded system with 8 PSK, $n_T = 2$, $n_R = 2$ and 3 bps/Hz (courtesy of [9])

3.3 Space-time Block Codes

In the hope of reducing the exponential decoder complexity of STTC, Alamouti proposed a simple transmit diversity scheme [13], known as space-time block coding. This scheme was later generalized by Tarokh *et al.* [30], to an arbitrary number of antennas. Unlike space-time trellis codes, these codes have the property of having a simple maximum likelihood-decoding scheme at the receiver. The block diagram of the receiver for 2 transmit and 2 receive antennas is shown in Figure 3.8. A space-time block code is defined as a n x n_T matrix, G, where n is the block length of the code and n_T is the number of transmit antennas. For example, the space-time code matrix which uses 2 transmit antennas is,

$$\mathbf{G}_2 = \begin{bmatrix} s_1 & s_2 \\ -s_2^* & s_1^* \end{bmatrix}. \tag{3.11}$$

The i-th column in $\mathbf{G}_2$ is the transmitted constellation point (from the modulation scheme) on the i-th antenna and the 1st row corresponds to the symbols transmitted at time t and the elements of the 2nd row are symbols transmitted at $t+T$, where T is the symbol period. The channel transfer matrix is given by,

$$\mathbf{H} = \begin{bmatrix} h_{11} & h_{12} \\ h_{21} & h_{22} \end{bmatrix}, \tag{3.12}$$

where the elements of $\mathbf{H}$ are defined in the same way as in section 2.1.2. Assuming that the channel coherence time is greater than a block length and there are $n_R = 2$ receive antennas, the received signals at time t are given by,

$$\begin{aligned} r_1 &= h_{11}s_1 + h_{12}s_2 + z_1 \\ r_2 &= h_{21}s_1 + h_{22}s_2 + z_2 \end{aligned} \tag{3.13}$$

and the received signals at $t+T$ are

$$\begin{aligned} r_3 &= -h_{11}s_2^* + h_{12}s_1^* + z_3 \\ r_4 &= -h_{21}s_2^* + h_{22}s_1^* + z_4 \end{aligned}, \tag{3.14}$$

where z_j are the complex random variables representing the receiver thermal noise. The combiner (shown in Figure 3.8) constructs the following two signals,

$$\begin{aligned} \tilde{s}_1 &= h_{11}^*r_1 + h_{12}r_3^* + h_{21}^*r_2^* + h_{22}r_4^* \\ \tilde{s}_2 &= h_{12}^*r_1 - h_{11}r_3^* + h_{22}^*r_2 - h_{21}r_4^* \end{aligned}. \tag{3.15}$$

Expanding this set of equations (using Equation (3.13) and (3.14)),

$$\begin{aligned} \tilde{s}_1 &= \left(h_{11}^2 + h_{12}^2 + h_{21}^2 + h_{22}^2\right)s_1 + h_{11}^*z_1 + h_{21}^*z_3 + h_{12}z_2^* + h_{22}z_4^* \\ \tilde{s}_2 &= \left(h_{11}^2 + h_{12}^2 + h_{21}^2 + h_{22}^2\right)s_2 - h_{11}z_2^* - h_{21}z_4^* + h_{12}^*z_1 + h_{22}^*z_3 \end{aligned}. \tag{3.16}$$

These combined signals are fed to the ML detector. The decision criteria for choosing s_i for the signal s_1 is given by,

$$\begin{aligned}&\left(h_{11}^2+h_{12}^2+h_{21}^2+h_{22}^2\right)\left|s_i\right|^2+d^2\left(\tilde{s}_1,s_i\right)\\&\le\left(h_{11}^2+h_{12}^2+h_{21}^2+h_{22}^2\right)\left|s_k\right|^2+d^2\left(\tilde{s}_1,s_k\right),\forall i\neq k\end{aligned}, \tag{3.17}$$

where $d(\cdot)$ is the Euclidean distance. Similarly, the detector chooses s_i for the signal s_2 when Equation (3.18) is satisfied [13],

$$\begin{aligned}&\left(h_{11}^2+h_{12}^2+h_{21}^2+h_{22}^2\right)\left|s_i\right|^2+d^2\left(\tilde{s}_2,s_i\right)\\&\le\left(h_{11}^2+h_{12}^2+h_{21}^2+h_{22}^2\right)\left|s_k\right|^2+d^2\left(\tilde{s}_2,s_k\right),\forall i\neq k\end{aligned}. \tag{3.18}$$

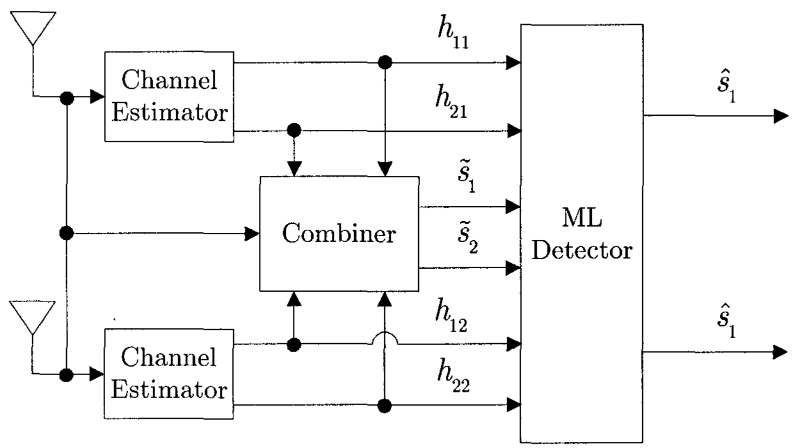

Figure 3.8: The block diagram of the receiver for the space-time block coding scheme for n_R = 2 (courtesy of [32])

It is important to note that there is no memory between consecutive blocks and the block length is typically very short (a maximum of $n = 8$ was shown in [31]). To improve performance, usually a more powerful code such as the Reed-Solomon [32] or turbo codes are concatenated with the space-time block code [33]. Further work incorporated the space-time block code in a multi-user detector, which used a MMSE interference suppression technique [32]. The performance of the space-time block code using 2 transmit / 2 receive antennas is shown in Figure 3.9. To reach a BER of 10^{-5}, a channel SNR (P/σ^2) of 9.9 dB or an E_b/N_0 value of 6.9 dB is required.

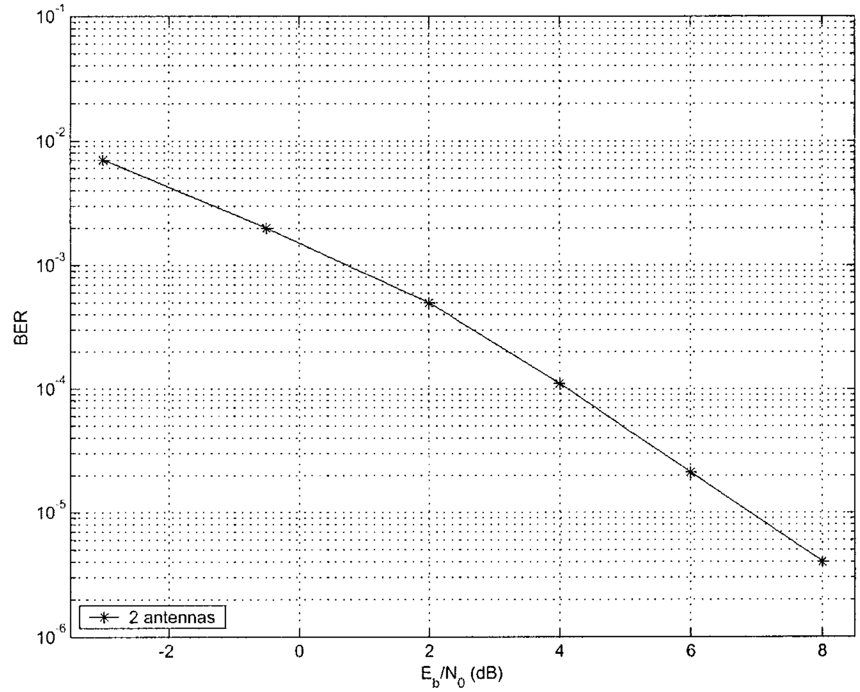

Figure 3.9: Performance of the space-time block coded system with BPSK, $n_T = 2$, $n_R = 2$ and 1 bit/s/Hz (courtesy of [13])

3.4 Turbo Coded Modulation

To improve the performance of space-time codes, Stefanov *et al.* proposed combining turbo codes with space-time coding [10]. Their system model consisted of a parallel concatenated encoder, whose outputs are punctured and then fed to a modulator, which was then transmitted on n_T antennas. The block diagram of the transmitter is shown in Figure 3.10.

The input to the modulator requires n bits for every output symbol. To reduce the correlation of adjacent bits, an interleaver is added between the parallel concatenated encoder and the modulator, so that systematic and parity bits are assigned to different modulated symbols. Also, in the event of deep fading, it distributes the burst errors evenly in the packet. The 4 PSK modulation scheme is shown in Figure 3.11.

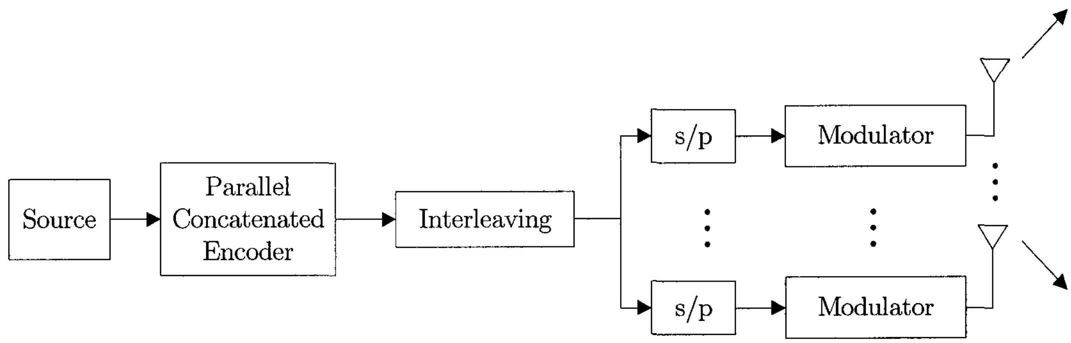

Figure 3.10: The schematic block diagram of the transmitter with a parallel concatenated encoder (courtesy of [10])

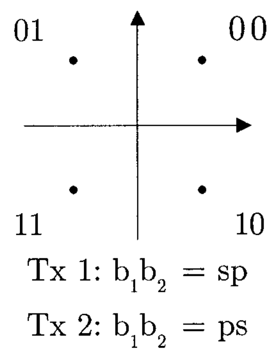

Figure 3.11: The 4 PSK modulation scheme used; s-systematic bit, p-parity bit (courtesy of [10])

The receiver computes the log-likelihood ratios using the modulated symbols from the antennas. After deinterleaving, the turbo decoder uses these log-likelihoods as if they are observations from BPSK modulation over an AWGN channel [10]. The block diagram of the receiver is shown in Figure 3.12.

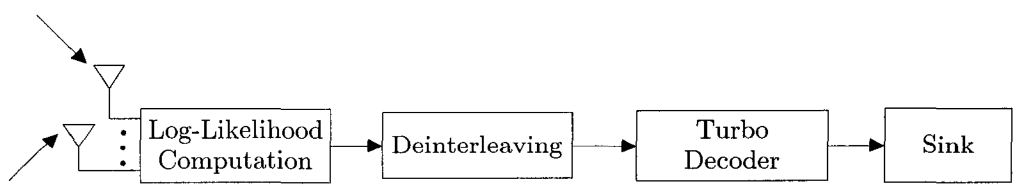

Figure 3.12: The schematic block diagram of the receiver (courtesy of [10])

The received signal at the j-th antenna is given by [10],

$$r_j = \sum_{i=1}^{n_T} \alpha_{ij} c_i + z_j \,. \tag{3.19}$$

where n_T is the number of transmit antennas, c_i are the complex symbol outputs of the modulator, which belong to the set of constellation points, $\mathcal{A} = \{c_i\}_{i=1}^{2^n}$ and z_j are modelled as independent samples of zero mean complex Gaussian random process with a variance of $N_0/2$ per dimension. Hence, the received signals, $r_1 \ldots r_{n_R}$ correspond to nn_T coded bits, $\mathbf{b}$,

$$\mathbf{b} = \left(b_1, \ldots b_n, b_{n+1}, \ldots, b_{nn_T}\right). \tag{3.20}$$

The group of bits, $b_{(i-1)n+1}, \ldots, b_{in}$ is used to select the constellation point for the i-th antenna, c_i, $i = 1, \ldots, n_T$ [10]. The log-likelihood ratio for the w-th element of $\mathbf{b}$, is given by,

$$\Lambda(b_w) = \log \frac{P\left[b_w = 1 \middle| r_1 \ldots r_{n_R}\right]}{P\left[b_w = 0 \middle| r_1 \ldots r_{n_R}\right]}, \tag{3.21}$$

which can also be written as,

$$\Lambda(b_w) = \log \frac{\sum_{\mathbf{b}:b_w=1} P\left[r_1 \ldots r_{n_R}, \mathbf{b} \text{ is transmitted}\right]}{\sum_{\mathbf{b}:b_w=0} P\left[r_1 \ldots r_{n_R}, \mathbf{b} \text{ is transmitted}\right]}. \tag{3.22}$$

Since, the modulation is a one to one mapping, $\mathbf{b}$ can be replaced with $\mathbf{c}$. By Baye's rule, the joint probability can be replaced with the conditional probability in Equation (3.22). A product of probabilities can further replace the conditional probability, as $r_1 \ldots r_{n_R}$ are independent given $\mathbf{c} = (c_1 \ldots c_{n_T})$,

$$P\left[r_1, \ldots, r_{n_R} \middle| \mathbf{c}\right] = \prod_{j=1}^{n_R} P\left[r_j \middle| \mathbf{c}\right]. \tag{3.23}$$

Hence, substituting for the noise statistics, the log-likelihood ratio of b_w becomes,

$$\Lambda(b_w) = \log \frac{\sum_{\mathbf{c}:\mathbf{c}=f(\mathbf{b}),b(w)=1} \prod_{j=1}^{n_R} \exp\left(-\frac{\left|r_j - \sum_{i=1}^{n_T} \alpha_{i,j} c_i\right|^2}{N_0}\right)}{\sum_{\mathbf{c}:\mathbf{c}=f(\mathbf{b}),b(w)=0} \prod_{j=1}^{n_R} \exp\left(-\frac{\left|r_j - \sum_{i=1}^{n_T} \alpha_{i,j} c_i\right|^2}{N_0}\right)}, \tag{3.24}$$

where $f(\cdot)$ defines the mapping from $\mathbf{b}$ to $\mathbf{c}$ and the receiver is assumed to have complete channel state information ($\alpha_{i,j}$ is known). Figure 3.13 illustrates the performance of the turbo coded modulation scheme. A block faded channel is assumed where the path gains are constant for a period of $l = 130$ channel uses. The turbo codes with an interleaver size of 5200 information bits after 10 iterations, performs 8 dB better than the corresponding 16 state space-time trellis code [10].

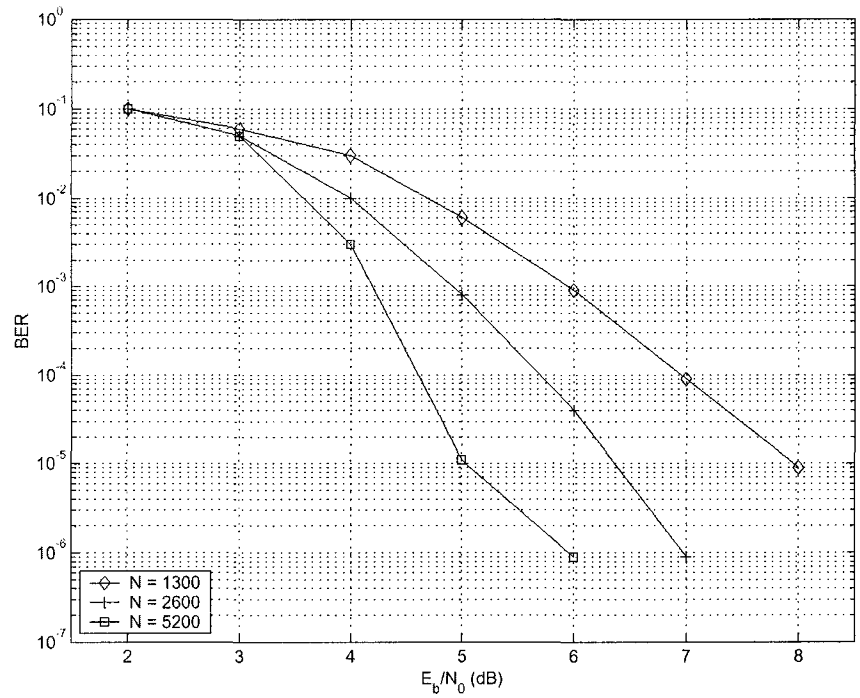

Figure 3.13: Performance of the turbo coded modulation system with 4 PSK, $n_T = 2$, $n_R = 2$, and 2 bits/s/Hz (courtesy of [10])

3.5 Turbo Space-Time Processing

Aryavistakul in [11] proposed two new coded layered space-time architectures, where he modified the structure that Foschini had suggested in [8], to accommodate iterative processing. Again, a quasi-static random Rayleigh channel model is assumed, where the fading is stationary within a data block, but statistically independent between different data blocks. The first architecture applies coding across multiple signal processing layers (LST-I, LST stands for layered space-time) and the other applies independent coding within each layer

(LST-II). The block diagram of these two systems is shown in Figure 3.14 and Figure 3.15.

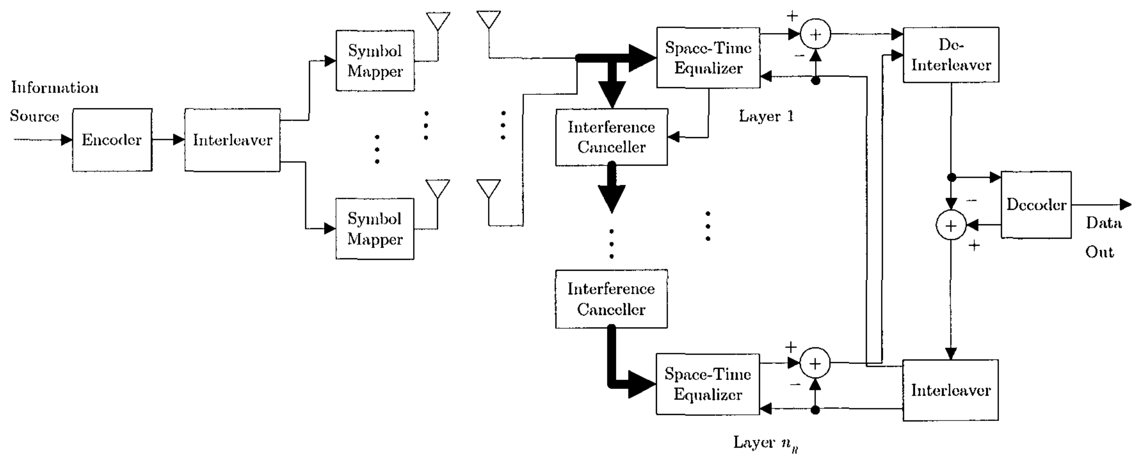

Figure 3.14: The block diagram of the LST-I architecture (courtesy of [11])

In the first system, the encoded outputs are interleaved and multiplexed onto n_T streams and modulated. At the receiver, the outputs of the n_R antennas (where n_R is assumed to be equal to n_T) are decoupled through a space-time equalizer and an interference canceller. This output is deinterleaved and the entire data block is passed to the decoder. The extrinsic information from the decoder can then be reinterleaved and passed back to the soft decision space-time equalizer, which would complete the 1[st] iteration. Using these decisions, the interference canceller can remove the effect of the 1[st] antenna.

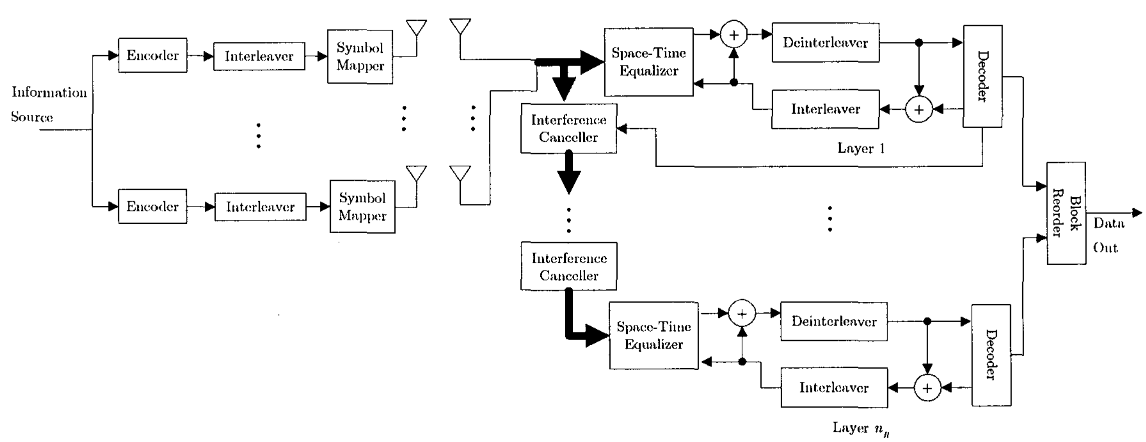

Figure 3.15: The block diagram of the LST-II architecture (courtesy of [11])

In the second approach, the information bits are divided into n_T streams and fed to n_T parallel encoders. The encoded outputs are then interleaved and modulated. At the receiver, each of the n_T streams ($n_R = n_T$) are decoupled and independently deinterleaved and decoded. The output of LST-II produces n_T information blocks at a rate of $1/n_T$ times the output rate of LST-I [11], hence preserving the overall rate. As can be seen by the above structure, the interference canceller uses the extrinsic information from the decoder, which is more reliable than the data decisions produced by the space-time equalizer.

Before a discussion on the performance of these two systems, the space-time equalizer should be considered. The block diagram of the space-time equalizer is shown in Figure 3.16. The outputs of the antennas are fed to n_R linear feedforward filters given by $W_j(f)$. The filtered outputs are combined and sampled at the symbol rate. The sampled signal is fed to the MAP processor, which applies the BCJR algorithm to produce the apriori probabilities on the modulated bits as described in section 2.4.3. The tentative hard decisions (which are found by quantizing these apriori probabilities) produced by the MAP processor are fed to the feedback filter $B'(f)$. This output is subtracted from the sampled signal and is the input to the MAP processor at the next iteration [11].

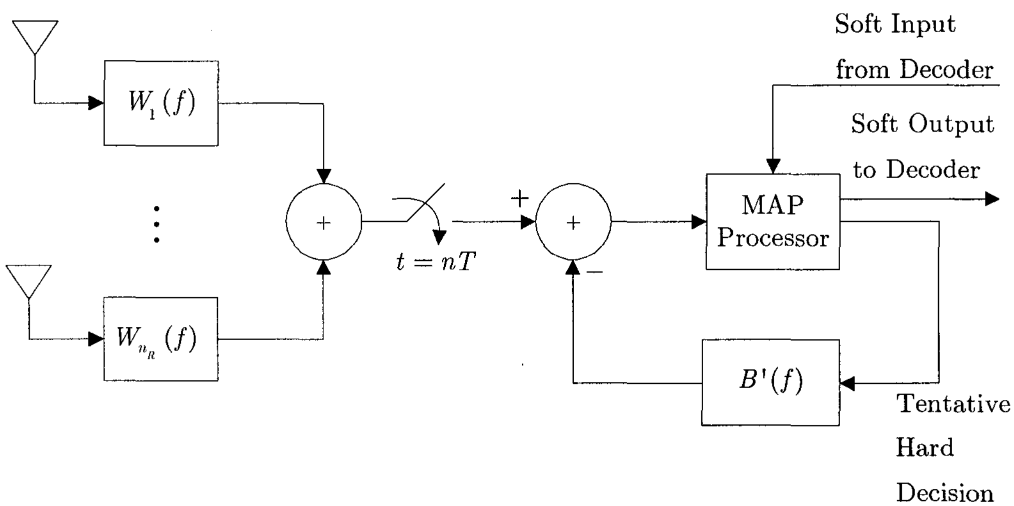

Figure 3.16: The block diagram of the space-time equalizer with MAP processing (courtesy of [11])

The performance of both these systems was studied by varying the number of transmit and receive antennas. It was found that the LST-I performed poorly for $n_T = n_R = 2$ as the decision errors prevent the system from approaching low block error rates regardless of the number of iterations. When the number of antennas is increased to 4, the error floor is lowered. With 3 iterations, the effect of the decision errors almost completely disappears when using soft decisions (at the output of MAP processor in the space-time equalizer) [11]. The LST-I performance for n_T = 2, 4, and 8 antennas after 6 iterations is shown in Figure 3.17. Since the block size is 400 bits and the rate of the system is n_T bps/Hz (as the modulation scheme is 8 PSK and the rate of the code is 1/3), LST-I reaches a bit error rate of 10^{-5} at –5.7 dB for the 8 antenna system. Hence, this system is approximately 5.1 dB away from the capacity limit (the capacity limit is calculated using Equation (2.16), where the ½ is dropped as the channel matrix is complex).

The performance of LST-II for n_T = 2, 4, and 8 after 6 iterations is shown in Figure 3.18. Unlike in LST-I, very little improvement is observed after 2 iterations. Therefore, for a large number of transmit and receive antennas, coding across the layers provides better performance than independent coding within each layer. However with the two transmit and two receive antennas, the former is heavily affected by decision errors and therefore provides poorer performance than the latter [11]. For the LST-II system, a BER of 10^{-5} is reached at an SNR of –3.5 dB for the 8 antenna system, which is 7.3 dB away from the capacity limit.

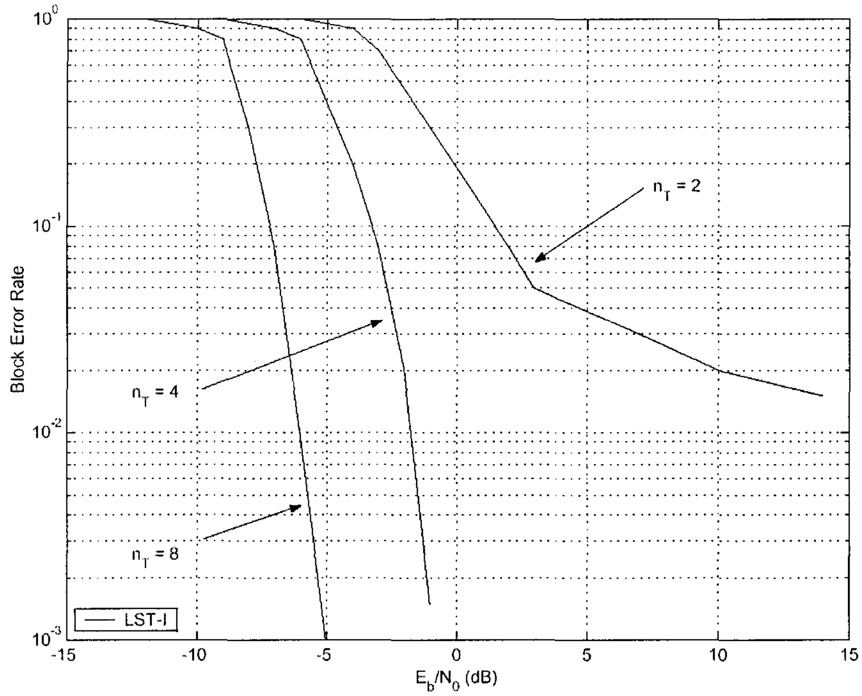

Figure 3.17: LST-I performance with $n_T = n_R = 2, 4, 8$ and n_T bits/s/Hz (courtesy of [11])

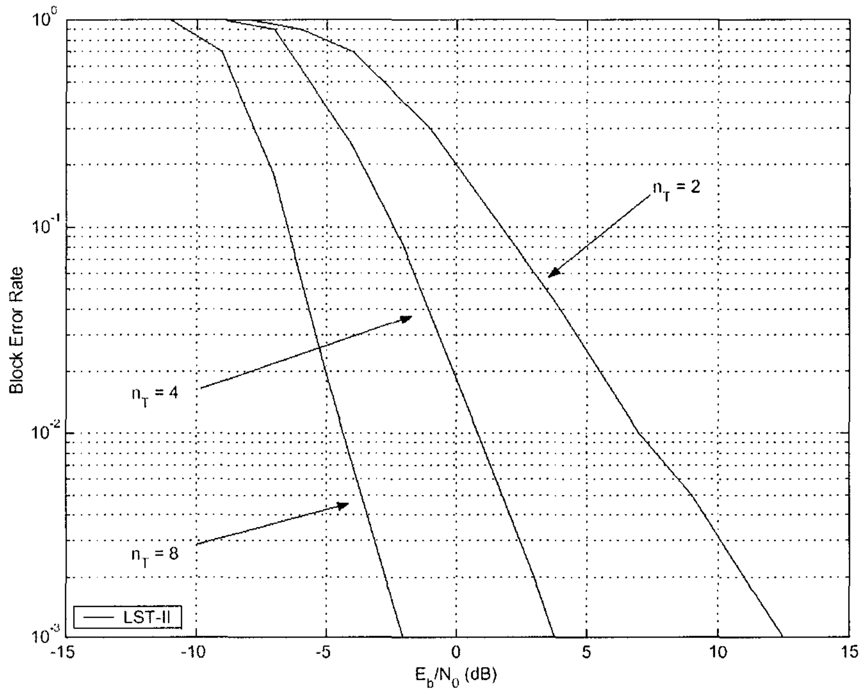

Figure 3.18: LST-II performance with $n_T = n_R = 2, 4, 8$ and n_T bits/s/Hz (courtesy of [11])

3.6 Chapter Summary

In this chapter, previous work in the field of antenna diversity systems was discussed. In particular, each system was described and its performance results were stated.

The prototype developed by Bell labs, known as V-BLAST, was shown to achieve very high spectral efficiency, however, the required channel SNR (P/σ^2) was in the order of 24 dB. At these SNRs, the receiver simply decorrelates all the received samples as there exists very little additive noise. Due to these high SNRs, this system is more suited for fixed wireless networks.

Space-time trellis codes, developed by Tarokh *et al.*, combined coding with antenna diversity. Although the spectral efficiency was much lower than V-BLAST, the system performed at lower channel SNRs (P/σ^2). However the complexity of the joint decoder at the receiver grew exponentially with the diversity level and transmission rate (keeping the number of antennas constant).

To reduce this complexity, Alamouti and then Tarokh *et al.* constructed space-time block codes. These codes were much simpler in their construction than the previous, hence having reasonable complexity at the receiver. However this system did not perform as well as the space-time trellis codes. In both cases, the reduced performance was due to weak codes.

Stefanov *et al.* and Ariyavisitakul, respectively applied turbo codes and iterative processing to an antenna diversity system. As expected, the systems performed significantly better than the previous systems: Stefanov's 4 state, 2 antenna was 8 dB better than the 16 state, 2 antenna space-time trellis system and Ariyavisitakul's 8 antenna system performed about 5.1 dB from the capacity limit. Although Ariyavisitakul had the lowest E_b/N_0 of all previous systems, a great deal of signal processing is required at the transmitter and receiver.

Chapter 4 Turbo Coded Diversity Transceivers

Previous systems required high SNRs to achieve low bit or frame error rates in quasi-static Rayleigh fading channels. To achieve transmission at much lower SNRs, the proposed system combines turbo coding with antenna diversity. The system design and the performance under different scenarios of varying antennas, and code rates will be described. Finally the performance of the proposed system will be compared to the capacity limit.

4.1 Proposed Coded Diversity System

The block diagram of the transmitter and receiver of the n_T transmit and n_R receive antenna system is shown in Figure 4.1 and Figure 4.2 where $n_T = n_R$. The systematic and parity bits (which are interleaved) of the parallel concatenated encoder are uniformly divided onto n_T antennas. Fading on the MIMO channel is spatially uncorrelated, quasi-static and Rayleigh. At the receiver, the n_R streams are received, deinterleaved, demultiplexed into two observations ($\mathbf{y}_1$ and $\mathbf{y}_2$ from section 2.5.2) and fed to the turbo decoder, which has the same structure as in section 2.5.2. All the blocks, which are dashed, are not essential for the system to function, however they may be used to improve performance.

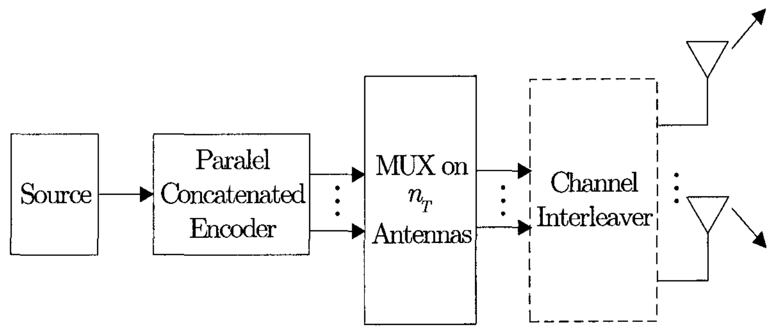

Figure 4.1: The schematic block diagram of the transmitter of the proposed system

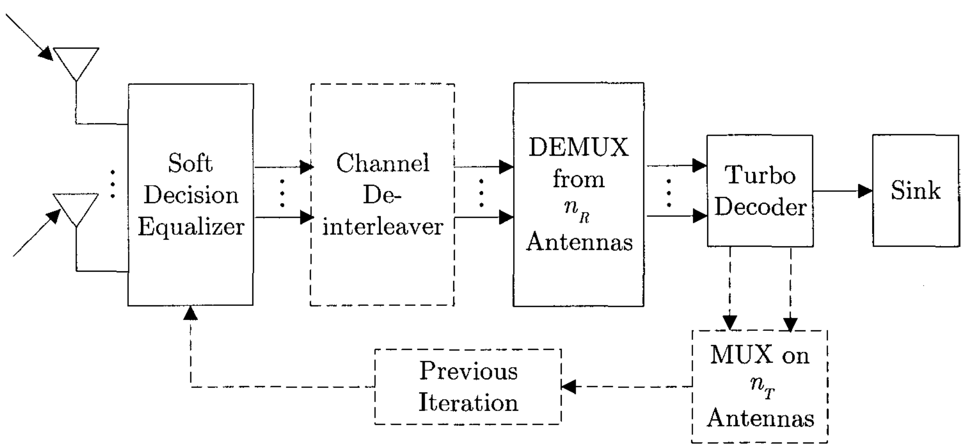

Figure 4.2: The schematic block diagram of the receiver of the proposed system

The Matlab (v5.3) simulation environment was used to simulate all the following systems. To decrease simulation time, the BCJR algorithm, which was used as the soft decision decoder, was compiled into an executable using the Matlab to C compiler. The simulation time that was required to generate the curves was in the order of 1.5 days for the small packet, 2 antenna system to 5 days for the small packet, 4 antenna system with turbo equalization. These simulations were carried out on a PIII 733 MHz processor with 384 MB RAM. It was found that as long as the program did not require more memory than the on-board RAM, the simulation time per bit were the same for the larger packet.

4.2 The 2 Transmit and 2 Receive System

In this section, the performance of the 2 transmit and 2 receive system will be discussed. Also it will be assumed that the parallel concatenated encoder is of rate 1/3 and the constituent encoders are described by the trellis shown in Figure 2.10. Although all the graphs are expressed in terms of the normalized SNR, E_b/N_0, this section and the following will express this quantity simply as SNR.

4.2.1 Performance on a Uniformly Faded Channel

In this system, there exists a uniform fade over the whole packet. If one of the streams experiences a deep fade, then 1/2 of the bits are lost. In such packets, the decoder cannot correct too many of the bits, and therefore it is expected that the BER curve will have a slow roll off. The system's performance is shown in Figure 4.3.

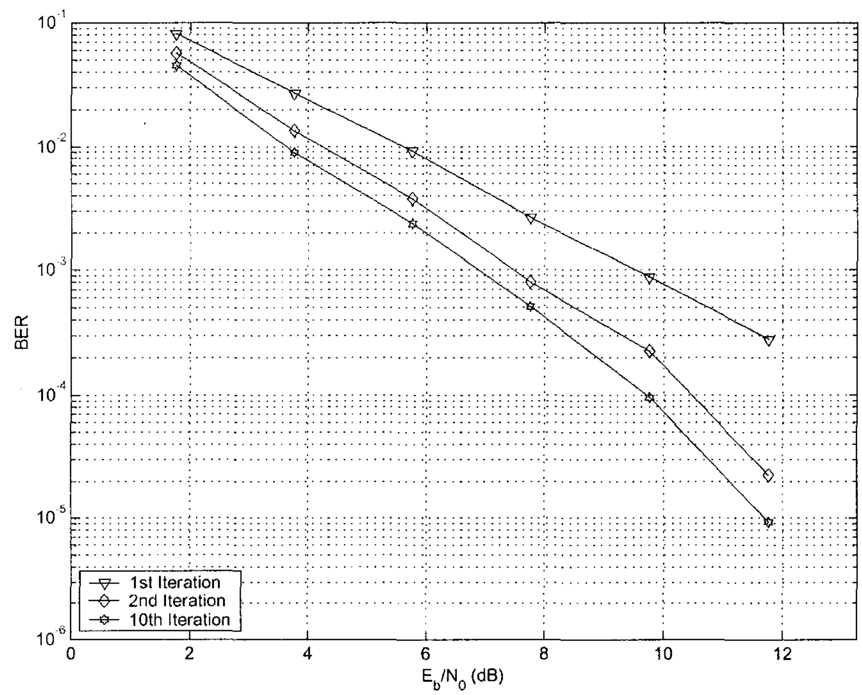

Figure 4.3: The performance on a uniformly faded channel (2 transmit / 2 receive)

As was predicted, a high SNR is required for achieving low BERs, i.e., a BER of 10^{-5} is reached at 11.7 dB. Also it was observed that although there was some gain in the first couple of iterations, the last five iterations did not provide any significant improvement.

4.2.2 Performance on a Block-Faded Channel

Although quasi-static fading is assumed, the fades usually remain constant for l channel uses. Tarokh *et al.* in [9] assumed that l is 130 and this will be assumed here as well. Hence, if a deep fade occurs, only 260 bits (130 × 2 antennas) will be lost instead of half the packet. Since the turbo code is quite powerful, it is assumed that it should perform better than in the previous case. The performance curve of this system is shown in Figure 4.4.

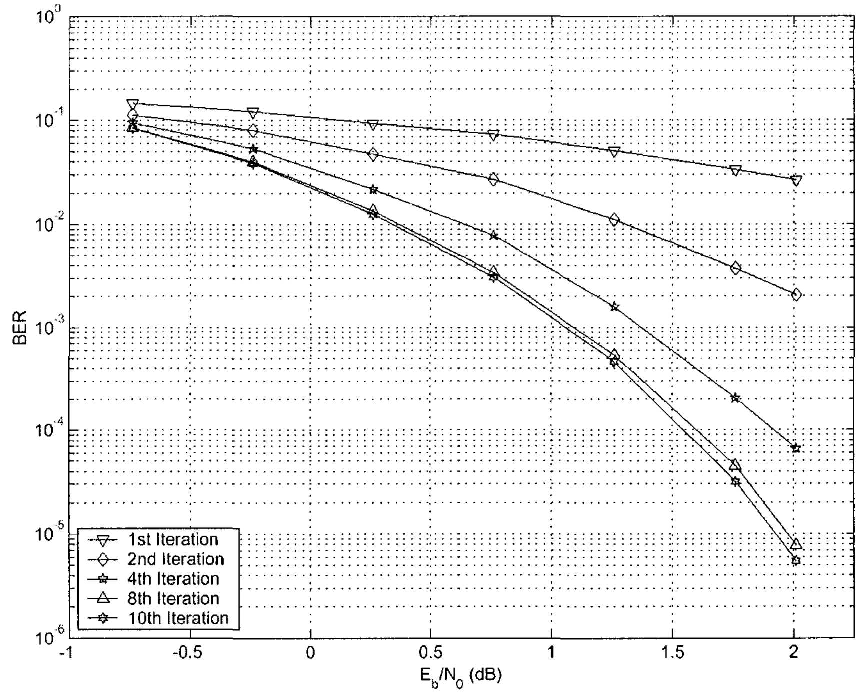

Figure 4.4: The performance on a block faded channel (2 transmit / 2 receive)

An SNR of 1.92 dB is required to reach a BER of 10^{-5}, which is a gain of 9.78 dB over the previous system. As in the preceding case, the last five iterations do not provide any significant improvement. This is probably due to fades, which still knock out too many parity bits, resulting in a saturation of the performance.

4.2.3 Performance on a Fully Interleaved Channel

In the previous set-up, it is possible to have consecutive deep fades knocking out many parity bits in the same packet. Although this does not occur often, these packets would reduce the performance of the system. Ideally the decoder could correct errors in a packet if the channel changed at the symbol level and if the receiver knew the channel matrix. This scenario is not realistic, but it can be mimicked if an interleaver is placed before the transmitter. This interleaver, known as a channel interleaver, would permute the data such that each element in the interleaved output comes from a different packet. Hence, the channel interleaver would require N packets to permute a block of N bits. The receiver would receive all N packets and then deinterleave and demultiplex them back into their appropriate codewords. Although some bits may be lost due to deep fades, the majority will not be, allowing the turbo decoder to correctly decode the packet. Hence, it is expected that the performance on a fully interleaved channel should be better than the previous scenarios. The performance curve of this system is shown in Figure 4.5.

An SNR of 0.91 dB is required to reach a BER of 10^{-5}, which is an improvement of 1.01 dB over the previous system. This gain is due to channel interleaver, which implies that the added signal processing seems to be worthwhile.

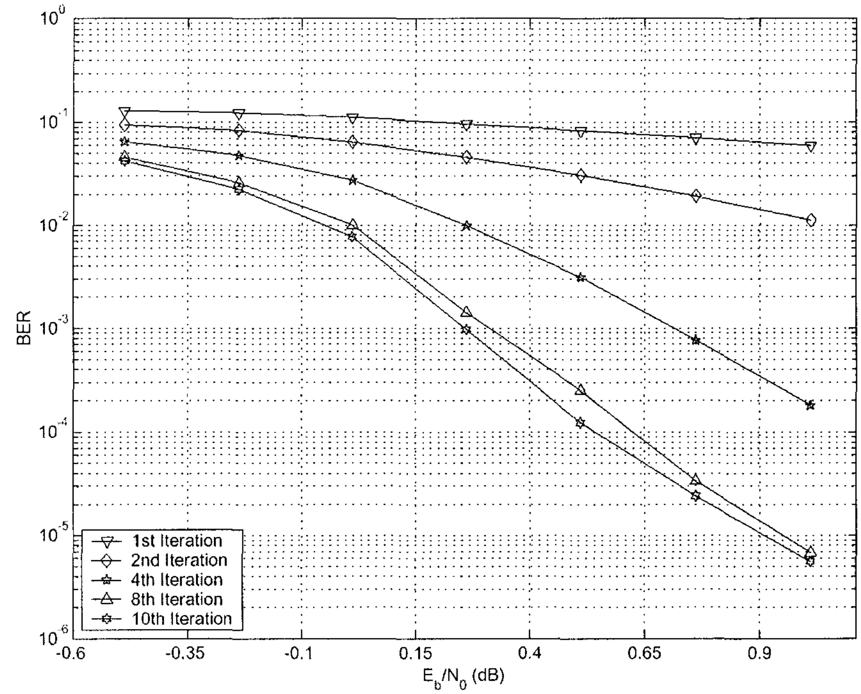

Figure 4.5: The performance on a fully interleaved channel (2 transmit / 2 receive)

4.2.4 Performance with Turbo-Equalization

In Figure 4.2, the soft decision equalizer can be brought into the iterative loop with the decoder while still maintaining a fully interleaved channel (indicated by the dotted feedback line). The receiver will now perform turbo equalization over the transmitted data. The performance curve of this system is shown in Figure 4.6.

A bit error rate of 10^{-5} is reached at –0.52 dB, which is a gain of 1.43 dB over the previous system. This gain was mostly realised in the last five iterations, which implies that turbo equalization improves the reliability of the parity bits. Clearly having the decoder trade extrinsic information on the codewords with the equalizer provides a significant gain.

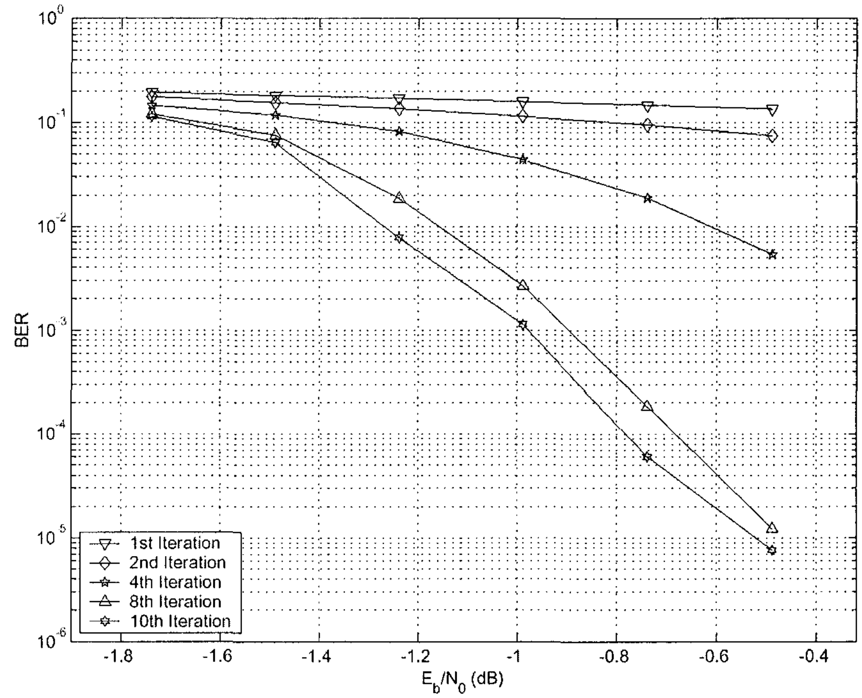

Figure 4.6: The performance on a fully interleaved channel with turbo equalization (2 transmit / 2 receive)

4.2.5 Performance with a Larger Packet Size

In section 2.5.1, it was indicated that the performance of a parallel concatenated code would increase if a larger interleaver between each constituent encoder was used. Therefore the packet size was increased to 18400 (which is 10 times bigger than the previous cases) and the simulation of the system on a fully interleaved channel without and with turbo equalization was rerun. The performance curves for these two scenarios are shown in Figure 4.7 and Figure 4.8, respectively.

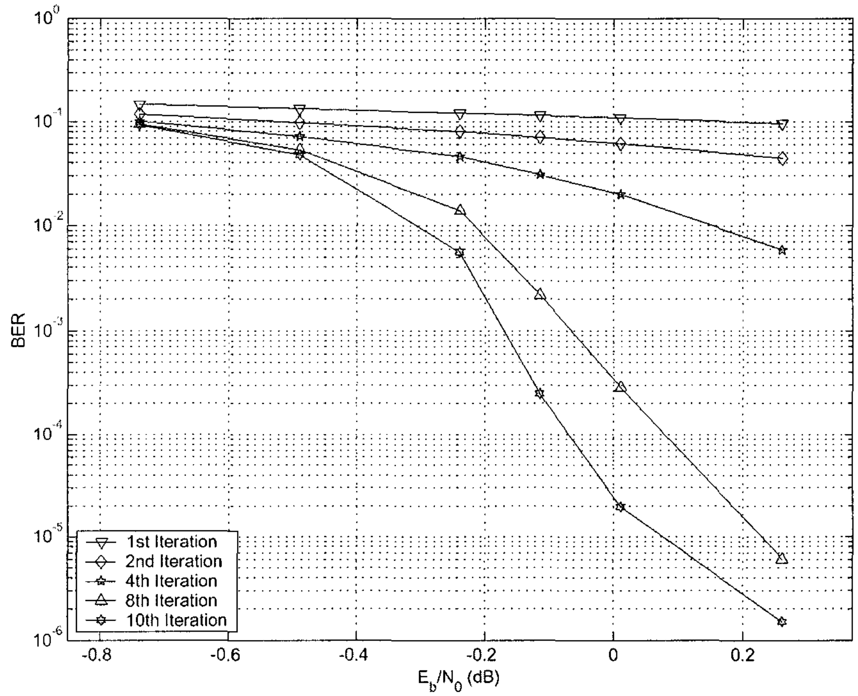

Figure 4.7: The performance on a fully interleaved channel for a larger packet (2 transmit / 2 receive)

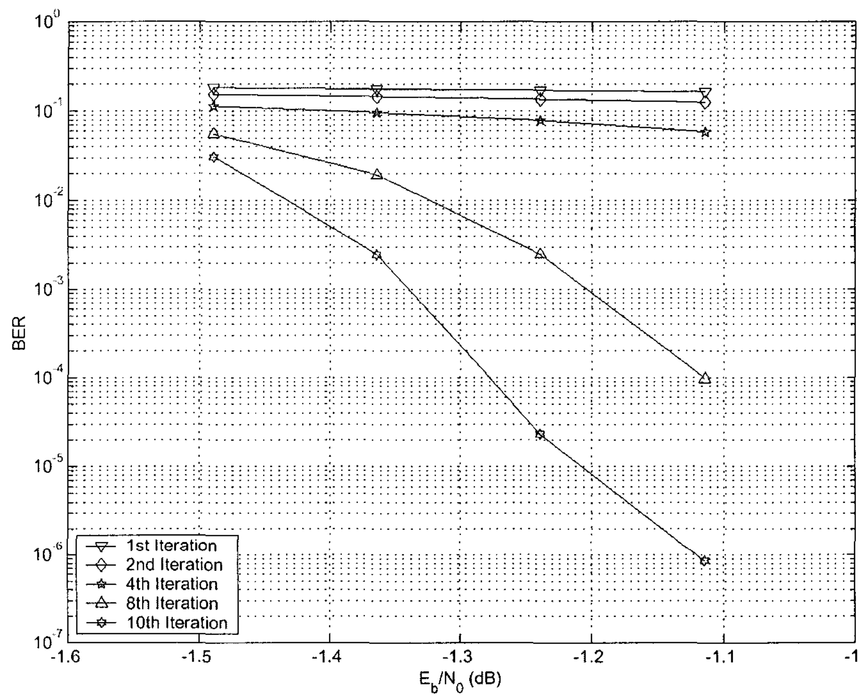

Figure 4.8: The performance on a fully interleaved channel with turbo equalization for a larger packet (2 transmit / 2 receive)

At a BER of 10^{-5}, the required SNR is 0.08 dB and −1.21 dB for the fully interleaved and turbo-equalized systems, respectively. This is a gain of 0.83 dB and 0.69 dB with respect to the corresponding smaller packet size systems. In the turbo-equalized scenario, there exists a large gap between the 8^{th} and 10^{th} iterations, which suggests that a more iterations would result in an additional performance improvement. Unlike curves for the packet size of 1840, these curves require a smaller falling range, i.e., 1 dB and 0.375 dB versus 1.4 dB and 1.25 dB for the fully interleaved channel and turbo equalized, respectively.

4.3 The 4 Transmit and 4 Receive System

In this section, the performance of the 4 transmit and 4 receive system will be discussed. Also, it will be assumed that the parallel concatenated encoder is of rate 1/5 and the constituent encoders have a trellis that is shown in Figure 2.13. The general FSM encoder trellis was used as it performed significantly better than the RSC encoder trellis of Figure 2.10.

4.3.1 Performance on a Uniformly Faded Channel

In this case, as in the 2 antenna system, the fade is uniform over the whole packet. If one of the streams experiences a deep fade, then 1/4 of the bits are lost. Hence to reach low BERs, high SNRs will be required and the curve will have a slow roll off. The performance curve of this system is shown in Figure 4.9.

As expected, a high SNR is required for achieving low BERs, i.e., a BER of 10^{-5} is reached at 4.29 dB. Although there is some improvement in the first five iterations, subsequent gain in the next five iterations is not as significant.

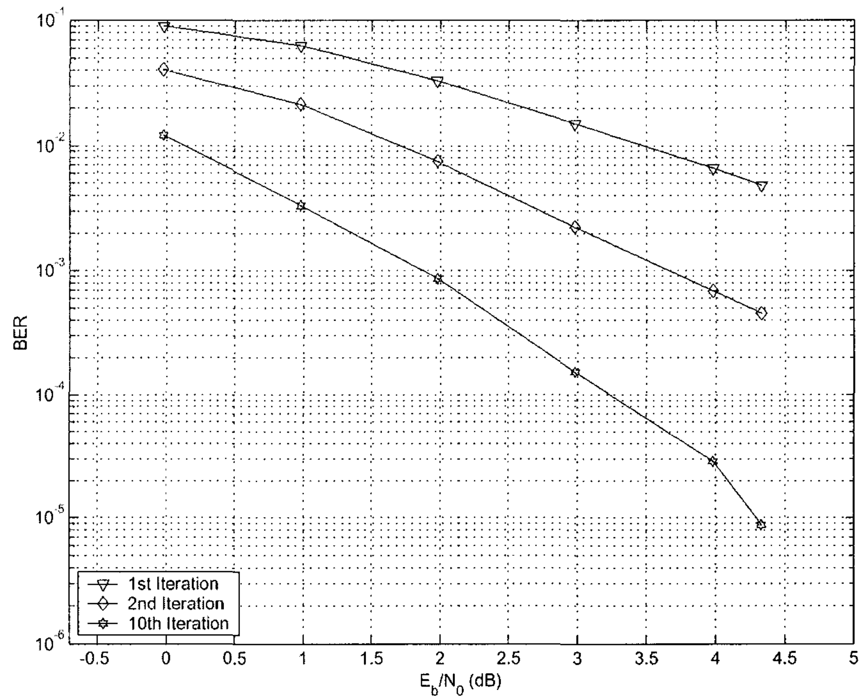

Figure 4.9: The performance on a uniformly faded channel (4 transmit / 4 receive)

4.3.2 Performance on a Block-Faded Channel

In this section, the fading will be assumed to be constant for 130 channel uses. This system's performance should be better than the corresponding 2 antenna system as there are more parity bits. The performance curve of this system is shown in Figure 4.10.

Clearly the system performs better in a block-faded channel than a uniformly faded channel. An SNR of –0.43 dB is required to reach a BER of 10^{-5}, which corresponds to a gain of 4.72 dB over the previous system. Unlike the 2 antenna system, there exists a uniform improvement in the performance as the turbo decoder iterates. This is probably because there are enough parity bits to provide good extrinsic information to the decoder even in deep fades. There is almost a 2.35 dB gain at a BER of 10^{-5} between the corresponding 2 and 4 antenna system. This gain is due to the added diversity and coding advantage (4 vs. 2 and 1/5 vs. 1/3).

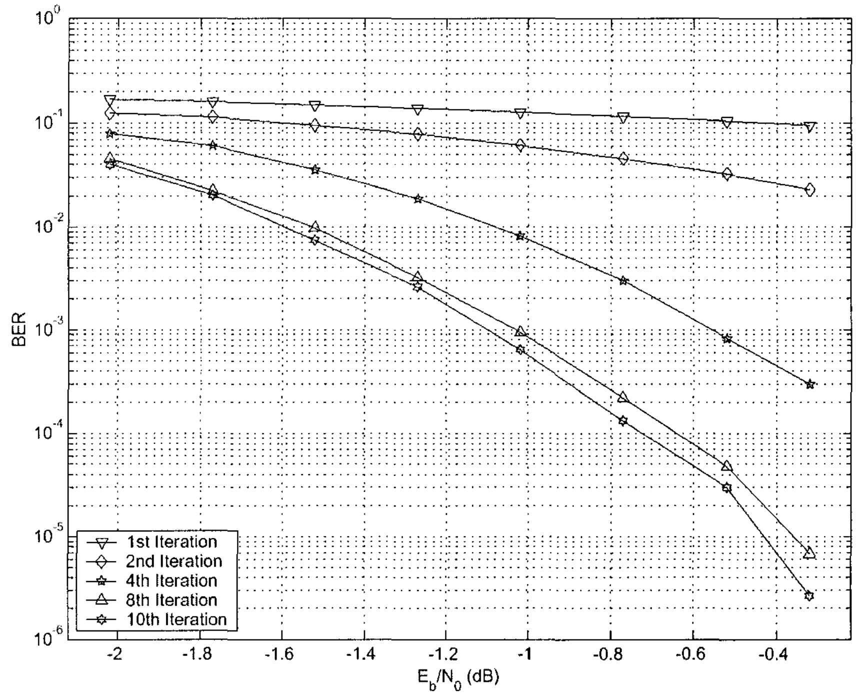

Figure 4.10: The performance on a block faded channel (4 transmit / 4 receive)

4.3.3 Performance on a Fully Interleaved Channel

In this section, the performance of the 4 transmit and 4 receive will be considered where the channel interleaver is present at back and front ends of the transmitter and receiver, respectively. The performance curve of this system is shown in Figure 4.11.

To reach a BER of 10^{-5}, an SNR of -1.14 dB is required, which is 0.71 dB better than the previous system. This gain is due to adding the channel interleaver. Also, there seems to be a significant performance improvement in the last five iterations.

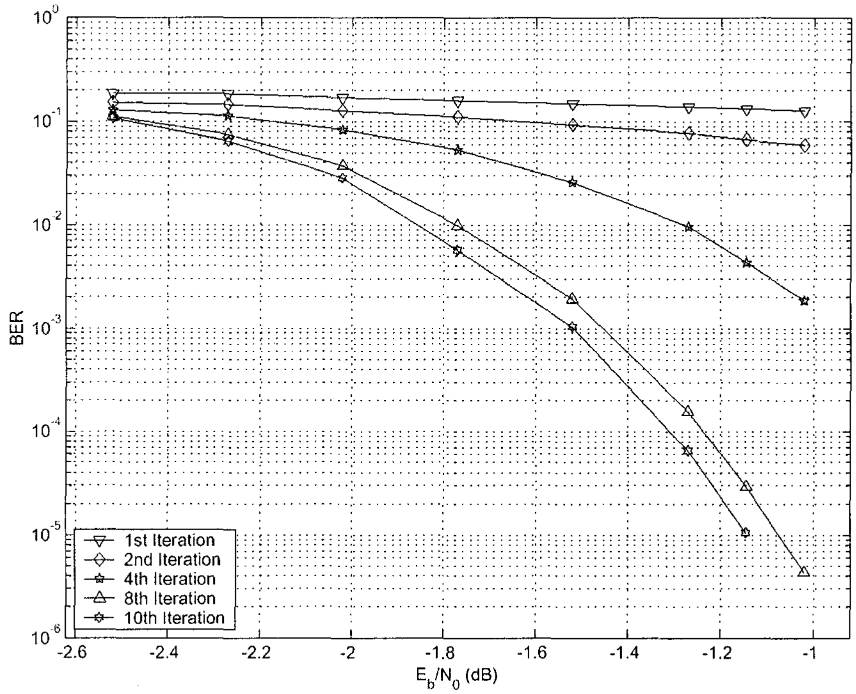

Figure 4.11: The performance on a fully interleaved channel (4 transmit / 4 receive)

4.3.4 Performance with Turbo-Equalization

Similar to the 2 antenna case, the soft decision equalizer can be brought into the iterative loop, which can realise another performance improvement. The performance curve of this system is shown in Figure 4.12.

A BER of 10^{-5} is reached at –2.52 dB, which is a gain of 1.38 dB over the previous system. As in the 2 antenna case, a significant gain can be realised when equalization and turbo decoding is performed jointly.

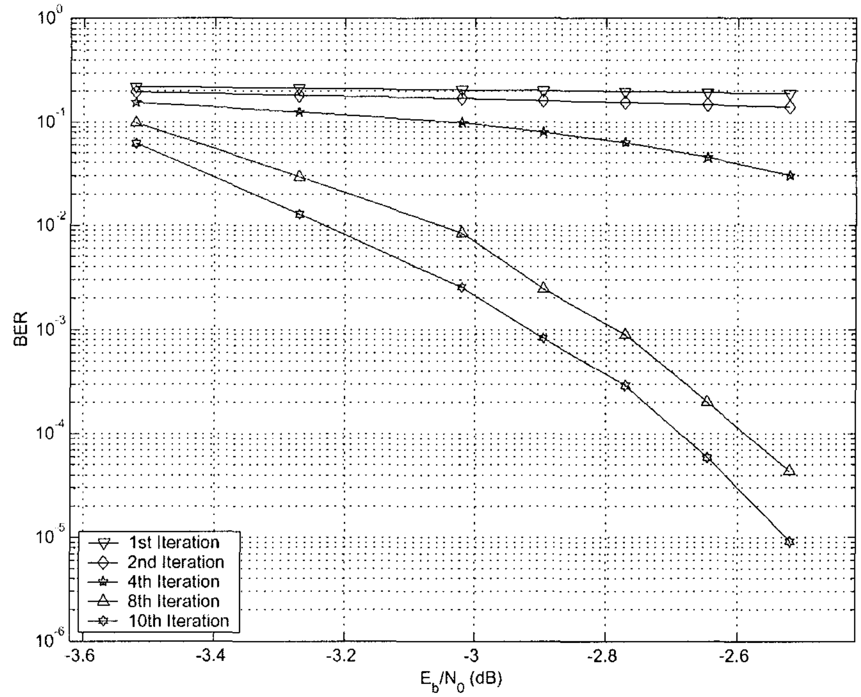

Figure 4.12: The performance on a fully interleaved channel with turbo equalization (4 transmit / 4 receive)

4.3.5 Performance with a Larger Packet Size

In this section, the performance of the 4 transmit and 4 receive will be considered where the packet size is increased 10 times. The performance curve for the fully interleaved and turbo-equalized systems are shown in Figure 4.13 and Figure 4.14, respectively.

At a BER of 10^{-5}, the required SNR is –1.89 dB and –3.27 dB for the fully interleaved and turbo equalized systems, respectively. Hence, by increasing the interleaver size, 0.67 dB and 0.75 dB was gained in performance compared to the corresponding small packet systems. In the turbo-equalized scenario, a significant gain exists between the 8^{th} and 10^{th} iteration, which suggests that more iterations would further improve performance. Also, the BER curve falls almost uniformly until a particular SNR, after which, the BER curve falls very steeply. Unlike curves for the packet size of 1840, these curves require a very small falling range, i.e., 0.38 dB versus 1.5 dB for the 18400 and 1840 packet sizes, respectively.

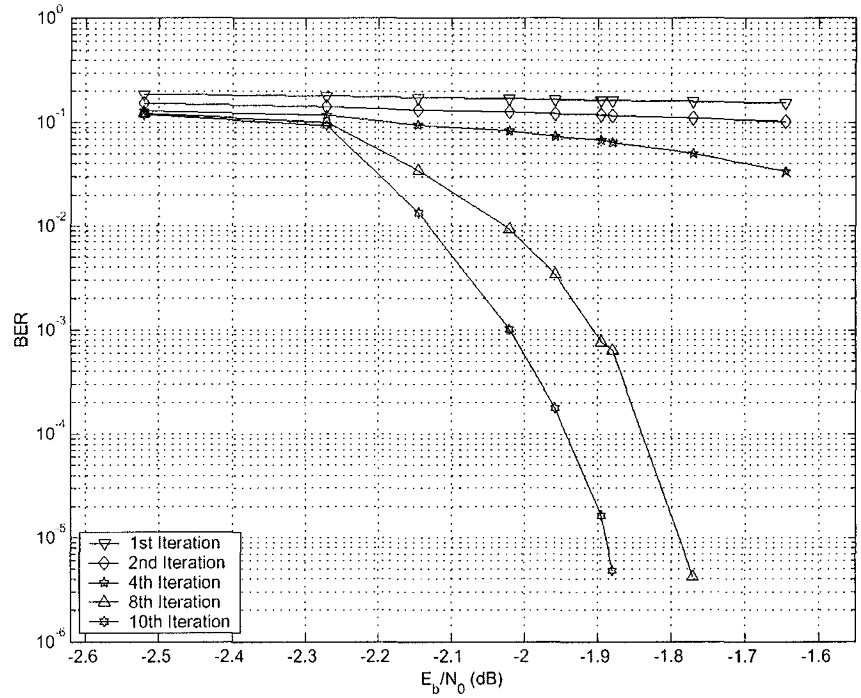

Figure 4.13: The performance on a fully interleaved channel for a larger packet (4 transmit / 4 receive)

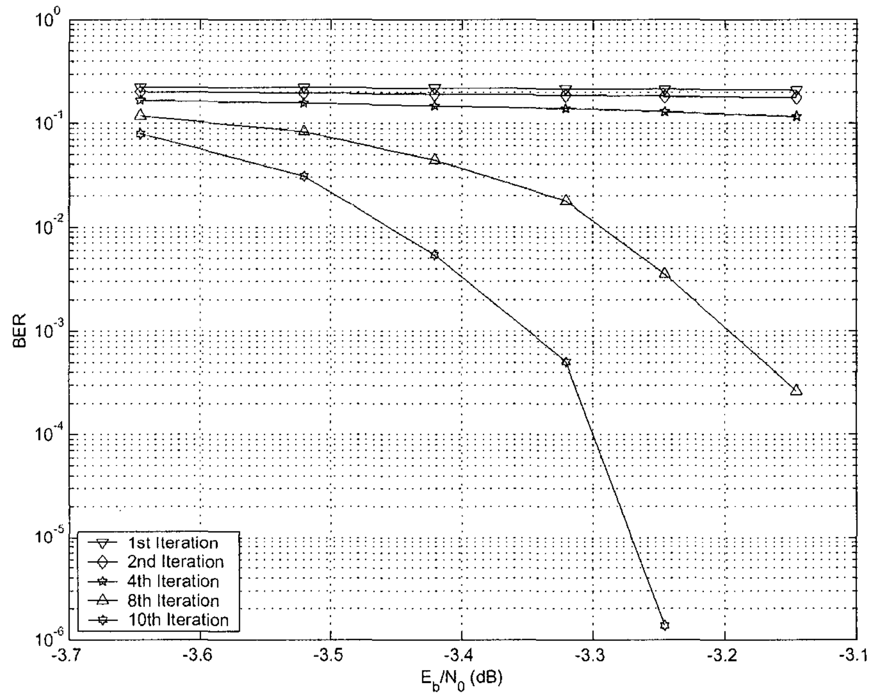

Figure 4.14: The performance on a fully interleaved channel with turbo equalization for a larger packet (4 transmit / 4 receive)

4.4 Asymmetric MIMO Channels

Unlike the mobile terminal, the receiver or the base station has more signal processing power available to it. Hence, it is conceivable to put more receive antennas on the base station, to better detect and decode the signal. If a system has 2 transmit and 3 receive antennas, referring to the discussion in section 2.1.2, the transmitted data exists as points in a 2-dimensional plane, but the channel maps these points into a 3-dimensional space. Thus there exists greater separation between the received points, which the decoder can then use to increase its performance. As a topic of further study, the number of receive antennas was varied in the above systems, to see how much the performance would increase. Figure 4.15 and Figure 4.15 illustrates the performance of the 2 and 4 transmit antenna systems on a fully interleaved channel with turbo equalization where the number of receive antennas was increased to 3 and 6, respectively.

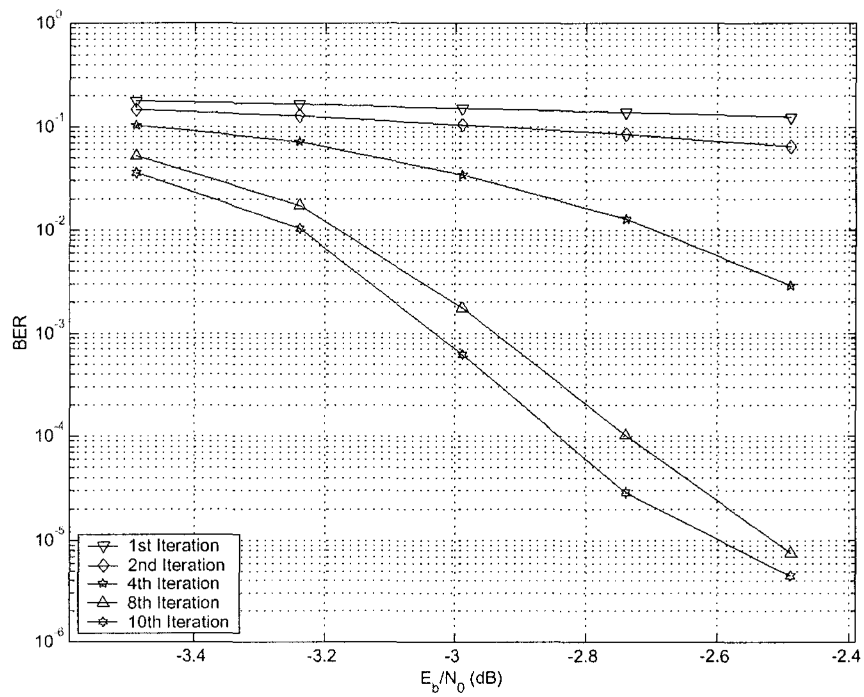

Figure 4.15: The performance on a fully interleaved channel with turbo equalization (2 transmit / 3 receive)

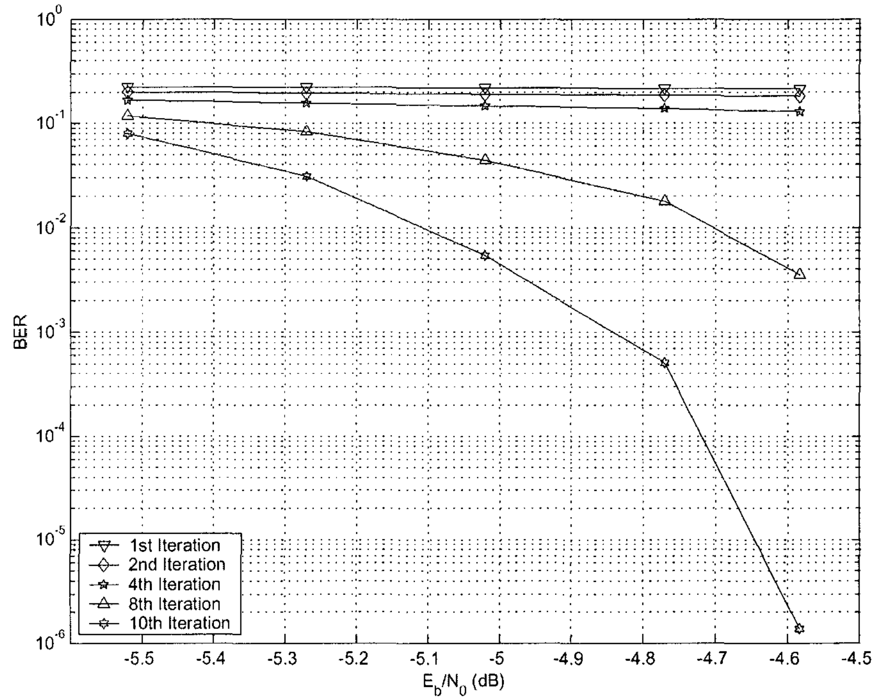

Figure 4.16: The performance on a fully interleaved channel with turbo equalization (4 transmit / 6 receive)

To reach a bit error rate of 10^{-5}, an SNR of –2.59 dB and –4.64 dB was required for the 2 and 4 antenna systems, respectively. Therefore, adding 50 % more receive antennas corresponds to a gain of about 2 dB.

4.5 Performance Comparison of the Space-Time Systems

In section 2.2.2, a numerical technique to calculate the MIMO capacity for a changing **H** was provided. In this section, the performance of the above systems will be measured with respect to this capacity limit. The rates of transmission for the 2 and 4 antenna systems are R = 2/3 bps/Hz and R = 4/5 bps/Hz, respectively (R_m is 1 for BPSK and R_c is 1/3 and 1/5 for the 2 and 4 antenna systems, respectively). In Equation (2.16), the normalized SNR, E_b/N_0, can be adjusted so that C_T (capacity calculated at the T-th iteration, where T is 100, 000) is approximately equal to R. The results of this capacity analysis for the symmetric system are shown in Table 3.

Table 3: Capacity bounds for the symmetric turbo equalized systems

System	E_b/N_0 (dB) from Simulation at a BER of 10^{-5}	Capacity Limit (dB) as BER $\rightarrow 0$	Difference (dB)
2 Antenna System (18400)	-1.21	-2.40	1.19
4 Antenna System (18400)	-3.27	-5.60	2.33

Although the 4 antenna system reaches the same bit error rate as the 2 antenna system at a lower SNR, it is about 1.15 dB further from the capacity limit than the 2 antenna system. The reason as to why the 4 antenna system performs worse is that the general FSM code shown in Figure 2.13 should be further optimized (by adjusting the state transitions, input and output labels) in the context of the 4 branch parallel concatenated encoder. A summary of the capacity analysis for the asymmetric system is shown in Table 4.

Table 4: Capacity bounds for the asymmetric turbo equalized systems

System	E_b/N_0 (dB) from Simulation at a BER of 10^{-5}	Capacity Limit (dB) as BER $\rightarrow 0$	Difference (dB)
2, 3 Antenna System (1840)	-2.59	-4.40	1.81
4, 6 Antenna System (1840)	-4.64	-7.50	2.86

For the asymmetric scenario, the difference between performance and the capacity limit increased by about 0.6 dB to 1.81 dB and 2.86 dB for the 2 and 4 antenna systems, respectively. The increased separation is due to the fact that additional coding was not added to take full advantage of the increased diversity gain.

4.6 Practical Considerations

The equation to determine the throughput of the system is given by,

$$Throughput = \frac{Clock\ frequency \times Pipeline\ factor \times ASIC\ factor}{\#\ of\ Clock\ cycles/sample/iteration \times \#\ of\ iterations}. \quad (4.1)$$

The limiting factor in the system throughput is the decoder as it is more complex than the encoder. Currently, Xilinx has developed a 3GPP compliant turbo codec for the Virtex II FPGA device which requires 3 clock cycles/bit/iteration of the turbo decoder [52]. Since the equalizer is simply a lookup table, it is assumed to add 1 more clock cycle per bit/iteration. Therefore, Equation (4.1) results in a throughput of 1 Mbps at a clock frequency of 40 MHz. If the decoder was implemented on an ASIC, then a further gain of two can be achieved. This gain is because an ASIC has less overhead than a corresponding FPGA implementation [53]. The throughput can potentially be increased to 20 Mbps when a pipelining option is used, where it is assumed the number of turbo decoder blocks is equal to the number of iterations. Other than an increase in the size of the chip, this throughput would be the same for the 4 antenna system.

4.7 Chapter Summary

In this chapter, the design of the proposed coded antenna diversity system with its performance results were presented. The performance was shown to increase significantly when the number of antennas was increased from 2 to 4 and the coding rate decreased from 1/3 to 1/5. Performance was increased by fully interleaving the transmitted data, joint equalization and decoding and using longer packets. The performance analysis showed that turbo equalization on a fully interleaved channel for the larger packet (18400 bits) with 2 and 4 antennas performed within 1.19 dB and 2.33 dB of the Shannon limit, respectively. The asymmetric systems performed slightly worse and are about 1.81 and 2.86 dB from the capacity limit, respectively.

Chapter 5 Conclusion

5.1 Summary

The presence of fading in wireless environments increases the error probability and stipulates the use of good coded diversity schemes. Diversity schemes have been used in fading channels and in particular antenna diversity has been shown to increase the capacity of a wireless communication link significantly. Good channel codes, which add redundancy and memory to the transmitted data, are required to achieve this increased capacity. In 1993, Berrou *et al.*, proposed a new encoding and decoding scheme, commonly referred to as turbo codes, which are capable of achieving near capacity performance on an AWGN channels [6]. In this work, we proposed a power efficient turbo coded antenna diversity system and investigated its performance on a quasi-static Rayleigh fading channel.

In Chapter 2, we described the baseband equivalent fading model when there exist multi element antenna arrays at the transmitter and receiver. This model, termed the multi input multi output (MIMO) channel, is memoryless, and it has fades that are spatially uncorrelated between the antennas and independent from one fade to the next. Under this assumption, the channel capacity is an average of the capacities under different realisations of the channel transfer matrix. Since the analytical expression is difficult to calculate [7], we briefly describe a numerical technique to evaluate the channel capacity. After establishing the MIMO channel capacity, the construction of parallel concatenated encoders and the process of turbo decoding were presented, which also included the concept of turbo equalization.

Chapter 3 considered previous work in the field of coded space-time processing. In particular, the V-BLAST architecture [8], the space-time trellis codes [9], space-time block codes [13], turbo coded modulation with antenna diversity [10] and layered space-time architecture with iterative processing proposed in [11] were explored. We observed that although the V-BLAST system could send more bits through the channel (26 bps/Hz), the channel SNR (P/σ^2) that was required could only be supported through a large power supply. Although space-time trellis codes and space-time block codes operate at lower channel SNRs, these SNRs are still high for the rates of transmission (3 bps/Hz and 1 bps/Hz, respectively). In [10], turbo codes were applied to antenna diversity, which resulted in significantly better performance than the corresponding space-time trellis code. However, Stefanov *et al.* were still quite far from the capacity limit. In [11], a layered space-time architecture with iterative processing was proposed. This system was within 5.1 dB of the capacity limit, with a medium rate of transmission (8 bps/Hz) using 8 antennas. However, this performance was achieved with significant signal processing at the receiver.

In Chapter 4, the design and simulation results of the proposed system were presented. The system design was motivated by the performance of parallel concatenated codes on a single input and single output Gaussian channel, and the ability of antenna diversity to improve performance in fading channels. To achieve a further performance gain, a soft decision equalizer was at the front end of the receiver. We explored the performance under symmetric antenna configurations with 2 and 4 antennas. In each configuration, five cases were considered: uniform fading, block fading, fully interleaved channel, turbo equalization on a fully interleaved channel and increased packet size. Figure 5.1 and Figure 5.2 illustrate the performance of these 5 cases with respect to the capacity bound for the 2 and 4 antenna systems respectively.

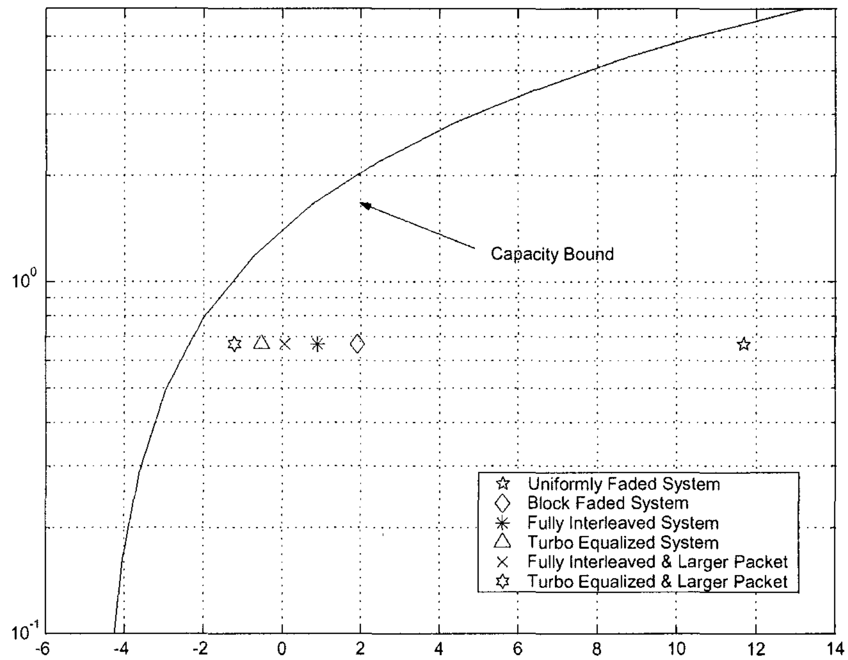

Figure 5.1: Performance results for 5 different cases of the 2 antenna system

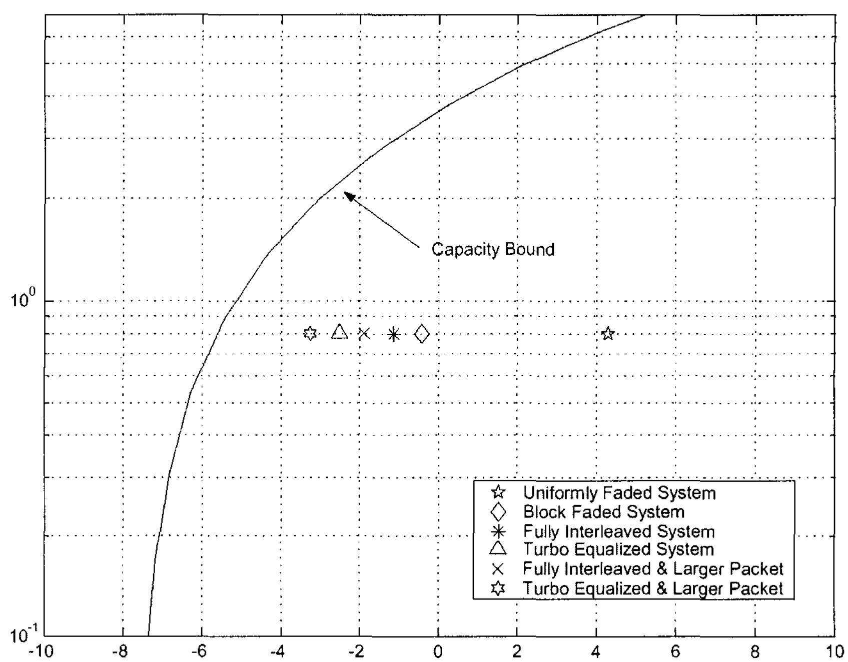

Figure 5.2: Performance results for 5 different cases of the 4 antenna system

From the above figures, it is clear that the turbo-equalized system performed significantly better than any other case. The best performance was the system with turbo equalization on a fully interleaved channel for the larger packet. These systems reached 10^{-5} at an E_b/N_0 of –1.21 dB and –3.27 dB, which are 1.19 dB and 2.33 dB from the Shannon limit for the 2 and 4 antenna cases, respectively. As a topic of further study, the number of receive antennas was increased, to observe if the above gain was due to diversity alone or due to a combination coding and diversity. If 50 % more receive antennas were added, the performance increased by about 2 dB for the 2 and 4 antenna systems. However, the resulting systems were about 1.81 and 2.86 dB away from the capacity limit. Clearly increasing the number of antennas without an appropriate decrease in the coding rate is not accompanied with an increase in performance with respect to the Shannon limit.

Compared to previous literature, this is the first coded antenna diversity system, which is closest to the capacity limit on a quasi-static Rayleigh MIMO fading environment. These systems reach small BERs (10^{-4} – 10^{-5}) at negative channel SNRs and negative E_b/N_0s, i.e., the power of the signal is less than the noise. In fact, the best 4 antenna symmetric system reaches a BER of 10^{-5} at a channel SNR of –1.23 dB or an E_b/N_0 value which is 1.66 dB lower than the –1.6 dB limit for reliable communication on a SISO system[1] [37]. Such low SNRs are well suited for finite power mobile terminals in the field. Using a CDMA modulation scheme, a 2.5 MHz bandwidth per user can support 2 Mb/s (which is the maximum rate of transmission in the current 3GPP standard [54]) with the 4 antenna system (rate of transmission is 0.8 bps/Hz).

[1] Recently it has been shown that MIMO systems have the potential to outperform the –1.6 dB bound [7]. The proposed coding scheme, to the best of our knowledge, is the first one to overcome this limit, with negative channel SNRs.

5.2 Future Research Directions

This thesis has focused on power efficient transmission on quasi-static Rayleigh fading MIMO channels. This objective has been successfully achieved by combining iterative decoding and antenna diversity schemes. As an area of further research, this system can be extended to high spectral efficiencies by changing the coding schemes to higher rate codes and (or) by changing the modulation. Other areas of research are to use a more sophisticated interleaver, and to evaluate these systems in a non-Rayleigh environment, for example, Ricean. Finally it would be interesting to apply this space-time scheme in the context of a multi-user scenario where the interference from other users must also be considered.

References

[1] J. Proakis, *Digital Communications.* New York: McGraw Hill, 1989

[2] C. E. Shannon, "A Mathematical theory of communication", *Bell System Technology Journal*, vol. 27, pp. 379-423 and 623-656, 1948

[3] R. Lucky, "The precious radio spectrum", *IEEE Spectrum*, pp. 90, September 2001

[4] R.W Hamming, "Error detecting and error correcting codes", *Bell System Technology Journal*, vol. 29, pp. 147-160, 1950

[5] G. D. Forney Jr., "The Viterbi algorithm", *IEEE Trans. on Commun.*, vol. 61, pp. 268-278, March 1973

[6] C. Berrou, A. Glavieux and P. Thitimajshima, "Near Shannon limit error-correcting coding and decoding: turbo-codes (1)", *Proc. ICC '93*, Geneva, Switzerland, pp. 1064-1070, May 1993

[7] E. Telatar, "Capacity of multi antenna Gaussian channels", *European Transactions on Telecommunications*, Vol. 10, No. 6, pp. 585-595, Nov/Dec 1999

[8] G.J. Foschini, "Layered space-time architecture for wireless communications in a fading environment when using multi-element antennas", *Bell Labs Technical Journal*, vol. 1, no. 2, pp. 41-59, Autumn 1996

[9] V. Tarokh, N. Seshadri, and A.R. Calderbank, "Space-time codes for high data rate wireless communication: performance criterion and code

construction", *IEEE Trans. Inform. Theory*, vol. 44, no. 2, pp. 744-765, Mar. 1998

[10] A. Stefanov, T. Duman, "Turbo coded modulation for wireless communications with antenna diversity", *Proc. of IEEE VTC '99*, vol. 3, pp. 1565-1569, September 1999

[11] S. L. Ariyavisitakul, "Turbo space-time processing to improve wireless channel capacity", *IEEE Tran. Commun.*, Vol. 48, No. 8, pp. 1347-1359, August 2000

[12] N. Mysore, J. Bajcsy, "Combined Turbo Coding and Turbo Equalization in a Wireless System with Antenna Diversity", to appear in *IEEE Proc. of VTC '02*, May 2002

[13] S.M Alamouti, "A simple transmit diversity technique for wireless communications", *IEEE J. Select Areas Commun.*, vol. 16, pp. 1451-1458, Oct. 1998

[14] W. Jakes, *Microwave Mobile Communications.* New York: IEEE Press, 1974

[15] M. Godbout, H. Leib, "A transmit diversity coding framework for cellular systems", Proceedings of CCECE (CD-ROM), May 2001

[16] T. M. Cover and J. A. Thomas, *Elements of Information Theory.* New York, New York: John Wiley and Sons, Inc., 1991

[17] J. Bajcsy, "Lecture Notes For Digital Communications II (304-623)", taught at McGill University in the Winter semester of 2001

[18] J. Bajcsy and H. Kobayashi, "On Obtaining the BCJR Algorithm via Path Counting," *Proc. of ISITA 2000*, pp. 192-194, Honolulu, HI, November 2000.

[19] L. Bahl, J. Cocke, F. Jelinek and J. Raviv, "Optimal decoding of linear codes for minimizing symbol error rate", *IEEE Trans. on Information Technology.*, vol. 20, pp. 278-284, March 1973

[20] J. Hagenauer, P. Hoeher, "A Viterbi algorithm with soft decision outputs and its applications", *Proc. GLOBECOM '89*, Dallas, Texas, Nov. 1989, pp. 47.1.1 – 47.1.7

[21] M. Shoemake, C. Heegard, "Computationally efficient turbo decoding with the bi-directional Viterbi algorithm (BIVA)", *IEEE Symposium on Information Theory*, pp. 228, July 1997

[22] A.J. Viterbi, "Error bounds for convolutional codes and an asymptotically optimum decoding algorithm", *IEEE Trans. on Information Theory*, vol. IT-13, pp. 260-267, April 1967

[23] R. M. Fano, "A heuristic discussion of probabilistic decoding", *IEEE Trans. Information Theory*, vol. IT-9, pp. 64-74, Apr. 1963

[24] S. Dolinar, D. Divsalar, "Weight distributions for turbo codes using random and nonrandom permutations", *JPL TDA Progress Report 42-122*, August 15, 1995

[25] D. Raphaeli, Y. Zarai, "Combined turbo equalization and turbo decoding", *IEEE Commun. Letters*, vol.2, no.4, pp.107-109, Apr. 1998

[26] A. Roumy, I. Fijalkow, D. Pirez, "Joint equalization and decoding: why choose the iterative solution?", *Proc. of IEEE VTC'99,* pp. 2989-2993, September 1999

[27] G.J. Foschini and M.J. Gans, "On limits of wireless communications in a fading environment when using multiple antennas", *Wireless Personal Communications*, pp. 311-335, Mar. 1998

[28] P.W. Wolniansky, G.J. Foschini, G.D. Golden, R.A. Valenzuela, "V-BLAST: an architecture for realizing very high data rates over the rich scattering wireless channel", *Proc. ISSSE*, pp. 295-300, 1998

[29] G.D. Golden, G.J. Foschini, R.A. Valenzuela, P.W. Wolniansky, "Detection algorithm and initial laboratory results using the V-BLAST space-time communication architecture", *Electronics Letters*, Vol. 35, No. 1, pp. 14-15, Jan. 1999

[30] V. Tarokh, H. Jafarkhani, A.R. Calderbank, "Space-time block codes from orthogonal designs", *IEEE Trans. Inform. Theory*, vol. 45, pp. 1456-1467, July 1999

[31] V. Tarokh, H. Jafarkhani, A.R. Calderbank, "Space-Time Block Coding for Wireless Communications: Performance Results", *IEEE J. Select Areas Commun.*, Vol. 17, N0. 3, pp. 451-460, March 1999

[32] A. Naquib, N. Seshadri, A.R. Calderbank, "Applications of space-time block codes and interference suppression for high capacity and high data rate wireless systems", in *Proc. Conference Record of the 32nd Asilomar Conference*, vol. 2, pp. 1803-1810, Nov. 1998

[33] G. Bauch, "Concatenation of space-time block codes and "turbo" - TCM", in *Proc. IEEE Int. Conf. On Commun.*, pp. 1202-1206, June 1999

[34] G. D. Forney, Jr. *Concatenated Codes.* MIT Press, Boston: Cambridge, 1966

[35] P. Robertson, "Illuminating the structure of code and decoder of parallel concatenated recursive systematic (turbo) codes", *Proc. of GLOBECOM '94*, San Francisco, USA, pp. 1298-1303, Nov. 1994

[36] C. Douillard, M. Jezequel, C. Berrou, A. Picart, P. Didier, A. Glavieux, "Iterative correction of intersymbol interference: turbo-equalization", *Europ. Trans. on Telecommun. (ETT)*, Vol. 6, pp. 507-511, Sept.-Oct. 1995

[37] J. Proakis and M. Salehi, *Communication Systems Engineering* 4th ed. New York: Prentice Hall, 1996

[38] J. Proakis, D. Manolakis, *Digital Signal Processing: Principles, Algorithms and Applications.* Upper Saddle River, New Jersey: Prentice Hall, 1996

[39] A. Picart, P. Didier, A. Glavieux, "Turbo-detection: a new approach to combat channel frequency selectivity", Proc. ICC'97, pp. 1498-1502, June 1997

[40] G. Bauch, H. Khorram, J. Hagenauer, "Iterative equalization and decoding in mobile communications systems", *Proc. European Personal Mobile Communications Conference*, pp. 301--312, October 1997

[41] E. Hall, S.G. Wilson, "Design and analysis of turbo codes on Rayleigh fading channels", *IEEE J. Selected Areas Commun.*, pp. 160-174, Feb. 1998.

[42] V. Tarokh, N. Seshadri and A.R. Calderbank, "A space-time coding modem for high-data-rate communications", *IEEE J. Selected Areas Commun.*, vol. 16, N0. 8, pp. 1459-1478, Oct. 1998

[43] B. Yeap, T. Liew, J. Hamorsky, L. Hanzo, "Comparative study of turbo equalizers using convolutional codes and block-based turbo codes for GMSK modulation", *Proc. IEEE VTC '99,* pp. 2974-2978, September 1999

[44] T. Liew, B. Yeap and J. Woodard and L. Hanzo, "Modified MAP algorithm for extended turbo BCH codes and turbo equalizers", *Proc. of the First International Conference on 3G Mobile Communication Technologies* 2000, p.185-189, March 2000

[45] M. Tüchler, R. Kötter, A. Singer: "Turbo equalization: principles and new results", submitted to *IEEE Trans. on Commun.*, September 2000

[46] R. Gozali, "Space-time coding and MIMO channels: a tutorial", *The Propagator*, Vol. 11, No. 2, pp. 11-13, Fall 2000. (Electronic Copy found at http://www.mprg.org/publications/Propagator/Fall00.pdf)

[47] D.S. Shiu, G.J. Foschini, M.J. Gans, J.M.Kahn, "Fading correlation, and its effect on the capacity of multielement antenna systems", *IEEE Trans. on Comm.*, vol. 48, No. 3, 2000

[48] A. Roumy, I. Fijalkow, A.J. Grant, D. Pirez, "Analysis of the iterative process of the Turbo-equalizer", submitted to *IEEE Trans. on Sig. Processing*, Feb. 2001

[49] J. Bajcsy, C. V. Chong, D. Garr, J. Hunziker, and H. Kobayashi, "On iterative decoding in some existing systems", *IEEE J. Select Areas Commun.*, Vol. 19, No. 5, pp. 883-890, May 2001

[50] R. Valenzuela. *V-BLAST High Level Overview.* June 15 2001. <http://www.bell-labs.com/project/V-BLAST/high-level-overview.html>

[51] R. Valenzuela. *A V-BLAST Tutorial.* Bell Labs. June 15 2001. <http://www.bell-labs.com/user/rav/4V-BLASTTutorial06.pdf>

[52] Xilinx Logicore, "3GPP Compliant Turbo Convolutional Codec V1.0", Product specification, May 2001. <http:// www.xilinx.com/ipcenter/

turbo_convol_lounge/#additional_information>

[53] ALV, *TechTalk - The ALVMTCF*, January 20, 2002. < http://www.alvgmbh.de/tt_mtcf/tt_mtcf.html>

[54] *3GPP Specifications*, January 20, 2002. The latest version is available from ftp://ftp.3gpp.org/specs/latest/, previous specifications can be found at ftp://ftp.3gpp.org/specs/archive/.